Mechanisms of Ciliary Targeting of the Olfactory Cyclic Nucleotide-Gated Channel

by

Paul Michael Jenkins

A dissertation submitted in partial fulfillment
of the requirements for the degree of
Doctor of Philosophy
(Pharmacology)
in The University of Michigan
2010

Doctoral Committee:

Associate Professor Jeffrey Randall Martens, Chair
Professor Lori L. Isom
Professor Benjamin L. Margolis
Associate Professor Kristen J. Verhey

To my family

ACKNOWLEDGEMENTS

I would like to first extend my sincerest gratitude to my research mentor, Dr. Jeffrey R. Martens. The time I have spent in his laboratory has shaped me both professionally and personally. His drive and dedication to science serve as a model that I strive towards every day. The past few years have been extremely rewarding for me due to his friendship, patience, and continual mentoring. I would not be where I am today without his guidance.

I would also like to acknowledge my thesis committee members, Dr. Lori Isom, Dr. Ben Margolis and Dr. Kristen Verhey. I have been extremely lucky to have a committee that not only acted as thesis advisors, but also as collaborators, mentors, and friends.

I would like to thank the numerous members of the Martens laboratory, present and former: Kristin Arendt, Dave Dudek, Nikhil Iyer, Sajida Jackson, Qiuju Li, Dyke McEwen, Jeremy McIntyre, Sarah Schumacher, Laurie Svoboda, Kristin van Genderen, Eileen Vesely, Tiffney Widner, Liz Williams, Kendra Yum, and Lian Zhang. Your antics in lab have kept me alternating between sanity and insanity and have left me with many good memories.

Special thanks to the many collaborators I have worked with in my time spent in graduate school: the Benjamin Margolis laboratory, including Albert Liu and especially

Toby Hurd for advice and technical help; the Donna Martin laboratory, including Elizabeth Hurd, Wanda Layman, and Jennifer Skidmore for assistance with the *in situ* hybridization experiments; the Yehoash Raphael laboratory, especially Lisa Beyer, for help with the electron microscopy; and the Margaret Gnegy laboratory, including Bipasha Guptaroy, Cheryse Furman, Rong Chen and Kathryn Luderman for help with the radiolabeling experiments. I would also like to acknowledge my funding from the Pharmacological Sciences Training Program, Hearing Balance and Chemical Senses Training Grant, and the National Institute on Deafness and Other Communication Disorders.

I would like to show appreciation to my parents, Beverly and Richard, as well as my siblings, Ken and Katie, for their support through the years. Finally I would like to thank my wife, Jackie, and our daughter, Molly, for all of the great times. Your love and unconditional support have been so important to me throughout graduate school. I could not have done it without you. Thank you all so much.

TABLE OF CONTENTS

LIST OF FIGURES

LIST OF ABBREVIATIONS

ACIII	adenylyl cyclase type III
B-SIT	brief smell identification test
BBS	Bardet-Biedl Syndrome
CNG channel	cyclic nucleotide-gated channel
EOG	electroolfactogram
FRAP	fluorescence recovery after photobleaching
GBC	globose basal cell
HA	hemagglutinin
HBC	horizontal basal cell
IFT	intraflagellar transport
JIP	JNK-interacting protein
LCA	Leber congenital amaurosis
MDCK	Madin Darby Canine Kidney cells
MTOC	microtubule organizing center
NGS	normal goat serum
OE	olfactory epithelium
OR	odorant receptor
OSN	olfactory sensory neuron
PACS-1	phosphofurin acidic cluster sorting protein-1
PF	paraformaldehyde
shRNA	short hairpin RNA
SRO protein	Stomatin-related olfactory protein
TBB	4,5,6,7-tetrabromobenzotriazole
TRP channel	transient receptor potential channel
YFP	yellow-fluorescent protein

CHAPTER 1

OLFACTORY CILIA: LINKING SENSORY CILIA FUNCTION AND HUMAN DISEASE

SUMMARY

The olfactory system gives us an awareness of our immediate environment by allowing us to detect volatile airborne stimuli. The components necessary for detection of these odorants are compartmentalized in the cilia of olfactory sensory neurons. Cilia are microtubule-based organelles, which can be found projecting from the surface of almost any mammalian cell, and are critical for proper olfactory function. Mislocalization of ciliary proteins and/or the loss of cilia cause impaired olfactory function, which is now recognized as a clinical manifestation of a broad class of human diseases, termed ciliopathies. Future work investigating the mechanisms of olfactory cilia function will provide us important new information regarding the pathogenesis of human sensory perception diseases.

Chapter 1 published as Jenkins, P.M., McEwen, D.P., and Martens, J.R. (2009). Olfactory cilia: linking sensory cilia function and human disease. Chem Senses *34,* 451-64. For copyright release, please see Appendix I.

INTRODUCTION

Inhalation of odorants across the surface of the olfactory epithelium (OE) initiates the olfactory signaling cascade, which involves the binding of odorants to receptors localized on the cilia of olfactory sensory neurons (OSNs). In the well-described canonical pathway, activated odorant receptors (ORs) act through a stimulatory G protein-coupled mechanism to activate adenylyl cyclase type III (ACIII) and increase the ciliary concentration of cAMP. Olfactory cyclic nucleotide-gated (CNG) channels open in response to cAMP binding and allow the depolarization of the OSN that is further amplified by the Ca^{+2}-activated Cl^{-} channel. All of these components necessary for odorant detection are enriched in olfactory cilia, and perturbation in the localization of these components or in the cilia themselves causes impaired olfactory function. Despite this critical ciliary compartmentalization, there is a relative paucity of information regarding membrane transport to this microtubule-based organelle. The revelation that most neuronal cells types possess a cilium, a unique cellular compartment whose function remains obscure, has stimulated interest in the segregation of proteins and the functional specialization of these membrane subdomains. One cell type where the ciliary function is well-described is the OSN. In this chapter, I will focus on olfactory cilia including structure and function, developmental formation and relation to human disease.

Anatomy of the Olfactory Epithelium

The main OE is a stratified epithelium composed of several cell types (Figure 1.1A). Supporting cells, termed sustentacular cells, contain many microvilli on their apical surface and have been shown to play a role in water-balance, regulation of mucous ion composition (along with the Bowman's glands), drug metabolism, and purinergic modulation of odor sensitivity [1-4]; however their precise function remains unknown. In addition to sustentacular cells, there are also five other distinct microvillous cell types in the OE that are found in much lower abundance. These cells, while sharing the common feature of microvilli, are distinct in their morphological characteristics and distribution [5-8]. A population of olfactory stem cells, termed basal cells, lies immediately superficial to the basal lamina and is responsible for the generation of new cells within the OE. The basal cell layer is composed of two types of cells: the globose basal cell (GBC) and the horizontal basal cell (HBC) (For review see [9]).

The OSN is the main sensory cell, which contains the elements of the olfactory sensory cascade (Figure 1.1B). OSNs are bipolar neurons with long axons projecting through the bony cribriform plate into the olfactory bulb, and relatively short dendrites terminating in a specialized ending termed a dendritic knob (Figure 1.1B). The dendritic knob contains multiple basal bodies from which the olfactory cilia project into the mucous of the OE [10-11] (Figure 1.1A-B).

Olfactory Cilia Structure

Cilia are nearly ubiquitous organelles that can be found projecting from the surface of most mammalian cell types (Reviewed in [12]). These cilia are generally

divided into classes based on their axonemal structure and motility. The structural component of the cilium, the axoneme, is most often composed of 9 doublets of microtubules arranged symmetrically around a central core. Cilia which contain a pair of microtubules within the central core are said to be in the (9+2) configuration, whereas those that lack the central pair contain the (9+0) configuration. Historically, cilia of the (9+2) configuration have been termed motile, whereas those of the (9+0) configuration have been termed non-motile or primary cilia. Motile (9+2) cilia (and their longer cousins, flagella) utilize structures called dynein arms along with the energy from ATP hydrolysis to generate movement, and play important roles in fluid flow, sexual reproduction, and airway clearance. In the nasal mucosa, respiratory cilia are (9+2) motile and can be easily distinguished by their rhythmic movement. Non-motile (9+0) cilia are commonly found as single primary cilia that help regulate cell-cycle progression, oncogenesis, and renal function. However, these ultrastructural classifications are not always steadfast. For example, rare motile (9+0) cilia can be found in the embryonic node where they function in the development of proper left-right asymmetry in the body [13]. Non-motile (9+2) cilia can be found in sensory organs [14-15]. Another prominent ciliated cell type in the nasal mucosa is the OSN. Although these cells possess cilia that have the (9+2) microtubule configuration normally found in motile cilia, they lack the dynein arms necessary for movement, and are thus rendered immotile [14]. Interestingly, some non-mammalian vertebrates, such as goldfish and frogs [16-17], display motile olfactory cilia, which have an axoneme resembling that of respiratory cilia in their proximal segments and are suggested to play a role in odorant clearance [18-19].

Axoneme

Much of the current knowledge about the structure of olfactory cilia can be credited to early electron microscopy studies [11, 16, 20-21]. These reports demonstrated that the mammalian olfactory cilium is approximately 50-60 microns in length and is divided into two distinct sections termed the proximal and distal segments. The thicker proximal segment projects 2-3 microns from the basal body in a (9+2) configuration with a thickness of around 300 nanometers [22]. The distal segment projects the remaining ~50 microns and dwindles down to an axonemal configuration of 1-4 singlet microtubules, most commonly consisting of a pair of singlet microtubules (Figure 1.1C) [22]. The distal segments of the olfactory cilia are oriented parallel to the epithelial surface. Because there are numerous cilia (10-30) per cell and because of the large distance they project from the dendritic knob there is substantial overlap of cilia from different OSNs [22]. This intertwined mat of cilia increases the sensory surface of the OE by over 40 times thus increasing our ability to detect odorants [23].

The ciliary axoneme is composed of long strands of α and β tubulin dimers, which form the structural backbone for the cilium (reviewed in [24-25]). These microtubules provide the roadway for molecular motors, such as kinesins and dyneins, to transport cargo into and out of the cilium. Olfactory ciliary axonemes are oriented with the plus end located in the distal tip of the cilium (Figure 1.1C), which means that plus end-directed motors carry cargo to the tip of the cilium, while minus end-directed motors are responsible for the return of cargo (reviewed in [24-25]).

Recently a number of post-translational modifications of tubulin have been discovered to play functional roles in the regulation of cargo transport (reviewed in [26]). Many modifications to tubulin have been found on the ciliary axoneme, including acetylation (α), polyglutamylation ($\alpha + \beta$), polyglycylation ($\alpha + \beta$), and detyrosination (α). While all of these modifications have been detected in olfactory cilia, their precise functional relevance is poorly understood [27-28]. However, a recent study found that zebrafish lacking an enzyme responsible for polyglutamylation exhibited a loss of olfactory cilia [27], indicating a role for post-translational tubulin modifications in assembly or maintenance of olfactory cilia. It is unclear if these modifications are uniform along the length of the ciliary axoneme.

In addition to changes in the axoneme structure, there is evidence for heterogeneity in protein content along the length of the cilium. The proximal and distal cilia segments may represent distinct subcellular compartments. During development, signaling proteins appear to localize differentially between these two regions. In newly-formed cilia, the olfactory signaling proteins are more evenly distributed between the proximal and distal segments. In mature cilia the signaling molecules, such as $G\alpha_{olf}$, ACIII, and CNG channel, appear to preferentially localize to the long distal segment where the odorant presumably first makes contact with the OSN [22, 29-30]. This clustering of signaling molecules at the site of odorant exposure may increase the efficiency of odorant-stimulated signaling.

Lipid Composition

The microtubule-based axoneme is encased by the lipid bilayer in the form of a membrane sheath, which, given the importance of lipids in cellular signaling, most certainly plays a critical role in olfactory signaling. The canonical olfactory signaling pathway includes several peripheral and transmembrane proteins; therefore, there likely exists a dynamic reciprocity between odorant signaling proteins and membrane lipids in olfactory cilia such that perturbation of membrane lipids can affect olfactory signaling.

Recently, there is growing evidence for the role of lipid membrane microdomains, enriched in cholesterol and sphingolipids, in the organization of olfactory signaling proteins [31-33]. In OE, Schreiber and colleagues [32] demonstrated that the G protein and adenylyl cyclase isoforms involved in odorant signaling associate with lipid rafts. They also reported that G_{olf} and ACIII interact with the cholesterol binding protein, caveolin, and that disruption of the caveolin interaction inhibits odorant-induced cAMP production in OSNs. Additionally, the recently identified stomatin-related olfactory (SRO) protein [33-34] has been shown to associate with lipid rafts in olfactory cilia and bind both caveolin and ACIII. Importantly, anti-SRO antibodies stimulated cAMP production in fractionated cilia membranes suggesting that rafts and/or a caveolin/lipid/protein complex regulate odorant signaling [33]. However, the study of lipid rafts and membrane organization in cilia and membranes in general has been hampered by the lack of quantitative biophysical approaches. Nevertheless, early ultrastructural data from the Menco laboratory comparing olfactory cilia membranes to that of respiratory cilia led them to conclude that that the outer leaflet membranes of

olfactory cilia are thicker than inner leaflets [17]. This is consistent with a potential enrichment of sphingolipids that are localized almost exclusively to the outer leaflet [35]. The enrichment of certain lipids is further supported by work in invertebrates that has shown that the ciliary membrane of *Paramecium* is highly enriched with sphingolipids [36]. These investigators later showed that ciliary membrane excitability in the same invertebrate model was sensitive to sterol composition [37]. Others have reported that there is an enrichment of cholesterol in the ciliary shaft, but not the necklace region, of epithelial cilia that extends during ciliogenesis [38]. Surprisingly however, there is virtually no information regarding the precise lipid composition of this important membrane structure in the olfactory system.

Ciliary Necklace

One clearly delineated microdomain of the ciliary membrane can be found where the lipid membrane sheath meets the dendritic knob. This membrane specialization is termed the "ciliary necklace" and likely represents the transition zone between the cytoplasm and the ciliary compartment. This highly ordered domain is marked by a spiraling array of membrane particles [39-41], which connect to the basal body just below the ciliary axoneme [42]. While most cilia types possess a ciliary necklace, olfactory cilia typically have more strands per cilium than their respiratory counterparts, although the physiological relevance of this is unknown [41]. The formation of the ciliary necklace precedes ciliogenesis as a patch of membrane, and in malformed cilia there are still necklace-like structures [41, 43]. Interestingly, some ciliary transport proteins have been found to be localized at the ciliary necklace indicating that it may serve as a cargo

docking site connecting the ciliary shaft to the protein complexes at the base of the cilium [44].

Basal Body

The basal body is a modified centriole that migrates to the plasma membrane prior to ciliogenesis (Figure 1.3). The basal bodies are duplicated *en masse* in the cell body of the OSN before they migrate to the dendritic knob (Figure 1.3A) [11, 28, 45-46]. Basal bodies, like the ciliary axoneme, are composed of nine sets of microtubules arranged in a radial symmetry (Figure 1.1C). However, basal bodies are composed of polymers of triplet microtubules rather than the doublet microtubules seen in the axoneme. The basal body serves as the microtubule organizing center (MTOC) in the dendritic knob with the axonemal tubules projecting from the basal body, such that the plus ends orient toward the distal tip of the cilium [47].

In addition to serving as MTOCs for the ciliary axoneme, the basal bodies are associated with electron-dense satellite particles that appear to also be MTOCs [47]. These organizing centers serve as nucleation sites for microtubules that project from the dendritic knob back through the dendrite towards the cell body [48]. Some of the MTOCs are connected to the basal body through a sheath of material that surrounds the basal body and thickens at its proximal end. The basal bodies and sheath are connected to the plasma membrane through 9 struts which correspond to the electron-dense endings which anchor to the plasma membrane (Figure 1.1C) [41].

Ciliary Rootlet

The ciliary rootlet is a cytoskeletal feature found projecting from the basal body in many ciliated cells and believed to participate in anchoring of cilium [49]. Although the structural components of the ciliary rootlet are beginning to be elucidated [50], still very little is known about its function. It seems unclear if olfactory cilia possess a rootlet [51-53]; however OSNs have been shown to express components of the ciliary rootlet in a localization consistent with the dendritic knob/basal body region [53-54]. More work is necessary to definitively demonstrate the presence or absence of an olfactory ciliary rootlet.

Ciliogenesis

The olfactory placode first appears in the mouse at embryonic day 9 (E9) post-fertilization [10-11, 20-21, 28, 55]. At E10, the olfactory placode invaginates and forms the olfactory pit which is composed primarily of two cell types: a population that is electron dense (proliferative basal cells) and those that appear light (differentiated OSNs) [10-11, 20-21, 55]. At E11, the dendrites begin to form and extend toward the apical surface. Also, the olfactory pit deepens and forms recesses which will eventually become the olfactory turbinates [10-11, 20-21, 55]. During this time, the primary site of OSN growth and maturation is the deep recesses of the olfactory pit [10-11, 20-21, 55].

By E11, several morphological changes occur in OSNs, representing the initial stages of ciliogenesis. First, in the perinuclear region of these neurons, numerous microtubules and microfilaments form and extend vertically toward the apical surface [11, 20, 56]. Second, the distal end of the dendrite now extends into the lumen of the

nasal cavity, where it begins to swell and form the dendritic knob (Figure 1.3B-C) [11, 20, 56]. Finally, and perhaps most importantly, centriole duplication occurs and groups of centrioles accumulate in the perinuclear region of the neuron (Figure 1.3A) [11, 20, 56].

By E12, the rate of OSN proliferation increases, and these OSNs begin to develop well-formed dendrites and dendritic knobs filled with mitochondria, small coated vesicles, and numerous microtubules [11, 20, 56]. The microtubules in the dendritic knob are arranged in two distinct populations; one is arranged concentrically around the periphery of the knob while the other is arranged longitudinally and extends deep into the dendrite [11, 20, 56]. In addition, the centrioles that were duplicated at E11 begin to migrate to the dendritic knob and eventually disperse singly around the knob periphery where they associate with the plasma membrane (Figure 1.3C). Ciliogenesis commences when a single, primary cilium of approximately 1 μm extends into the nasal cavity [11, 20, 28, 56]. As new cilia form, their microtubule-based axoneme elongates and the basal body, formed by the migrating centrioles, matures and is anchored at the plasma membrane (Figure 1.3C-D) [10-11, 28, 45-46]. By E13 or E14, multiple cilia up to 2 μm in length can be seen extending from a single dendritic knob (Figure 1.3D). Over the next several days, olfactory cilia continue to elongate and can reach up to 60 μm prior to birth. Intraflagellar transport (IFT), which will be discussed in more detail below, plays a key role in the transport of cargo responsible for the growth and maintenance of cilia [24-25]. In some species, the cilia will continue to grow and can reach up to 200 μm in length [16, 20, 57]. The multitudes of overlapping OSN cilia create a meshwork across

the surface of the OE, thus increasing the surface area of the OE up to 40 times and enhancing the sensitivity of odorant detection [17, 20].

In addition to ciliogenesis, the proper delivery of ciliary signaling proteins is essential for normal olfactory function. Most of the work examining developmental expression of olfactory signaling molecules has probed for mRNA expression using either RT-PCR, northern blot, or *in situ* hybridization analysis [28, 58-61]. Interestingly, there appears to be a differential temporal expression of the components necessary for odor detection. ORs, of which a subset begin to be expressed at E11, appear to be the first member of the signaling cascade to be expressed as determined by both mRNA and protein expression [28, 59-60]. This expression occurs prior to ciliogenesis, and thus the OR protein localizes in high density at the dendritic knob [28]. Surprisingly, this expression appears to be limited to a subset of ORs. For example, mOR256-17 and V1, two of the earliest detectable ORS, begin to express at E11 [28, 59-60], while mOR5, mOR14, mOR18-2, mOR37, mOR111-5, mOR124, and mOR171-24 begin to express around E12 [60-61]. Eventually the diversity of expression continues to increase during development thus allowing the expression of hundreds of ORs [58-60]. The physiological relevance of this temporal expression pattern remains unclear.

The downstream components of the olfactory signaling cascade appear to be expressed later in embryonic development. ACIII expression is first detected around E15, while G_{olf} and the CNG channel expression initiates at E16 and E19, respectively [58]. It is assumed that odor detection cannot occur until all proteins are present in olfactory cilia, thus the relevance of this temporal expression pattern remains unknown.

The protein expression of one specific OR, mOR256-17, has been used to track ciliogenesis [60]. As mentioned above, ORs begin their expression prior to the initiation of ciliogenesis. mOR256-17 accumulates at the dendritic knob in high density at this stage. Only after the cilia form and elongate (~E11) can the OR be properly localized initially to the knob and at the very proximal portions of the cilia. Once the cilia reach 2 μm or longer (~E12-13), mOR256-17 migrates almost exclusively to OSN cilia [60]. Interestingly, this work indicates that, at least in the case of mOR256-17, the protein can localize to the dendritic knob independent of any signal from the cilium.

INTRAFLAGELLAR TRANSPORT (IFT)

Cargo transport in cilia occurs through an evolutionarily-conserved process termed intraflagellar transport (IFT), which was first discovered in the laboratory of Joel Rosenbaum in *Chlamydomonas* [62]. Since cilia lack the necessary components for protein synthesis and no obvious vesicular structures have been observed within the cilium, cargo must be synthesized in the cell and carried into the cilia through IFT, which involves movement along microtubules by molecular motors in complex with transport molecules, called IFT particles (reviewed in [24-25, 63]). Since the basic mechanisms of IFT are widely conserved not only between cilia types, but also often between species, we presume that these mechanisms studied in invertebrates are also acting in mammalian olfactory cilia.

IFT involves bidirectional transport into and out of the cilium by molecular motors that utilize the energy from ATP hydrolysis to generate processive movement. The transport of cargo out of the cilium back into the cell is accomplished via the

cytoplasmic dynein motor [64], whereas anterograde transport towards the distal, plus-end of the cilium microtubules has been shown to involve kinesin motors [65] (Figure 1.1D). Work in *Caenorhabditis elegans* has shown that the formation and maintenance of the chemosensory ciliary axoneme and the delivery of cargo is accomplished through coordination of two anterograde kinesin motors: the heterotrimeric kinesin-II motor and the homodimeric OSM-3 [66]. The mammalian kinesin-II motor, consisting of KIF3a, KIF3b, and the accessory protein, KAP3, has also been found to be necessary for ciliogenesis (Figure 1.1D) [67]. However, differences are beginning to be recognized between specialized cilia types in invertebrates and mammals [68-69]. Expression of a dominant-negative KIF17, the mammalian homolog of OSM-3, impaired ciliary trafficking of the olfactory CNG channel, however it had no effect on cilia length as predicted by work in *C. elegans* [68-69]. Future studies are necessary to determine if these motors are also responsible for cargo transport in mammalian olfactory cilia. Interestingly, OSM-3 operates on singlet microtubules of the distal segments of *C. elegans* cilia [69]. Since olfactory cilia have such prominent distal segments and several signaling proteins, including the CNG channel, are found to be enriched in the distal segment, it seems likely that KIF17 is also functioning on distal segments in the mammalian olfactory cilium. Nevertheless, the differences in kinesin-2 motor coordination between the cilia of *C. elegans* and mammals highlight the need to further explore the mechanisms of IFT in mammalian olfactory cilia.

Using electron microscopy, IFT particles can be seen as electron-dense regions consisting of motors and IFT complexes found along the olfactory ciliary axoneme [16].

It is known that IFT motors associate with two distinct complexes of transport proteins called IFT proteins, which are named according to their molecular weight. These two complexes comprise 17 highly-conserved proteins, termed complex A and complex B [70]. Complex A consists of IFT144, 140, 139, 122, and possibly 43, while complex B consists of IFT 172, 88, 81, 80, 74/72, 57/55, 52, 46, 27, and 20. Defects in either complex can impair IFT and cause a host of human diseases (reviewed in [71]). A recent report demonstrated that mutation of the locus encoding the zebrafish homolog of IFT88 caused a loss of cilia from OSNs [72]. While the function of IFT proteins in many cases remains elusive, some IFT proteins have been shown to share significant homology with Golgi-localized clathrin trafficking machinery [73]. Interestingly, the clathrin AP-1 μ adaptor, UNC-101, has been shown to be responsible for the localization of ORs to the cilia of C. *elegans* [74]. In most cases, however, the precise role of the IFT complexes in mammalian olfactory cilia transport remains undefined.

Recent work in *C. elegans* suggests that there is a dynamic reciprocity between ciliary signaling and IFT-mediated ciliary structure maintenance. Mukhopadhyay *et al.* have shown that the loss of activation of the sensory signaling cascade modulates the structure of the AWB neuron modified sensory cilia [75]. This sensory signaling-dependent remodeling was shown to be dependent on kinesin-II as well as Bardet-Biedl Syndrome (BBS) proteins [75]. This is similar to a previous study showing that structure of AWC neuron cilia is also linked to sensory function [76]. While gross structural changes have been reported in mice deprived of odorant stimulation by naris occlusion [77], it would be interesting to examine ultrastructural changes in cilia architecture due to

loss of olfactory cues. Regardless, this suggests a potential feedback interaction between the IFT proteins involved in ciliary assembly and maintenance and those involved in odorant-induced signaling.

While we have learned a great deal about IFT from invertebrate models, the olfactory systems of invertebrates may not be homologous with those found in vertebrates [78]. Additionally, critical differences are beginning to be recognized even between cilia types within an organism. Therefore it is critical that we continue to elucidate the function of vertebrate, and specifically mammalian, olfactory cilia.

Regulation of Ciliary Protein Entry

Common to all organisms is the fact that only a subset of cellular proteins is able to gain access to the cilium, since it contains a protein population distinct from the extraciliary compartment [79]. It is widely believed that there must be a barrier to diffusion that restricts entry into the cilium. This selective gate is thought to occur at the basal body through interactions with a large complex of proteins (Figure 1.1D) [24-25]. One family of proteins that has been shown to be involved in the regulation of ciliary transport is the BBS family of proteins. Bardet-Biedl Syndrome is a pleiotropic ciliopathy that include phenotypes such as retinal degeneration, polydactyly, obesity, anosmia, and others (discussed in more detail below). There are 12 known BBS proteins (BBS1-12), which encode proteins involved in different stages of cilia transport. While there are a variety of ciliary phenotypes associated with defects in BBS proteins, loss of function of BBS1 and BBS4 caused impaired olfactory function [80-81]. Interestingly,

mice null for BBS1 or BBS4 may exhibit defects in olfactory cilia maintenance or assembly, although the mechanism for this defect remains unknown [80-81].

Mutation of the cilia/centrosomal protein CEP290 has been implicated in the specific mislocalization of olfactory G proteins [82]. Importantly, mutation in CEP290 did not globally alter cilia structure and all other olfactory signaling molecules tested were localized normally, indicating that in olfactory cilia, regulation of cargo entry is distinct for different proteins. Interestingly, CEP290 was recently shown to interact with the centriolar satellite protein PCM-1 in a retinal epithelial cell line [83]. PCM-1 has been shown to interact with BBS4 [84] and is dependent on the presence of BBS4 for proper ciliary localization [81]. Together, these reports represent the beginning of the discovery of the mechanisms of basal body/cilia function in the OSN, though much work remains to further elucidate this process.

Recently, the intracellular trafficking protein, phosphofurin acidic cluster sorting protein 1 (PACS-1) has been shown to localize to the base of human respiratory cilia and control the localization of nephrocystin 1 to the transition zone of respiratory cilia [85]. While PACS-1 has been shown to interact with acidic cluster-containing ion channels such as polycystin-2/TRPP2, TRPV4, and CLC-7 [81, 86], no direct role has been demonstrated in the control of ciliary localization of ion channels. Recent unpublished work from the Martens laboratory has found that this protein localizes to the dendritic knob of OSNs and is necessary for the localization of the olfactory CNG channel, but not ACIII, to olfactory cilia (Unpublished work, Martens laboratory). Interestingly, this mechanism is dependent on phosphorylation of PACS-1 and CNGB1b by CK2, thus

providing a mechanism for the subunit-dependent trafficking of the olfactory CNG channel [68]. Phosphorylation-dependent trafficking of olfactory signaling proteins may represent a mechanism for the tuning of the olfactory response. Another report demonstrated that ORs interact with β-arrestin in a phosphorylation-dependent manner, and that this interaction may be responsible for trafficking of ORs out of the cilium upon prolonged exposure to odorant [87]. Despite these reports, very little is known regarding the dynamic trafficking of proteins into and out of olfactory cilia either under normal conditions or in response to stimuli.

Growing interest in ciliary protein trafficking has led to the identification of amino acid sequences necessary for entry of cargo into cilia. For example, the "RVxP" motif originally identified in polycystin-2 [88], was found to be necessary for the ciliary delivery of the olfactory CNG channel [68]. Interestingly, a recent report demonstrated that the homologous "xVxP" motif in rhodopsin interacts with the small GTPase Arf4 and regulates trafficking of a ciliary targeting complex from the trans-Golgi network [89]. Additionally, several ORs were recently found to contain another ciliary targeting motif consisting of (AX[S/A]XQ) which was sufficient to drive ciliary localization of non-ciliary receptors [90]. The precise mechanisms by which these motifs control ciliary localization remain unknown. Interestingly, only a subset of ciliary proteins expresses these motifs indicating that there are multiple potential ciliary targeting motifs that most likely act through distinct ciliary entry mechanisms.

Due to the lack of rough endoplasmic reticulum, the dendritic knob is not a site for protein synthesis. This suggests that ciliary cargo must be synthesized in the soma

and transported down the length of the dendrite in order to gain access to the cilium. Therefore, a loss of somatodendritic trafficking of ciliary cargo could also cause ciliary dysfunction. For example, in *C. elegans*, mutation in the membrane protein ODR-4 causes a mislocalization of a subset of chemosensory receptors [91]. Because of the localization of ODR-4 to intracellular membranes within the soma, the authors conclude that this mislocalization could be due to a loss of ODR-4-mediated OR folding, sorting, or transport from the soma. Although this mechanism has yet to be seen in mammalian OSNs, given the difficulty expressing ORs in heterologous systems, it seems likely that mammalian OSNs possess a similar set of proteins necessary for proper OR transport.

Dynamics of Protein Movement within Olfactory Cilia

Although we are beginning to understand some of the mechanisms of ciliary cargo entry, we have virtually no information regarding the dynamics of cargo movement once inside the cilium. One might expect that members of signaling cascades, specifically transmembrane proteins, would move relatively slowly within the cilium and display long half-lives in order to increase the efficiency of the signaling cascade. Indeed, in fluorescence recovery after photobleaching experiments, the olfactory CNG channel moved within the cilium at a rate consistent with slow diffusion (t1/2 of recovery ~ 10 minutes) in a model system [68]. However, in *C. elegans* the TRPV channel OSM-9 moves along the ciliary membrane at rates comparable to IFT (~1-2 microns per second) [92]. One potential reason for the rapid movement of cargo in cilia would be the recycling of damaged signaling proteins, however at this point the dynamics of protein movement within olfactory cilia remains relatively unexplored.

Fate of Mistargeted Ciliary Cargo

As discussed earlier, the basal body serves as the nucleation site for the ciliary axoneme and appears to serve as a scaffold for a complex of proteins that regulate entry of cargo into the cilium. In addition to these functions, it appears that the basal body also acts as a site of organization of proteolytic machinery. For example, it has been shown that proteolytic enzymes are enriched around the centrosome [93]. Recently, another group demonstrated that disruption of basal body function by suppression of BBS4 impairs proteasome function [94]. This basal body/proteasome complex may serve to degrade improperly folded or mistrafficked ciliary cargo. For example, mice null for CNGB1b demonstrate very low levels of the remaining CNG subunits [95]. However, when these mice are treated with a proteasome inhibitor, the remaining channel subunits can be readily detected at the dendritic knob suggesting that the knob is serving as the site of proteolytic degradation.

CILIARY GENOMICS AND PROTEOMICS

Cilia contain a set of proteins distinct from the remainder of the cell [79]. In addition, the components necessary for odorant detection are all highly localized to cilia (Figure 1.2). Although we understand the function of a handful of these proteins, emerging areas of research are yielding new insights into other cilia-related genes and novel proteins that may be involved in olfactory signaling or ciliary structure and maintenance [54]. Recent advances in technology have vastly improved our ability to use bioinformatics as a tool to identify novel genes involved in various cellular processes, such as cilia formation and function. Hundreds of genes present in numerous ciliated

species have recently been identified to be important in cilia-related functions [54, 73, 96-100].

Although it is believed that cilia are widely conserved between cilia types, it is now becoming clear that differences exist both between species and between cilia types within one organism. Only a few studies have concentrated on identifying ciliary genes in mammals, with only a few focusing on olfactory cilia [54, 101-106]. Using genomics and proteomics, these studies have identified over 100 cilia-related genes of known and unknown function in OSNs [54, 101, 105-106]. These studies represent a solid starting point for the elucidation of the ciliary proteome; however, improved cilia purification methods should facilitate further study. Nevertheless, the challenge remains to demonstrate the function and physiological relevance of these ciliary proteins, especially in relation to human ciliopathies.

OLFACTORY CILIA AND HUMAN DISEASE

While the olfactory system is necessary for detecting odors and crucial for our sense of taste, it also plays important roles in our quality of life, health, and safety. Dysosmia (impaired sense of smell) or anosmia (loss of ability to smell) can prevent us from detecting signs of danger such as smoke or spoiled food, and also can lead to medical problems such as weight gain and poor nutrition [107]. Impaired olfactory function is estimated to affect 3-6 million Americans and over 50% of those over the age of 65 [108-109], however this may be a gross underestimate given that olfactory dysfunction frequently goes unreported [109]. While the leading causes of smell disorders in patients are injury due to head trauma, upper respiratory tract infections, and

chronic rhinosinusitis, in at least 20% of cases the underlying etiology remains unknown [110]. Olfactory dysfunction due to genetic mutations or neurodegenerative disorders affecting cilia is becoming increasingly recognized and better studied.

Olfactory Ciliopathies

One of the first documented cases of a human patient with anosmia presumably due to ciliary defects was in 1975 [111-112]. A biopsy from this patient, who suffered from congenital anosmia, revealed that, while the global architecture of the epithelium appeared normal, his OSNs were devoid of cilia, the cause of which is unknown [111]. It has only been within the past 5 years that patients with deficits in olfaction due to ciliary defects have been clearly identified [80-82]. In these cases, the olfactory deficits were shown two occur in two different pleiotropic diseases, Bardet-Biedl syndrome (BBS) and Leber congenital amaurosis (LCA).

BBS is highly pleiotropic with patients exhibiting mental disabilities, obesity, retinal degeneration, polycystic kidneys, hypertension, and hypercholesterolemia, which together may lead to premature death [113-116]. The varied effects are dependent upon mutations in one of 12 members of the BBS gene family, with the most severe mutations occurring in either BBS1 or BBS10 [116-120]. Several BBS proteins, BBS1-8, have been characterized as basal body proteins that are thought to regulate protein entry into the cilium [116]. Human mutations in two BBS proteins, BBS1 and BBS4, and genetic deletion of BBS1, BBS2, or BBS4 in mice resulted in severely impaired olfactory function [80-81, 121-122]. However, mutations in the BBS proteins do not seem to share a common underlying mechanism of olfactory dysfunction. For example, patients with

mutations in BBS1 are anosmic, most likely due to a loss of olfactory cilia, as the cilia are absent in the BBS1 null mouse model [80-81]. In the BBS2 null mouse, the status of olfactory cilia has not been examined, but both renal and retinal cilia are able to assemble [122]. Finally, in two different studies, patients with mutations in BBS4 exhibited decreased olfaction or anosmia [80-81]. The divergent phenotypes observed with mutation or loss of specific BBS proteins highlight the complex regulation of ciliogenesis as well as the assembly and maintenance of the axoneme. This is also true when comparing different ciliated cells from a single BBS null animal. For example, mice deficient in BBS4 have a diminished cilia layer in the OE which causes an almost complete loss of electroolfactogram response [81]. Similarly sperm from these null mice completely lack flagella [121]. However, these mice are still capable of ciliogenesis [121]. Renal epithelial cells from these animals possess cilia but demonstrate altered timing for axoneme extension [123], which may allow the age-dependent development of polycystic kidneys [124]. These results demonstrate the sensitivity of different cell types to alterations on BBS function and suggest that the manifestation of disease may reflect the extent to which complete elaboration of normal cilia is essential for a wildtype phenotype

A second example of a ciliary defect leading to olfactory impairment is a recent study investigating olfactory function in patients with Leber congenital amaurosis (LCA) [82]. LCA, first discovered by Theodor Leber almost 140 years ago [125], is a congenital retinal dystrophy accounting for more than 5% of inherited retinopathies [126]. LCA can occur due to mutations in several proteins of varying function, from retinoid

metabolism and phototransduction to cell-cycle progression [126]. Recent reports have also shown that LCA can be caused by mutations in the centrosomal/basal body protein, CEP290 [127-128]. Olfactory function was tested in the original LCA patient population with mutations in CEP290 using the Brief Smell Identification Test (B-SIT) [82]. For all patients tested, mutations in CEP290 resulted in severely impaired olfactory function despite a self-described normal sense of smell [82]. Using a mouse model, it was determined that the olfactory impairment was due to a mislocalization of the olfactory G-protein rendering the signaling pathway non-functional, despite cilia remaining intact [82]. Together, these studies suggest that olfactory dysfunction due to ciliary defects can occur by two separate mechanisms; 1) a complete loss of olfactory cilia, and 2) a defect in protein trafficking leading to a loss in olfactory signaling.

Although it is now clear that olfactory dysfunction is a clinical manifestation of a subset of ciliopathies, there appears to be a selective penetrance of phenotypes between different cilia in the body. For example, hypomorphic mutation in CEP290 causes anosmia and early-onset retinal degeneration without a renal phenotype [82, 129]. In addition, KIF17 is not essential for renal cilia maintenance, however is necessary for the maintenance of the rod outer segment, which is an extension of the modified connecting cilium [68, 130]. Despite the varying penetrance of ciliopathies, the assessment of olfactory function represents an attractive tool for pregenetic screening due to the low cost and minimally invasive nature of the procedure. In addition, screening for olfactory dysfunction may lead to the discovery of previously undescribed ciliary diseases. Finally, the finding that loss of olfactory cilia or perturbation in ciliary protein localization can

represent the underlying cause of olfactory dysfunction highlights the necessity for further elucidation of the mechanisms and molecular machinery necessary for ciliary transport in OSNs.

The OSN as a Site for Pathogen Entry

The mammalian olfactory system is unique in that it is the only region of the central nervous system that is directly exposed to the external environment [131-132]. It is estimated that the exposed surface of the OE, comprising the dendritic knob plus cilia, is around 23 cm^2 [131-132]. Together, this makes the OE a unique and vulnerable target for the entry of pathogens directly into the brain. Even though the OE is partially protected by the presence of the nasal mucous as well as high levels of metabolizing enzymes, such as cytochrome P450s, evidence exists that pathogens can enter the brain through the OE [131, 133-134]. In early 20^{th} century, it was shown that viruses could enter the monkey brain and that this was prevented by lesioning either the OE, the axon tracts, or the olfactory bulb [131, 135-137]. One of the major debilitating viruses shown to enter the brain via the OE was the poliomyelitus virus [135-137]. Today, the list of viruses able to infect the OE has expanded and includes some major viruses, such as adenovirus, herpes simplex, hepatitis, influenza A, and rabies, as well as many others [131]. A subset of these pathogens may enter exclusively through OSNs and specifically the cilia. For example, the olfactory cilia from a patient with sporadic Creutzfeldt-Jakob disease were positive for protease-resistant prion protein [138]. Following death, a neuropathological examination revealed nerve loss and gliosis in cerebral cortex, striatum, and cerebellum, suggesting that the olfactory cilia served as a site for pathogen

entry [138]. Therefore, the OE, specifically the OSN cilia, is likely a major target for pathogenic transmission of xenobiotics directly into the brain.

CONCLUSIONS

Olfactory dysfunction in the general population is frequent, affecting at least 2.5 million people in the U.S. alone. In at least 20% of the cases the etiology of the chemosensory disturbance cannot be identified. Recent evidence demonstrates that olfactory dysfunction is a clinical manifestation of an emerging class of human genetic disorders, termed ciliopathies, which involve defects in ciliary assembly and/or protein transport. Given the plasticity of the olfactory system and its regenerative properties, olfactory sensory neurons (OSNs) undergo a continual process of ciliogenesis and protein transport that is critical for olfactory function. Intrinsic mechanisms are present in OSNs that direct cell surface localization and selective ciliary compartmentalization of olfactory transduction proteins. Remarkably, the mechanisms and molecular machinery necessary for ciliary transport in OSNs are poorly understood. Future work in this area will afford new insights into the regulation of sensory perception while emphasizing that olfactory dysfunction represents an important clinical manifestation of ciliary disease.

ACKNOWLEDGEMENTS

This work was supported by National Institutes of Health grants DC009606 (JRM), GM007767 (PMJ), DC00011 (PMJ and DPM), and NRSA fellowship DC009524 (PMJ).

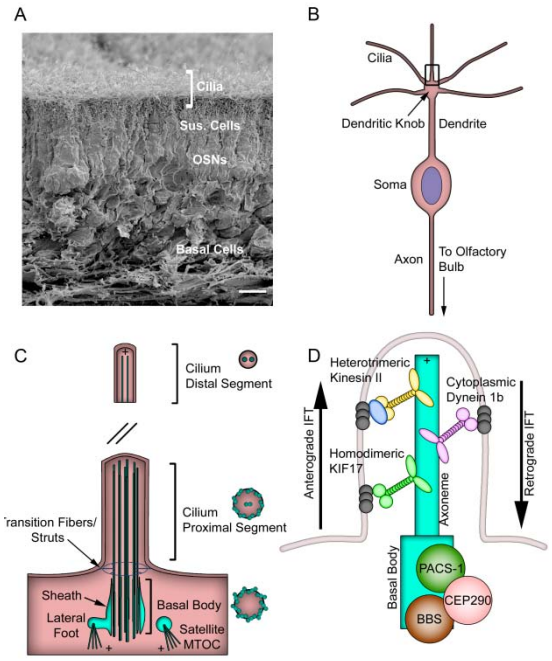

Figure 1.1 Anatomy of the Olfactory Epithelium and Olfactory Sensory Neuron

(A) Side view of a scanning electron micrograph at 1,030 x magnification from mouse OE. Mouse OE was dissected, fixed in glutaraldehyde, and processed for scanning electron microscopy as previously described [82]. Scanning electron micrographs were captured using an Amray 1910FE field emission scanning electron microscope at 5 kV. Images were recorded digitally with Semicaps software. Layers of the OE are labeled in white. Cilia layer marked by bracket. Sus. Cells = sustentacular cells. Scale bar represents 10 µm. (Image generously provided by Wanda Layman and Dr. Donna Martin, Department of Human Genetics, University of Michigan). **(B)** Cartoon representation of a single OSN. Boxed region of interest at base of cilium shown at higher magnification in panel C. **(C)** Cartoon representation of olfactory cilium and associated organelles. Cross sections of axonemal configuration from distal segment (top), proximal segment (middle), and basal body (bottom) shown on right. Solidi (//) mark transition from proximal to distal segments. MTOC = Microtubule Organizing Center. Break indicates transition from thick proximal segment to thin distal segment. + indicates plus end of microtubules. **(D)** Cartoon representation of the ciliary and basal body components involved in olfactory ciliary transport. Anterograde motors move cargo to the distal tip of the cilium. Heterotrimeric kinesin II is composed of KIF3a, KIF3b and KAP3 while KIF17 comprises a homodimer. The retrograde motor, cytoplasmic dynein 1b moves cargo back out of the cilium. IFT complexes are shown as grey circles.

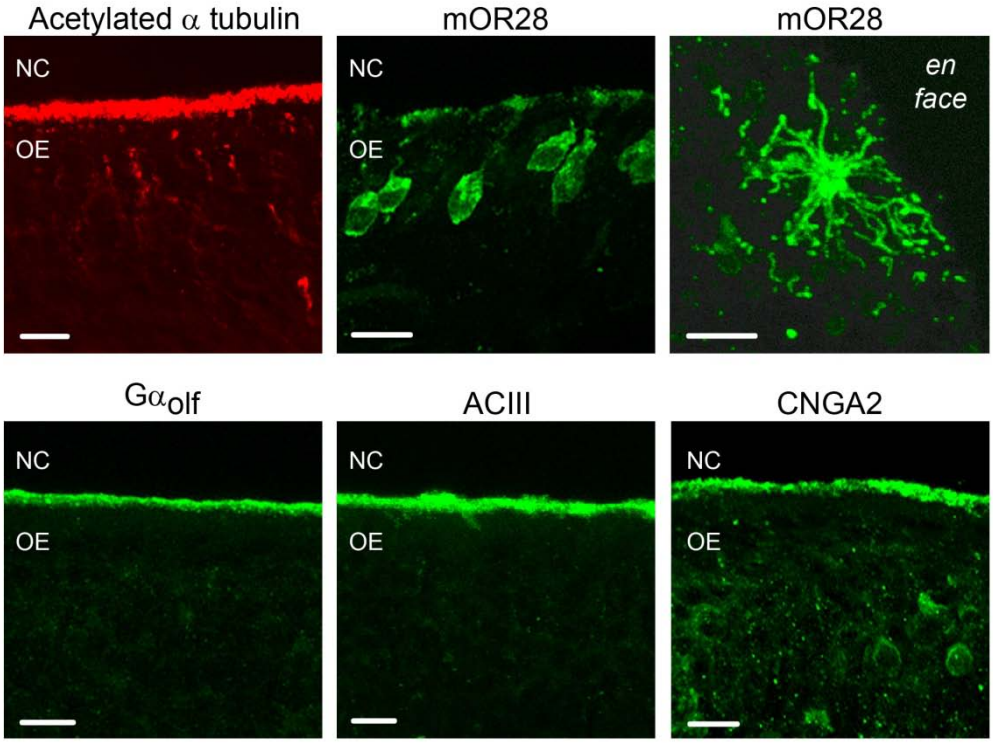

Figure 1.2 Localization of Olfactory Signaling Proteins to Cilia

Immunocytochemistry for olfactory signaling proteins was performed on 14 mm-thick sections of frozen mouse OE as described previously [82]. Acetylated α tubulin is a marker for the cilia layer. The odorant receptor mOR28 (top middle, antibody courtesy of Dr. Richard Axel) is localized throughout the OSN including the cilia, which can be more easily visualized in an *en face* section (top right). The olfactory G protein $G\alpha_{olf}$ (bottom left), adenylyl cyclase III (bottom middle), and CNG channel CNGA2 subunit (bottom right) are all enriched in the cilia layer. NC = nasal cavity, OE = olfactory epithelium. Scale bars represent 10 μm for all images except *en face* mOR28 (bar represents 5 μm)

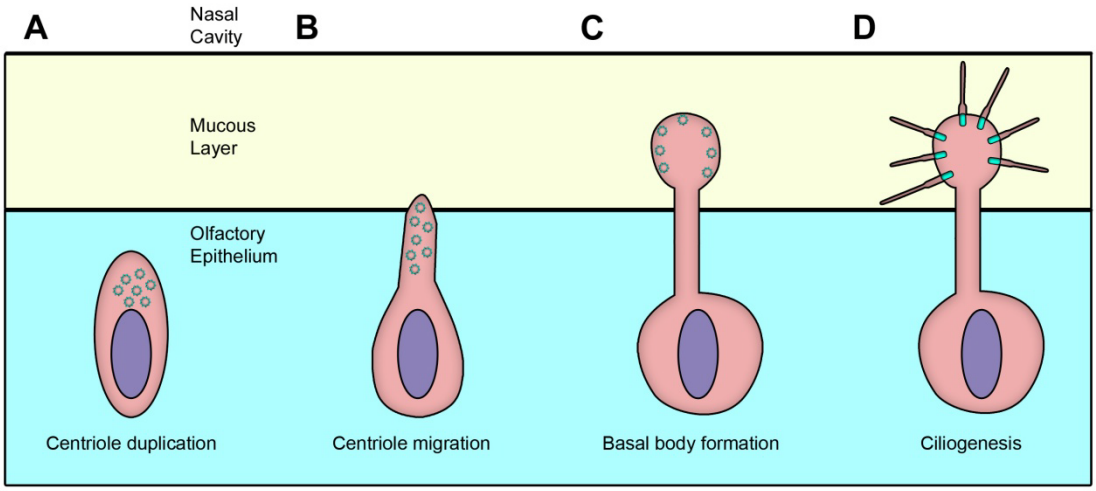

Figure 1.3 Steps of Ciliogenesis in the Olfactory Sensory Neuron

(A) In a developing OSN (at approximately E10 – E11) centrioles are duplicated *en masse* from the mother/daughter centrioles in the cell body before migrating along the developing dendrite towards the eventual dendritic knob **(B)**. **(C)** In the dendritic knob (at approximately E12-E14), centrioles are converted to basal bodies and anchored to the plasma membrane, and ciliogenesis begins as the ciliary axonemes extend from the basal body and elongate the cilia into the mucous layer where odorant transduction occurs (**D)** Interestingly, one single primary cilium of approximately 1 μm in length forms before the appearance of the remaining cilia.

CHAPTER 2

CILIARY TARGETING OF OLFACTORY CNG CHANNELS REQUIRES THE CNGB1B SUBUNIT AND THE KINESIN-2 MOTOR PROTEIN, KIF17

SUMMARY

Non-motile cilia on olfactory sensory neurons (OSNs) compartmentalize signaling molecules, including odorant receptors and cyclic nucleotide-gated (CNG) channels, allowing for efficient, spatially confined responses to sensory stimuli [139-141]. Little is known about the mechanisms of the ciliary targeting of olfactory CNG channels, composed of three subunits: CNGA2 CNGA4 and CNGB1b [142]. Recent reports suggest that subunit composition of the retinal CNG channel influences localization leading to disease [143-144]. However, the mechanistic role of subunits in properly targeting native olfactory CNG channels remains unclear.

Chapter 2 is published as Jenkins, P.M., Hurd, T.W., Zhang, L., McEwen, D.P., Brown, R.L., Margolis, B., Verhey, K.J., and Martens, J.R. (2006). Ciliary targeting of olfactory CNG channels requires the CNGB1b subunit and the kinesin-2 motor protein, KIF17. Curr Biol *16*, 1211-1216. For copyright release, please see Appendix I. I would like to acknowledge the Benjamin Margolis laboratory and Toby Hurd for providing reagents, critical review of the manuscript, and for the data shown in Figure 2.8A. Also I would like to thank the Kristen Verhey laboratory for providing the KIF17 plasmids and for review of the manuscript. Finally I would like to acknowledge the Jeffrey Martens laboratory including Dyke McEwen for the data shown in panels F and G of Figure 2.8 and Lian Zhang for the preparation of the CNG channel mutant constructs.

Here we show that heteromeric assembly with CNGB1b, containing a critical carboxy-terminal motif (RVxP), is required for ciliary trafficking of olfactory CNG channels. Movement of proteins within the cilia is governed by intraflagellar transport (IFT), a process that facilitates bi-directional movement of cargo along microtubules [24-25]. Work in *C. elegans* has established that heterotrimeric and homodimeric kinesin-2 family members play a critical role in anterograde transport [66, 69, 145]. In mammalian systems, the heterotrimeric KIF3a/KIF3b/KAP-3 complex plays a clear role in IFT; however, no role has been established for KIF17, the mammalian homolog of OSM-3 [146]. Here we demonstrate that KIF17 is required for olfactory CNG channel targeting, providing novel insights into mechanisms of mammalian ciliary transport.

RESULTS

To investigate the role of subunit composition in ciliary targeting of olfactory CNG channels, we expressed yellow fluorescent protein (YFP)-tagged CNGA2 in Madin Darby canine kidney (MDCK) cells. These cells contain a non-motile primary cilium extending from their apical surface and are an established heterologous system for the study of mammalian ciliary transport. When expressed alone, CNGA2-YFP was restricted to the cytoplasm, and failed to co-localize with acetylated tubulin (0/30 cells), which labels stabilized microtubules including the ciliary axoneme (Figure 2.1A, top). Coexpression of CNGA2-YFP with CNGA4 did not result in any detectable ciliary localization (0/20 cells) (Figure 2.1A, middle), but rather colocalization of the proteins in the cytoplasm (Figure 2.2). Surprisingly, co-expression of CNGA2-YFP with CNGB1b resulted in the targeting of channel protein to primary cilia where the YFP signal co-

localized with both acetylated tubulin (30/30 cells) (Figure 2.1A, bottom) and CNGB1b-3xFlag (Figure 2.2) in a punctate pattern along the entire length of the cilia (Figure 2.3). When expressed alone, both CNGA4 and CNGB1b were confined to the cytoplasm, consistent with reports that these subunits do not efficiently form tetramers capable of cell surface expression [147] (Figure 2.2).

Amino acid sequence comparison revealed a potential ciliary targeting motif (RVSP; amino acids 821 - 824) in the carboxy-terminus of CNGB1b (Figure 2.11A). The RVxP motif has been implicated in the ciliary localization of another membrane protein, polycystin-2 [88], and is absent from both the CNGA2 and CNGA4 subunits (Figure 2.11A). Mutation of positions R821, V822, and P824 to alanines (AASA mutant) resulted in the loss of ciliary targeting of CNGA2-YFP (Figure 2.11B, C), although this mutant CNGB1b subunit was still able to assemble with CNGA2 as determined by co-immunoprecipitation (Figure 2.5). In contrast, alanine substitution at position S823 had no effect on CNGA2 localization to cilia, suggesting a specific requirement for the RVxP motif (Figure 2.11D). Indeed, single alanine substitutions of positions R821, V822, or P824 led to a statistically significant decrease in ciliary targeting (Figure 2.6). These data are consistent with previous reports describing alanine substitutions of a putative flagellar targeting motif [148]. Notably, insertion of the RVSP motif 26 amino acids from the C-terminus of CNGA2 was not sufficient to confer targeting of CNGA2 to the primary cilia (Figure 2.11E). Together these data show that heteromeric assembly with CNGB1b is necessary, but not sufficient for targeting of olfactory CNG channels to cilia.

Having defined the subunit requirements for olfactory CNG channel targeting to cilia, we next sought to identify the motors responsible for transporting this cargo. Consistent with microtubule-based transport, destabilization of microtubule organization by demecolcine treatment resulted in a loss of cilia and accumulation of CNG channels at the basal body in MDCK cells (Figure 2.7). To test whether the main IFT anterograde motor kinesin-II plays a role in targeting of CNG channels, MDCK cells were transfected with a dominant-negative kinesin-II construct (KIF3aDN) that lacks the motor domain [149]. As predicted, expression of KIF3aDN resulted in a complete loss of cilia, consistent with its role in ciliary assembly and maintenance (Figure 2.7) [67, 150]. Another kinesin family member, KIFC3, has been implicated in transport of cargo to the minus-end of the microtubules at the apical surface of MDCK cells [151]. Interestingly, expression of a dominant-negative KIFC3 construct, did not affect targeting of CNG channels to the cilia (Figure 2.7). Together these results demonstrate that although the primary machinery for anterograde IFT previously characterized in invertebrates also participates in mammalian ciliary transport, the trafficking of CNG channels to cilia may occur through a novel mechanism.

A second kinesin-2 enzyme, the homodimeric OSM-3 kinesin, has been shown to transport IFT cargoes together with the heterotrimeric kinesin-2 (KLP20/KLP11/KAP-1) complex in *C. elegans* [25]. A role for the mammalian homolog of OSM-3, KIF17, in IFT has not been determined. Rather, KIF17 was proposed to have a brain-specific function in dendritic transport [146]. We show that KIF17 is endogenously expressed in MDCK cell cilia (Figure 2.8A) as well as in the ciliary layer of the olfactory epithelium

(Figure 2.8B), with a staining pattern indistinguishable from the ciliary-enriched type-III adenylyl cyclase (ACIII) [152] (Figure 2.9). Furthermore, KIF17 was coimmunoprecipitated with CNGA2 antibodies, demonstrating that endogenous CNG channels and KIF17 are part of a complex in native rat olfactory epithelium (Figure 2.8F, G). To test whether KIF17 plays a role in ciliary transport of CNG channels, MDCK cells were transfected with a dominant-negative KIF17 construct (KIF17DN). Expression of KIF17DN inhibited ciliary transport of CNG channels (CNGA2-YFP + CNGB1b) as no YFP fluorescence signal was detected in the cilia (Figure 2.8C) in any of the cells examined (0/11; Figure 2.8D). Mislocalization was specific for ciliary proteins as localization of apical and basolateral proteins were unaffected (Figure 2.10). In addition, expression of full-length KIF17 did not alter CNG channel targeting to cilia (data not shown). Interestingly, unlike KIF3aDN, expression of KIF17DN did not change the average length of primary cilia ($p=0.7564$ one-way ANOVA), indicating that these two motors may be functionally specialized in mammalian cilia (Figure 2.8E).

A major technical obstacle to the real-time study of protein movement in living cilia has been the successful expression of fluorescent-tagged proteins in vertebrate cilia. The ciliary targeting of the YFP-CNGA2 / CNGB1b complex provided a model to monitor movement of membrane proteins in MDCK cell primary cilia and permitted the first measurements of CNG channel mobility. We used fluorescence recovery after photobleaching (FRAP) to measure CNG channel dynamics in the ciliary compartment. For these experiments, CNGA2 channels were tagged with citrine, a photostable variant of YFP [153]. A 3-5 square micron region, in the middle of cilia lying horizontal in a

single confocal Z-plane was bleached (Figure 2.11A). Fluorescence within the bleached region was normalized to account for both prebleach intensity and photobleaching of the sample during recovery. Single exponential fit of the averaged data revealed that nearly 75% of the fluorescent signal recovers with a time constant of approximately 600 sec. (Figure 2.11B). The fact that 25% of the channel is immobile or of limited mobility would have been predicted based on its role as a transmembrane signaling protein [154]. Recovery of fluorescent channel signal in the cell body was nearly four times more rapid (Figure 2.12), illustrating the differences in ciliary and cellular trafficking. Fluorescence recovery in the cilia occurred from both sides of the bleached region (Figure 2.12). As a chemosensory signaling protein, the vast majority of ciliary CNG channel is likely localized within the plasma membrane. Technical limitations hinder the ability to resolve the combination of lateral diffusion within the plasma membrane and recovery due to IFT. The recovery timecourse in our experiments, therefore, most likely reflects membrane diffusion of a large population of channels that masks the minority of CNG protein undergoing IFT. This is supported by the fact that CNG channel recovery in cilia occurred slower than predicted for IFT (rates of 1-2 μm/sec). Of note, a similar time constant of recovery on the order of hundreds of seconds was recently reported for the lipid raft-associated Kv2.1 channel [155]. As CNGA2 targets to lipid raft microdomains [31], perhaps raft association confines the channel to a restricted diffusional microdomain.

DISCUSSION

Our studies demonstrate that heteromeric assembly with CNGB1b is needed for localization of olfactory CNG channels to cilia in MDCK cells. An RVxP motif conserved across species (including human) is necessary, but not sufficient, for ciliary targeting; however, its position within the CNGB1b sequence can vary. These results demonstrate a mechanistic role of CNGB1b subunits in proper ciliary targeting of olfactory CNG channels, and suggest a delegation of functional responsibilities among subunits.

Our results constitute the first demonstration of a role for KIF17 in mammalian ciliary transport. This kinesin-2 motor is not brain-specific [146], but rather is present in both MDCK cell cilia and OSNs. In vertebrate sensory cilia the Kif3a complex and KIF17 likely have partially redundant yet functionally distinct roles in IFT since the KIF3aDN resulted in a complete loss of cilia whereas the KIF17DN did not change average cilia length. This work provides strong support for the idea that OSM-3/KIF17 is an "accessory" IFT motor whose cilia-specific functions can cooperate with, yet functionally complement, the "canonical" Kif3a IFT motor [66, 69, 145]. Future experiments are required to determine whether KIF17 is important for the transport of other ciliary proteins or if this motor functions primarily on singlet microtubules at the distal segments. Interestingly, a recent report shows that a majority of olfactory CNG channels are localized to the distal segments of frog olfactory cilia [29]. The possibility remains that the Kif3a complex also contributes to ciliary targeting of CNG channels since expression of the KIF3aDN led to a complete loss of cilia. In addition, our work

also does not exclude the role of additional uncharacterized motors such as a mammalian homolog to the recently described KLP-6 in *C. elegans* [156].

EXPERIMENTAL PROCEDURES

Antibodies

Mouse anti-acetylated tubulin (used at 1:1000), polyclonal anti-Flag (1:1000), and mouse anti-FLAG M2 (1:1000) were obtained from Sigma-Aldrich (St. Louis, MO). Polyclonal rabbit anti-KIF17 was purchased from Abcam Inc. (Cambridge, MA). Polyclonal rabbit anti-adenylyl cyclase type III was from Santu Cruz Biotechnologies (Santa Cruz, CA). Mouse anti-NaK ATPase was obtained from Research Diagnostics Inc. (Concord, MA) and used at a 1:1000 dilution. Mouse anti-gp135 was used at a dilution of 1:1000. Mouse anti-CNGA2 (1:200) was a gift from Dr. U. Benjamin Kaupp. Goat-anti-mouse IgG labeled with Alexa 594, Alexa 647, or Bodipy FL, and Goat-anti-rabbit IgG labeled with Alexa 594 were obtained from Molecular Probes (Eugene, OR) and used at 1:1000.

Olfactory Epithelium Preparation

Briefly, Balb/C mice were decapitated at postnatal day 5, and the heads were sliced into 300μm coronal sections in ice-cold, slushy rat Ringer's solution (containing in mM: 140 NaCl, 5 KCl, 1 $MgCl_2$, 2 $CaCl_2$, 10 HEPES, and 10 glucose) using a Leica Microsystems VT 1000S Microtome (Bannockburn, IL). Sections were embedded in Tissue-Tek O.C.T. from Electron Microscopy Sciences (Hatfield, PA) and frozen on dry ice. Embedded sections were further sliced into 20μm sections on a Leica Microsystems CM1850

cryostat, and thaw mounted onto slides. Slides were air dried for 10 minutes, and fixed with 4% paraformaldehyde for 20 minutes at RT. Sections were permeabilized in PBS containing 0.1% Triton-X and 2% NGS for 2 hours. Tissue was incubated overnight at RT in a humidified chamber with primary polyclonal anti-KIF17 or anti-adenylyl cyclase type III antibodies diluted 1:1000 in PBS containing 2% NGS. Slides were rinsed 3 X 10' with PBS and incubated with 1:1000 Goat-anti-Rabbit IgG Alexa 594 for 2 hours at RT. After a final rinse (3 X 5 min in PBS), slides were dried for 5 min, and mounted using Prolong Gold.

For co-immunoprecipitation experiments 250g male Sprague-Dawley rats were deeply anesthetized using overdose of pentobarbital injected intraperitoneally and decapitated quickly. Skin was removed and head was bisected sagitally at the midline while immersed in ice cold rat Ringer's solution (containing in mM: 140 NaCl, 5 KCl, 1 $MgCl_2$, 2 $CaCl_2$, 10 HEPES, and 10 glucose). Exposed OE was dissected out, peeled from turbinates using forceps, and placed in Ringer's plus complete protease inhibitors (Roche Diagnostics, Indianapolis, IN) on ice. Tissue was then transferred to lysis buffer for coimmunoprecipitation.

Mutagenesis

The PCR primer pairs were used to synthesize a DNA fragment encoding the last 26 amino acids of CNGB1b (including RVSP) such that two BamH1 restriction site were introduced at both 5' and 3' ends. The DNA fragments were ligated into the BamHI sites immediately upstream of the RVSP motif and downstream of the stop codon of CNGB1b.

In addition the RVSP motif was mutated to AASA or RVAP. The primer sequences were as follows: Forward (AASA) 5'-CCG CCG GAG CCT TCA GTG AGG ATC GCT GCG AGT GCA GGC CCT GAT CCC GGG GAA CAG-3' , Reverse (AASA) 5-CTG TTC CCC GGG ATC AGG GCC TGC ACT CGC AGC GAT CCT CAC TGA AGG CTC CGG CGG-3', Forward (RVAP) 5'-GAT CCG TGT GGC TCC AGG CCC TGA TCC CGG GGA ACA GAC ACT ATC GGT GGA GAT GCT GGA AGA GAA GAA GGA GGA GGT GGA GTA GAG-3' and Reverse (RVAP) 5'-GAT CCT CTA CTC CAC CTC CTC CTT CTT CTC TTC CAG CAT CTC CAC CGA TAG TGT CTG TTC CCC GGG ATC AGG GCC TGG AGC CAC ACG-3'. Wild-type CNGB1b-3xFlag was digested with BamHI and then ligated using the BamHI-digested PCR fragments from above. For the generation of CNGA2-RVSP the primer pair was designed to insert the RVSP motif between position 649 and 652 of CNGA2-Citrine. The Quick Change Site-Directed Mutagenesis kit from Stratagene (La Jolla, CA) was used to generate the mutation using the primers indicated below. RVSP insert primer forward 5'-CAC AGT GCT AGA GAC CAA GAT GCG TGT GAG TCC AAA ACA GAA CCA TGA GGA TG-3'; RVSP insert primer reverse 5'-CAT CCT CAT GGT TCT GTT TTG GAC TCA CAC GCA TCT TGG TCT CTA GCA CTG TG-3'; AVSP insert primer forward 5'-GAT CGC TGT GAG TCC AGG CCC TGA TCC CGG GGA ACA GAC ACT ATC ATC GGT GGA GAT GCT GGA AGA GAA GAA GGA GGA GGT GGA GTA GCG-3'; AVSP insert primer reverse 5'-GAT CCT CTA CTC CAC CTC CTC CTT CTT CTC TTC CAG CAT CTC CAC CGA TAG TGT CTG TTC CCC GGG ATC AGG GCC TGG ACT CAC AGC-3'; RASP insert primer forward 5'-GAT CCG TGC GAG TCC

AGG CCC TGA TCC CGG GGA ACA GAC ACT ATC ATC GGT GGA GAT GCT GGA AGA GAA GAA GGA GGA GGT GGA GTA GCG-3'; RASP insert primer reverse 5'-GAT CCT CTA CTC CAC CTC CTC CTT CTT CTC TTC CAG CAT CTC CAC CGA TAG TGT CTG TTC CCC GGG ATC AGG GCC TGG ACT CGC ACG-3'; RVSA insert primer forward 5'-GAT CCG TGT GAG TGC AGG CCC TGA TCC CGG GGA ACA GAC ACT ATC ATC GGT GGA GAT GCT GGA AGA GAA GAA GGA GGA GGT GGA GTA GCG-3'; RVSA insert primer reverse 5'-GAT CCT CTA CTC CAC CTC CTC CTT CTT CTC TTC CAG CAT CTC CAC CGA TAG TGT CTG TTC CCC GGG ATC AGG GCC TGC ACT CAC ACG-3'

Immunoprecipitation

HEK-293 cells were washed twice with potassium-free PBS, scraped, and collected by centrifugation at 1,000 x g for 4 min. The pellet was resuspended in solubilization buffer (150mM NaCl, 50mM Tris, pH 7.4, 5mM EDTA, 1% TritonX-100, 0.02% NaN3, 250mM of NEM, and protease inhibitors; 1 ml per 60 mm dish) for 10 min at RT. After solubilization, the cells were spun at 4 °C at 10,000 x g for 20 min. The supernatant was collected and pre-cleared by treatment with 75 μl of protein-A Sepharose beads for 1 h with gentle mixing. The beads were then removed by centrifugation at 10,000 x g for 1 min at 4 °C, and the sample was incubated for 3 hours with either anti-GFP or anti-FLAG antibodies (1:500 dilution) and 100 μl of protein A-sepharose beads at 4 °C with gently mixing. The beads were removed by centrifugation at 10,000 x g for 1 min at 4 °C, and washed twice with solubilization buffer for 5 minutes. An equal volume of 2X SDS gel loading buffer was added to elute proteins, and the sample was heated at 100 °C for 2

minutes. The beads were removed by centrifugation at maximum speed for 1 minute. Immunoprecipitation samples (~60 µl) were loaded on a 4-12% Bis-Tris acrylamide gel (Invitrogen). After electrophoretic transfer to nitrocellulose, the membrane was incubated with either anti-FLAG or anti-GFP (1:2000, 1:5000 dilutions, respectively). Bound primary polyclonal antibody was detected with a 1:5000 dilution of horseradish peroxidase-conjugated goat anti-rabbit IgG (Zymed, San Francisco, CA), and visualized using the Renaissance Western blot chemiluminescence reagent according to the manufacturer's protocol (PerkinElmer Life Sciences, Wellesley, MA). Images were captured using the EpiChemi3 Darkroom (UVP Inc., Upland, CA).

Olfactory epithelium was prepared as described in Olfactory Epithelium Preparation, and homogenized in lysis buffer (10 mM Tris/Cl pH 7.5, 150 mM NaCl, 1 mM EDTA, 1% Nonidet-P40). Following homogenization, lysates were solubilized for 1 hr on ice and then centrifuged at 2000 x g for 5 min to remove insoluble material. Lysates were then incubated with 2 µg of either non-immune mouse serum (Sigma) or an anti-CNGA2 antibody conjugated to protein-G agarose beads (Sigma) on a rocker overnight at 4 C. Beads were washed three times with wash buffer (10 mM Tris/Cl pH 7.5, 150 mM NaCl, 1 mM EDTA, 0.1% Nonidet P-40) and resuspended in SDS sample buffer. Samples were run on a NuPAGE 4-12% Bis-Tris gel (Invitrogen) and transferred onto nitrocellulose membranes (Whatman). Immunoblots were then probed with a polyclonal anti-Kif17 primary antibody (1:1000; Abcam), followed by an anti-rabbit HRP-conjugated secondary antibody (1:5000; Zymed). Signal was detected using Western Lightning

chemiluminescence detection reagent (PerkinElmer Life Sciences, Inc., Boston, MA). Blots were stripped and reprobed with an anti-CNGA2 primary antibody (1:200). All blots were exposed for 15 min using a UVP BioImaging System (UVP, Inc., Upland, CA).

Cell culture, transfection, and immunocytochemistry

MDCKII cells were grown in DMEM containing 10% Fetal Bovine Serum and 1% Pen/Strep/Glutamine. Cells were kept at 37ºC in a humidified 5% CO_2 environment, and passaged weekly at 1:40. For experiments, cells were trypsinized and plated at high density in low Ca^{2+} media (S-MEM) containing 5% dialyzed FBS and 1% pen/strep on 6.5 mm diameter Transwell filter supports (0.4 μm pore size; Corning Costar, Acton, MA). After 4 hours, cells were fed with normal DMEM growth medium. Cells were fed every second day and allowed to grow for 5-7 days post-confluence before transfection.

For introduction of DNA, cells were rinsed three times with serum-free Opti-MEM and transfected using Lipofectamine and PLUS reagent. Briefly, 0.5 μg of each DNA was added to 150 μl of Opti-MEM. Six μl of PLUS reagent was added, mixed, and incubated for 15 minutes. In a separate tube, 6 μl of Lipofectamine reagent was added to 150 μl of Opti-MEM. After 15 minute incubation, the PLUS and the Lipofectamine mixtures were combined and allowed to incubate for an additional 15 minutes. This transfection cocktail was diluted with 1 ml of Opti-MEM and added to Transwells. Transfection was allowed

to proceed for 5 hours; then media was aspirated and replaced with normal growth media. Cells were allowed to incubate for 48 hours post-transfection.

For immunocytochemistry, Transwells were rinsed with PBS and fixed for 7 minutes in 4% paraformaldehyde. After 3x10 minute rinses in PBS, cells were incubated for 10 minutes in PBS containing 0.1% Triton-X100 and 2% normal goat serum (NGS). Cells were then incubated for 1 hour at RT in PBS containing 2% NGS and the appropriate dilutions of primary antibodies. Cells were then rinsed 3x10 minutes in PBS, reblocked for 10 minutes in PBS containing 2% NGS, and incubated for 1 hour in the dark with secondary antibodies diluted in PBS containing 2% NGS. After a final 3x 10 minute rinse in PBS, cells were mounted on slides using Prolong Gold AntiFade Reagent (Molecular Probes, Eugene, OR).

Confocal Imaging

Images of transfected cells displaying fluorescent signals were acquired on an Olympus Fluoview 500 confocal microscope using a 100×1.35 N.A. oil objective. Exposure times were adjusted so that the maximal pixel intensities were at least half saturation. Images were obtained by taking a series of stacks every 0.5 μm through the cell (generally 3-5 μm) and combining the images into a composite stack. To minimize effects of overexpression on CNGA2-YFP localization, only cells with low to mid levels of expressed protein were analyzed. Whereas the entire confocal stack containing sections through the whole cell were used to generate images for display, fluorescence intensity analysis and colocalization were measured in images generated only from focal planes

containing cilia. Contrast and brightness of composite images were further optimized using Adobe Photoshop CS version 8.0 (Adobe Systems Inc., San Jose, CA) on an Optiplex GX280 PC (Dell Inc., Round Rock, TX). Images were analyzed using ImageJ software (NIH, Bethesda, MA), and statistics were performed using Prism software from Graphpad Prism Software (San Diego, CA).

Quantification of Ciliary Targeting

Confocal stacks were analyzed using ImageJ software (NIH, Bethesda, MA). Signal from acetylated tubulin was used to mark cilia, and those confocal planes containing acetylated tubulin signal were collapsed into a 2-dimensional projection creating the ciliary 2-dimensional projection. In addition, the planes not containing tubulin signal were collapsed to create the non-ciliary 2-dimensional projection. A region of interest (ROI) was drawn around the cilium in the ciliary 2-dimensional projection of acetylated tubulin signal and then the same ROI was placed on the collapsed ciliary projection from the CNGA2-Citrine signal. Fluorescence was measured as arbitrary units per square micron. A ROI was drawn around the cell from the collapsed non-ciliary projection and CNG channel signal was quantified. In order to monitor ciliary enrichment of the CNG channel, the signal from the cilium was normalized to the signal from the cytoplasm and expressed as the ratio of ciliary pixel density to non-ciliary pixel density. Ratios were compared using the Student's two-tailed t test on Graphpad Prism Software (San Diego, CA).

Fluorescence Recovery After Photobleaching (FRAP)

Forty-eight hours after transfection, Transwell filters carrying cells were excised and inverted onto #1 round glass coverslips, covered with PBS, and inserted into a live-cell imaging Quick Change chamber with a heated base from Warner Instruments (Hamden, CT). 10 prebleach images were acquired at a resolution of 512x512 pixels at 3% laser intensity before bleaching a region of approximately 3-5 square microns at 100% laser intensity for 15 seconds. Recovery was measured by obtaining 512x512 images at 3% laser intensity every 5 seconds for indicated times. A single focal plane of 0.5-1 micron Z-resolution was imaged using a large confocal aperture to minimize effect of drift. Recovery of bleached region was background subtracted and normalized to both the initial region intensity relative to whole cell intensity and for photobleaching of sample during recovery. Total photobleaching of sample was generally less than 15% over entire period of recovery. Recovery kinetics were determined using a single exponential fit of the average data: $y = A(1e^{(-\tau * t)}) + c$, where A is amplitude, t is time, τ is the time constant, and c is the constant representing the relative fluorescence immediately post-bleach.

Kinesin Constructs

Dominant-negative kinesin motors were generated such that they contained the cargo-binding domain and a portion of the alpha-helical coiled-coil domain, however they lacked the remaining coiled domain and the kinesin motor domain. For KIF3aDN the construct encoded amino acids 525-702, the KIFC3DN construct was generated using amino acids 1-375, and the KIF17DN construct consisted of amino acids 801-1028.

Citrine-tagged KIF17 construct was created by subcloning full length Kif17 into the BglII and XbaI sites of pmCit-C1 by PCR using primers with appropriate restriction enzyme sites

ACKNOWLEDGEMENTS

We would like to thank Dr. U. Benjamin Kaupp at the Institut für Biologische Informationsverarbeitung, Jülich, Germany for generously providing the antibody to CNGA2. This publication was supported by grant number GM07767 from NIGMS (PMJ), grant numbers EY12837 (RLB) and DK069605 (BM) from NIH, and grant number 92a2f from the Polycystic Kidney Disease Foundation (TWH).

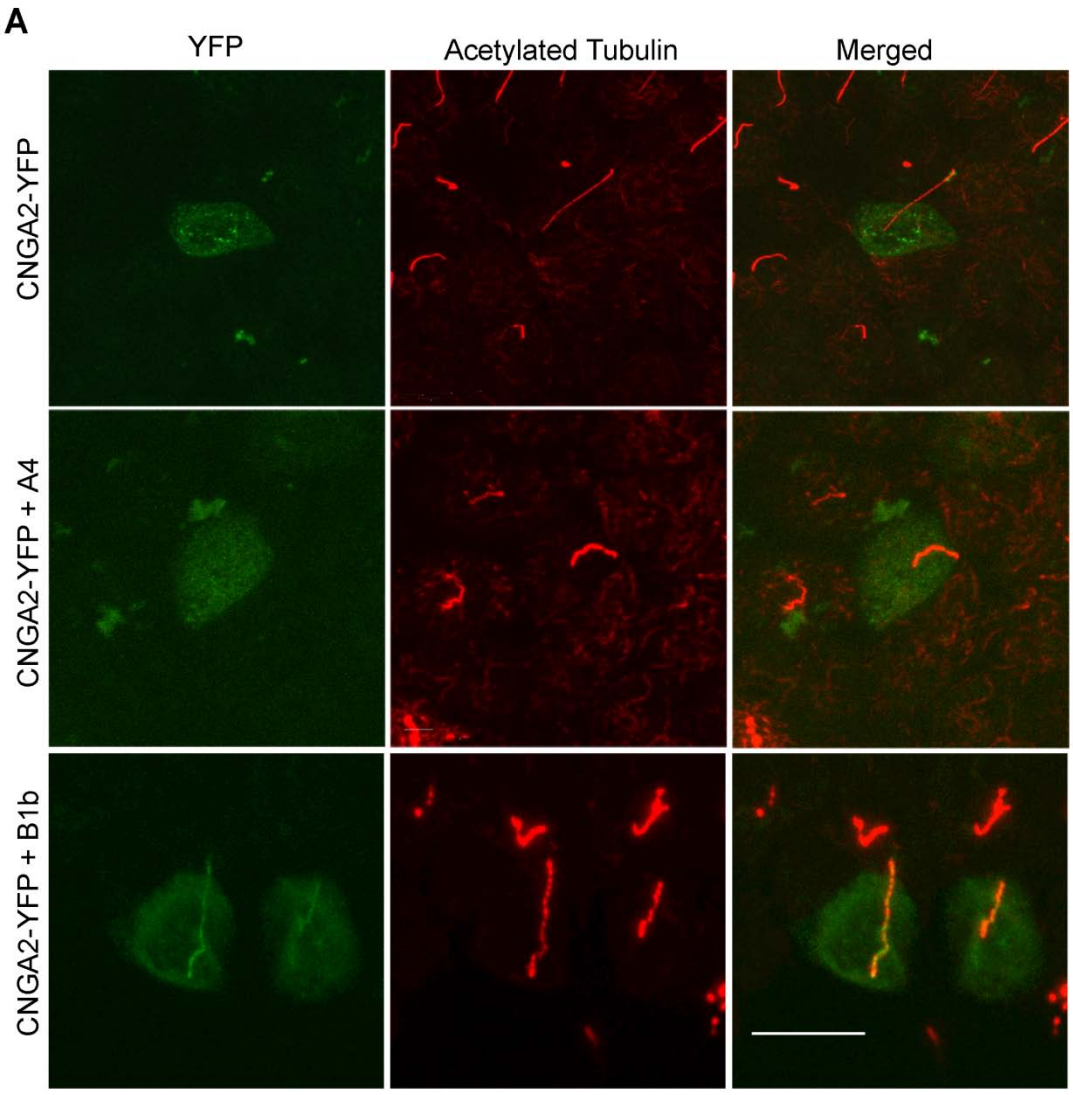

Figure 2.1 Ciliary Enrichment of CNGA2 Requires CNGB1b, but Not CNGA4.

(A) Representative images of MDCK cells transfected with CNGA2-YFP alone (top), CNGA2-YFP + CNGA4-3xFlag (middle), or CNGA2-YFP + CNGB1b-3xFlag (bottom). YFP fluorescence is shown at left (green) and immunostaining for acetylated tubulin is shown at center (red). Merged (right) signals from YFP and acetylated tubulin; yellow indicates colocalization. Bar represents 10 μm.

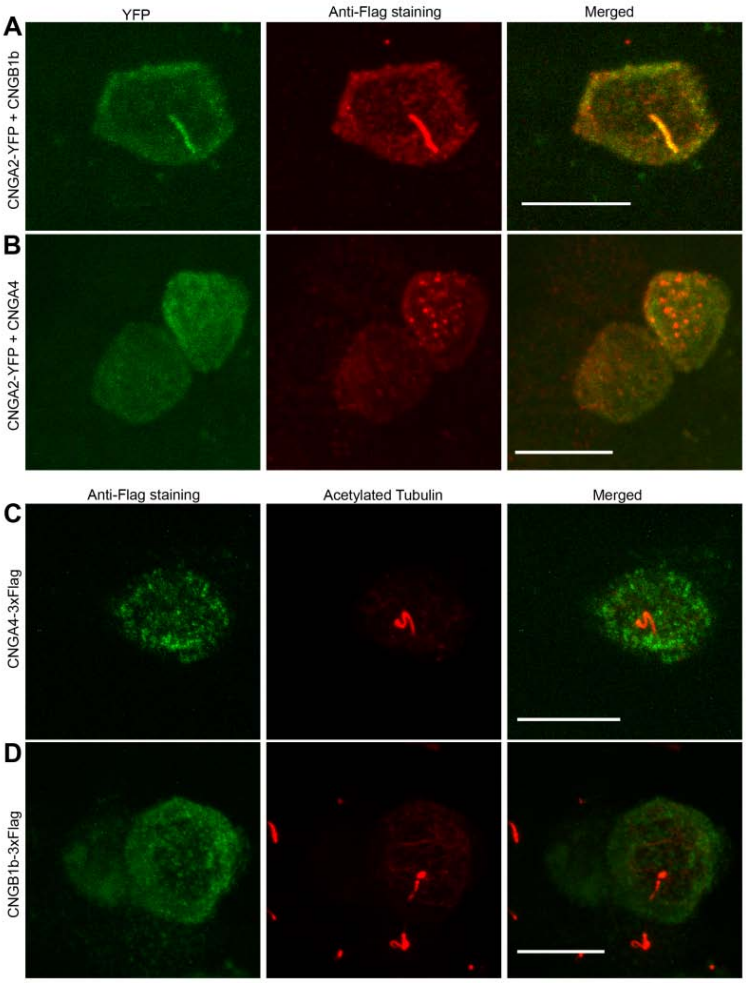

Figure 2.2 CNGB1b Colocalizes with CNGA2 in MDCK Cell Primary Cilia.

Representative images of MDCK cells grown on Transwell filters for 7-8 days post-confluence and transfected with **(A)** CNGA2-YFP + CNGB1b-3xFlag or **(B)** CNGA2-YFP + CNGA4-3xFlag. Cells were fixed, permeabilized, and immunostained 48 hours post-transfection with anti-acetylated tubulin antibodies (red). Merge of YFP and acetylated tubulin (Alexa 594) signal, shown in yellow, indicates colocalization. **(C, D)** Representative images of MDCK cells transfected with either **(C)** CNGA4-3xFlag and soluble CFP or **(D)** CNGB1b-3xFlag and soluble CFP. Cells were fixed, permeabilized, and immunostained 48 hours post-transfection with mouse anti-acetylated tubulin antibodies (red, center) and rabbit anti-Flag antibodies (green, left). Merge of acetylated tubulin (Alexa 594) and flag (Bodipy FL) signal shown on right. Bar represents 10 µm.

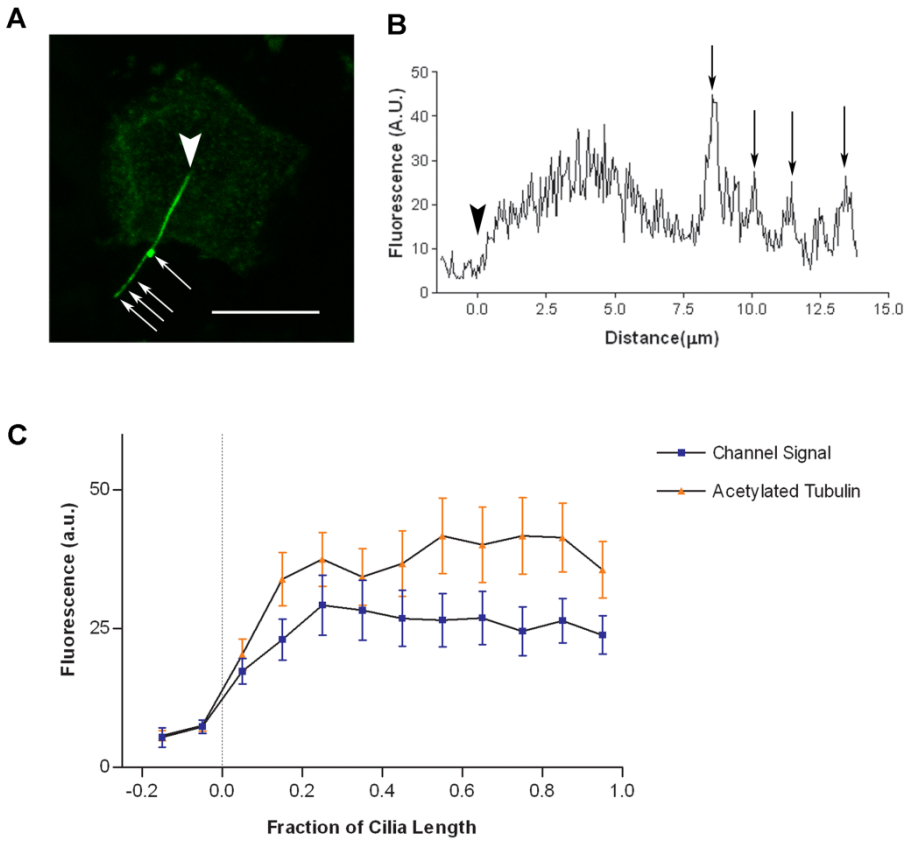

Figure 2.3 The CNG Channel is Evenly Distributed Along the Length of the Cilia.

(A) Representative image of MDCK cell transfected with CNGA2-Citrine (Green) and CNGB1b-3xFlag. Arrowhead marks base of cilium and arrows mark fluorescent puncta. Scale bar represents 10µm. **(B)** Fluorescence intensity plot of image from panel B. Arrowhead and arrows correspond to exact positions marked panel B. **(C)** Plot of normalized fractional cilia length versus average fluorescence intensity in arbitrary units (a.u.) for both channel signal (blue) and acetylated tubulin (orange) in cells expressing CNGA2-Citrine and CNGB1b-3xFlag. (n=10). Dotted line marks the beginning of cilia as determined by intensity of acetylated tubulin signal.

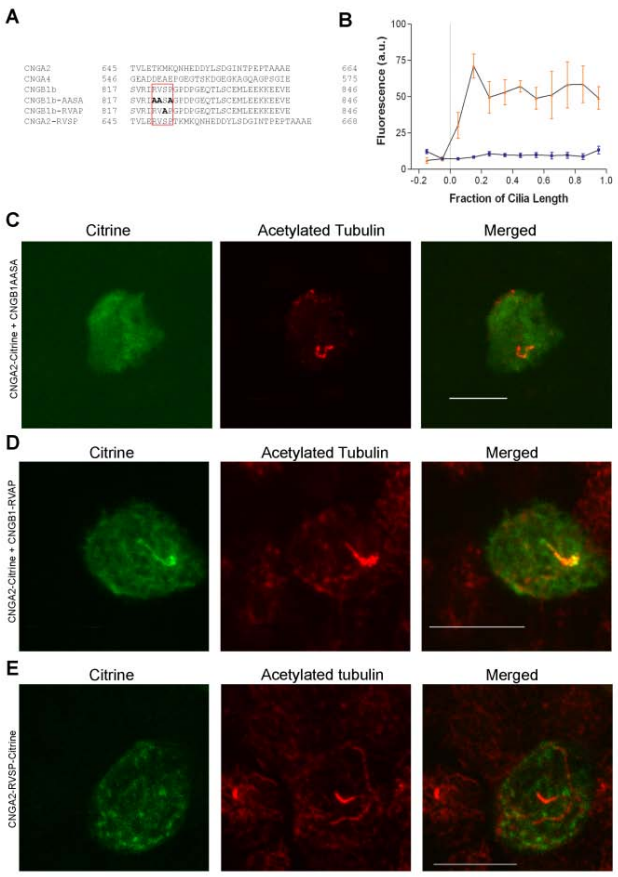

Figure 2.4 A Carboxyl-Terminal Motif in CNGB1b is Necessary, but Not Sufficient for Ciliary Trafficking of CNG Channels.

(A) Sequence alignment of final 30 carboxyl-terminal amino acids of wild-type CNGA2, CNGA4, CNGB1b, and mutant constructs. Alignment of the RVxP motif in CNG channel constructs is outlined in the red box. Amino acid substitutions and insertions are shown in bold. **(B)** Plot of normalized fractional cilia length versus average fluorescence intensity in arbitrary units (a.u.) for both channel signal (blue) and acetylated tubulin (orange) in cells expressing CNGA2-Citrine and CNGB1b-AASA-3xFlag (n=3). Dotted line marks the beginning of cilia as determined by concentrated acetylated tubulin signal. Values are mean ± SEM. **(C)** Representative image of MDCK cell transfected with CNGA2-Citrine (green, left), + CNGB1b-AASA-3xFlag mutant and immunostained with anti-acetylated tubulin (red, center) shown with merged image (right). Bar represents 10μm. **(D)** Representative image of MDCK cell transfected with CNGA2-RVSP-Citrine. Acetylated tubulin shown in (red). Scale bar represents 10μm. **(E)** Representative image of MDCK cell, transfected with CNGA2- Citrine (green) and CNGB1b-RVAP-3xFlag. Acetylated tubulin shown in (red). Merged image shown on right with yellow indicating colocalization. Scale bar represents 10μm.

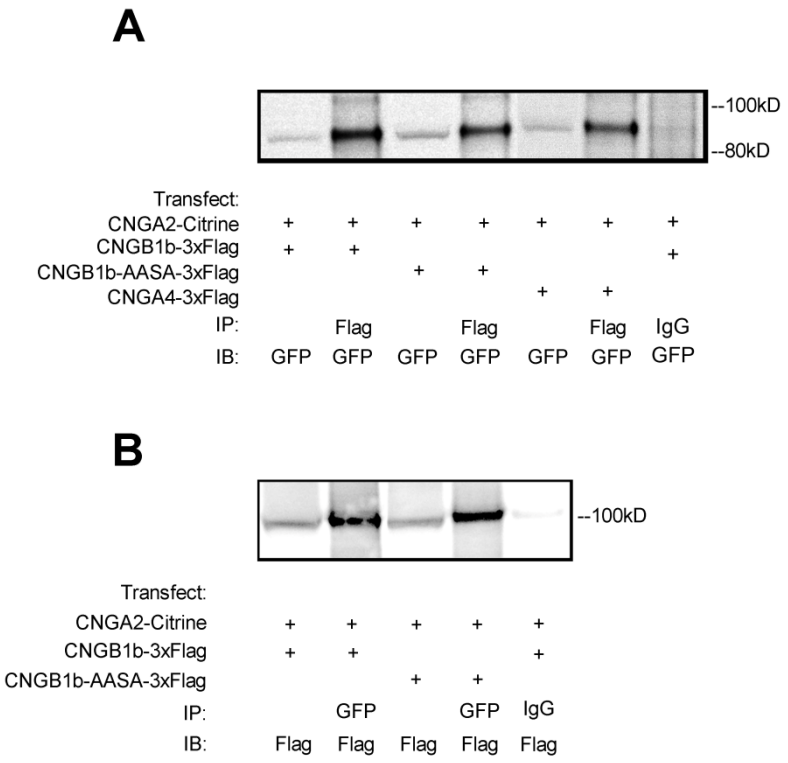

Figure 2.5 Mutant CNGB1b, as well as Wild-type CNGB1b and CNGA4 Co-assemble with CNGA2

MDCKII cells were transfected with CNGA2-Citrine and either CNGB1b-3xFlag, CNGB1b-AASA-3xFlag mutant, or CNGA4-3xFlag as indicated in *Materials and Methods*. **(A)** Immunoprecipitation with rabbit polyclonal anti-Flag antibody and immunoblotting with rabbit polyclonal anti-GFP. 5% detergent extract of transfected cells for each sample was used as starting material (lanes 1, 3, and 5) while the remaining 95% was split and immunoprecipitated with either rabbit anti-Flag (lanes 2, 4, and 6) or rabbit IgG (lane 7). **(B)** Immunoprecipitation with rabbit polyclonal anti-GFP antibody and immunoblotting with rabbit polyclonal anti-Flag. 10% of each sample was used as starting material (lanes 1 and 3) while the remaining 90% was immunoprecipitated with either rabbit anti-GFP (lanes 2 and 4) or rabbit IgG (lane 5). Apparent molecular weight markers are shown on the right.

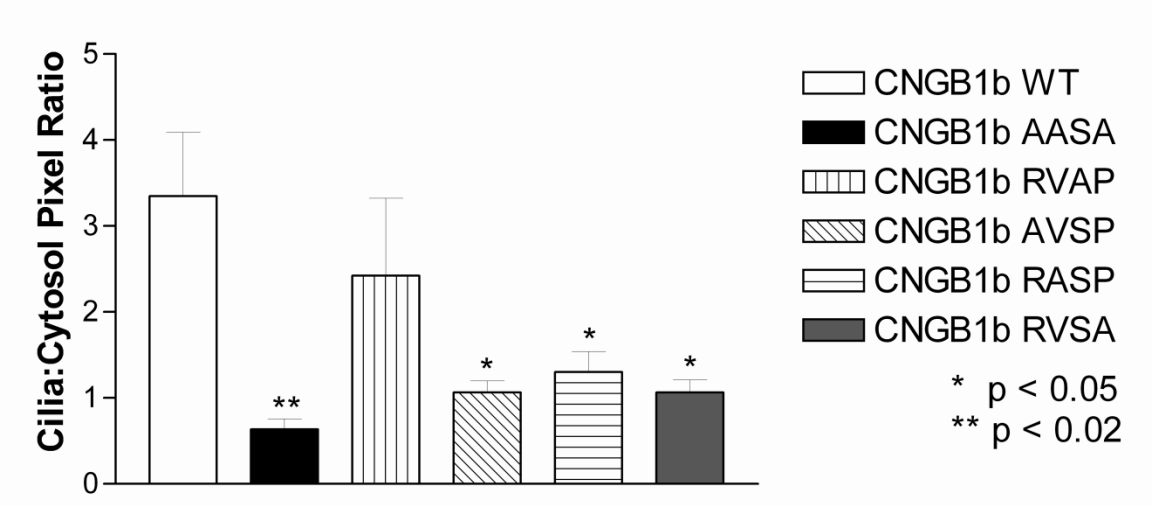

Figure 2.6 Effects of Single Alanine Mutations in the RVxP Motif of CNGB1b.

(A) Quantification of relative mean pixel intensities of the cilia versus the cytoplasm of MDCK cells transiently transfected with CNGA2-Citrine and CNGB1b mutants. Signal from acetylated tubulin was used to generate a ciliary region of interest (ROI) representing the cilium. Pixels were then quantified in the ciliary ROI using ImageJ software. In addition, a ROI was drawn representing the non-ciliary portion of the cell and also quantified. Results are expressed as the ratio of mean fluorescence intensity in the cilia versus cytoplasm. Mutation of R821, V822, and P824 to alanine in the CNGB1b-AASA mutant led to a loss of ciliary enrichment of the CNG channel. Alanine substitution of S823, however, had no significant effect on CNG channel ciliary targeting. Additionally each of the single substitutions of R821, V822, and P824 led to a statistically significant decrease in ciliary trafficking of the channel, however no single point mutation had as dramatic effect as seen in the CNGB1b-AASA mutant. Statistics were performed using the Student's two-tailed t test (n=5-8 for each group).

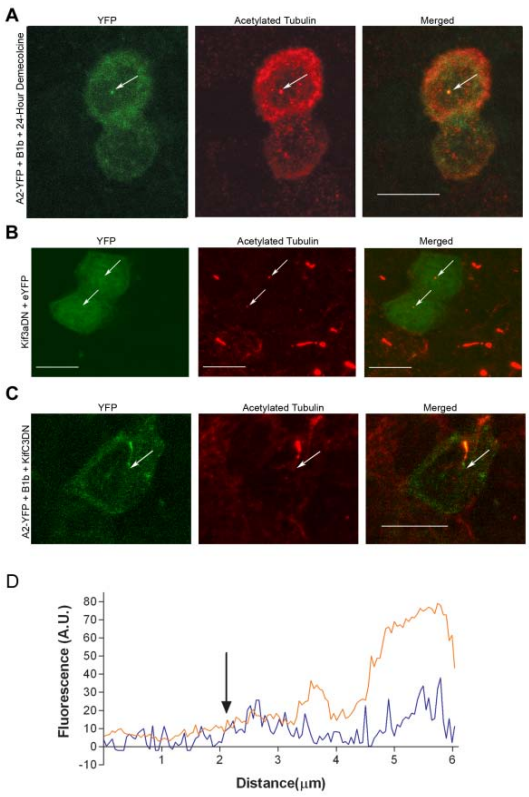

Figure 2.7 Effects of Demecolcine and Expression of Dominant-negative KIF Constructs on CNGA2 Localization.

(A) Demecolcine treatment removes the primary cilium from MDCK cells and channel accumulates at the basal body. Representative images of MDCK cells grown on Transwell filters for 7-8 days post-confluence and transfected with CNGA2-YFP + CNGB1b-3xFlag. Demecolcine (1 μg ml^{-1}) was added to cells 24 hours after transfection. Cells were fixed, permeabilized, and immunostained 48 hours post-transfection with anti-acetylated tubulin antibodies (red). Merge of YFP and acetylated Tubulin (Alexa 647) signal, shown in yellow, indicates colocalization. Bar represents 10 μm. **(B)** Expression of KIFC3 (1-375) dominant-negative does not affect localization of CNGA2+CNGB1b to the primary cilia of MDCK cells. Representative image of MDCK cell, transfected with CNGA2-Citrine, CNGB1b-3xFlag, and KIFC3-DN. Arrows mark base of cilia. Signal shown from CNGA2-citrine fluorescence (green), acetylated tubulin immunostaining (red), and merged image. Bar represents 10μm. **(C)** Fluorescence intensity plot of image from panel A. Arrow corresponds to exact position marked in panel A. Orange represents signal from acetylated tubulin staining and blue represents CNGA2-citrine fluorescence. **(D)** Expression of KIF3a (525-702) dominant-negative abolishes primary cilia of MDCK cells. Representative image of MDCK cell, transfected with CNGA2-Citrine, CNGB1b-3xFlag, and KIF3aDN. Arrows mark basal body. Signal shown from CNGA2-citrine fluorescence (green), acetylated tubulin immunostaining (red), and merge. Bar represents 10μm.

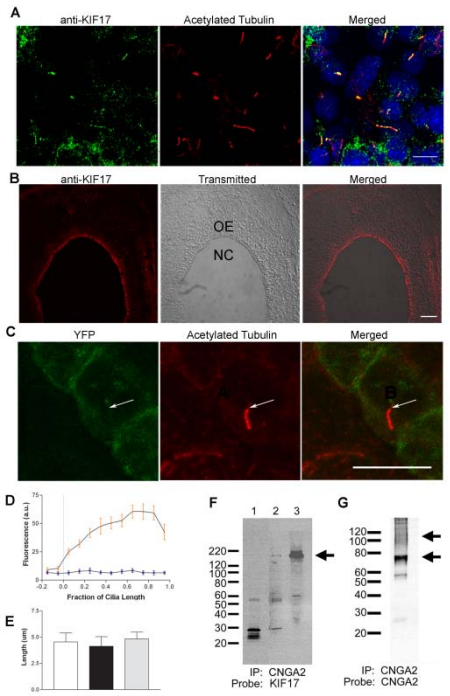

Figure 2.8 KIF17 is Endogenously Expressed in both MDCK Cells and OSNs and Mediates Ciliary Enrichment of the CNG Channel.

(A) MDCK cells stained with anti-KIF17 (green) and anti-acetylated tubulin (red). Merged images shown with DAPI (blue). Bar represents 10µm. **(B)** Mouse OE stained with rabbit polyclonal anti-KIF17 antibodies (red). Olfactory epithelium (OE), nasal cavity (NC). Bar represents 50 µm. **(C)** Representative image of MDCK cell, transfected with CNGA2-Citrine, CNGB1b-3xFlag, and myc-KIF17DN (801-1028). Arrowhead marks base of cilium. Signal shown from CNGA2-citrine fluorescence (left, green), acetylated tubulin immunostaining (center, red), and merge (right). Bar represents 10µm. **(D)** Plot of normalized fractional cilia length versus average fluorescence intensity in arbitrary units (a.u.) for both channel signal (blue) and acetylated tubulin (orange) from MDCK cells expressing CNGA2-Citrine, CNGB1b-3xFlag, and myc-KIF17DN (n=11). Dotted line marks the beginning of cilia as determined by concentrated acetylated tubulin signal. Values are mean ± SEM. (**E**) Average length of analyzed cilia from MDCK cells transfected with CNGA2-Citrine, B1b-3xFlag, and either no KIF17 (white, n=14), KIF17DN (black, n=10), or KIF17 full length (gray, n=5) constructs. KIF17DN had no statistically significant effect on cilia length (p=0.7551). Values are mean ± SEM. **(F)** KIF17 immunoprecipitates with CNGA2 in native rat olfactory epithelium. Lane 1 represents immunoprecipitation with nonspecific IgG as a negative control. Lane 2 shows immunoprecipitation with anti-CNGA2 antibodies (1:200), while Lane 3 is the starting material from rat olfactory epithelium. Blots were probed with anti-KIF17 (1:1000). Arrow indicates band for Kif17 with an approximate molecular weight of 170 kD. **(G)** Blot was stripped and reprobed with anti-CNGA2 antibodies (1:200). Arrows indicate bands for CNGA2 non-glycosylated (75 kD) and glycosylated form (90-150 kD).

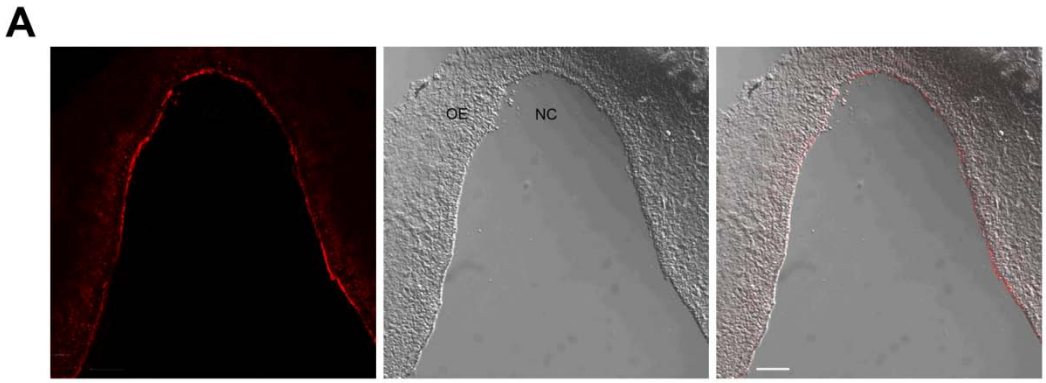

Figure 2.9 AC III is Enriched in the Ciliary Layer of the Olfactory Epithelium.

(A) 20 µm coronal section of p5 Balb/C mouse olfactory epithelium stained with rabbit polyclonal anti-adenylyl cyclase III antibody and goat-anti-mouse Alexa 594 (red). Olfactory epithelium (OE), nasal cavity (NC). Bar represents 50 µm.

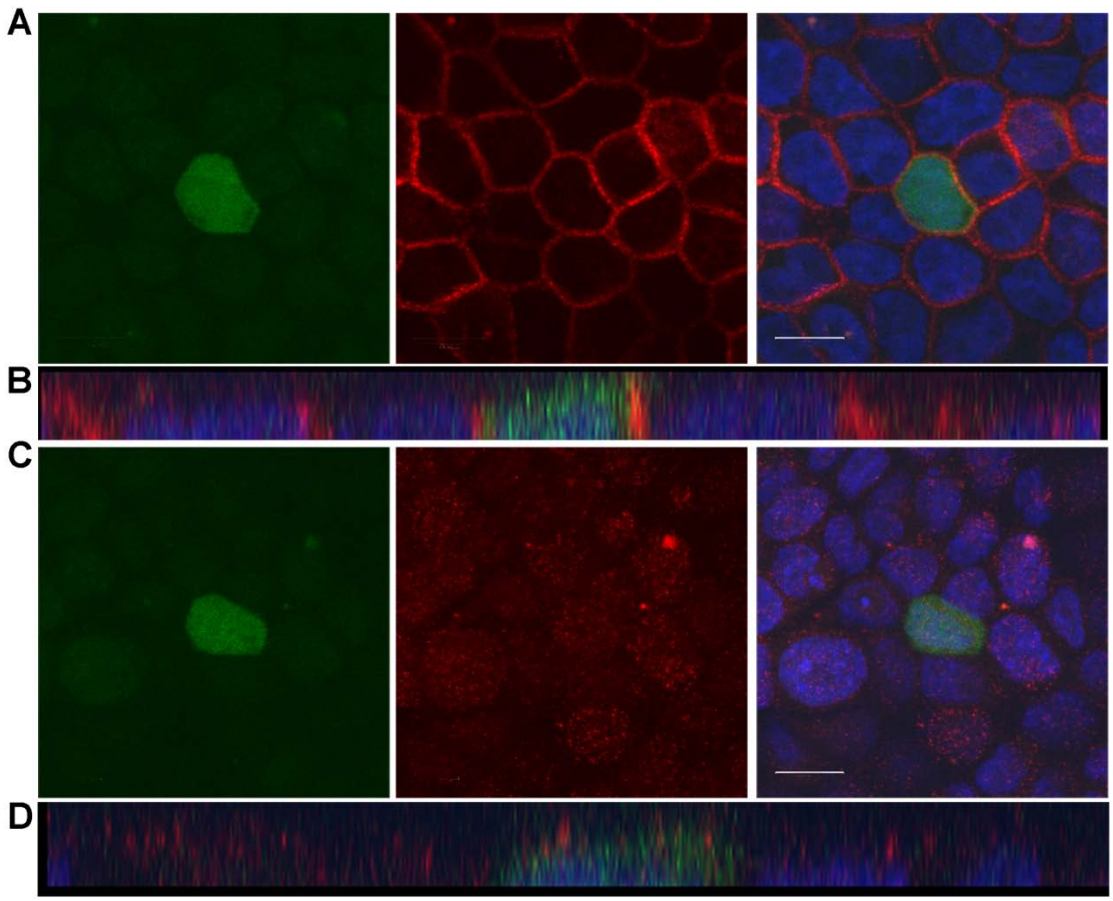

Figure 2.10 Expression of KIF17DN (801-1028) Does Not Affect Cell Polarity.

Representative images of MDCKII cells transfected with KIF17DN (801-1028) and soluble eYFP. **(A)** Signal shown from eYFP fluorescence as a marker of transfection (green), NaK ATPase immunostaining (red) marking the basolateral membrane, along with merged image containing nuclear staining with DAPI (blue). **(B)** X-Z view of cells in panel A **(C)** Signal shown from eYFP fluorescence as a marker of transfection (green), gp135 immunostaining (red) marking the apical membrane, along with merged image containing nuclear staining with DAPI (blue). **(D)** X-Z view of cells in panel C. Bar represents 10 μm for panels A, C.

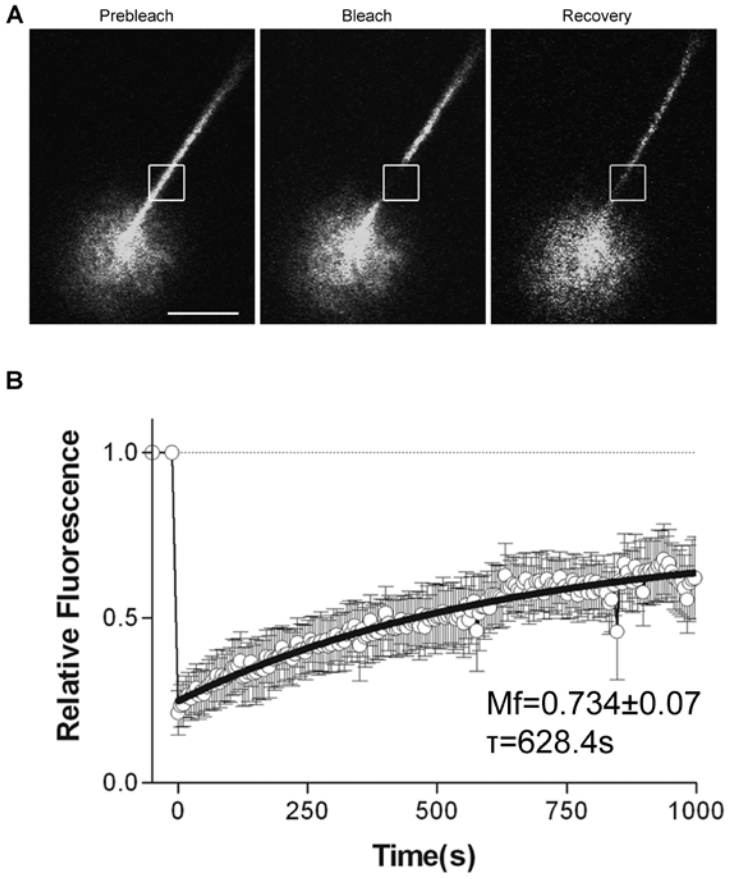

Figure 2.11 A Significant Fraction of CNG Channels is Mobile in the Primary Cilia of Madin-Darby Canine Kidney Cells.

(A) Selected images from a confocal FRAP experiment at 25ºC in living MDCK cells transfected with CNGA2-Citrine and CNGB1b-3xFlag showing fluorescence signal from CNGA2-citrine in cilia prebleach, immediately post-bleach (t = 0 s), and after recovery (t = 600 s). Box represents area of photobleach (dimensions of box). Bar represents 5µm. **(B)** Average recovery after photobleach for CNGA2-Citrine signal from the cilia of MDCK cells. Data shown are mean ± SE, *n* = 5 cells). The solid line through the data is a single-exponential fit to the average data. Fit parameters: mobile fraction = 0.734±0.07, τ = 628.4 s, and R^2=0.952. Values are mean ± SEM.

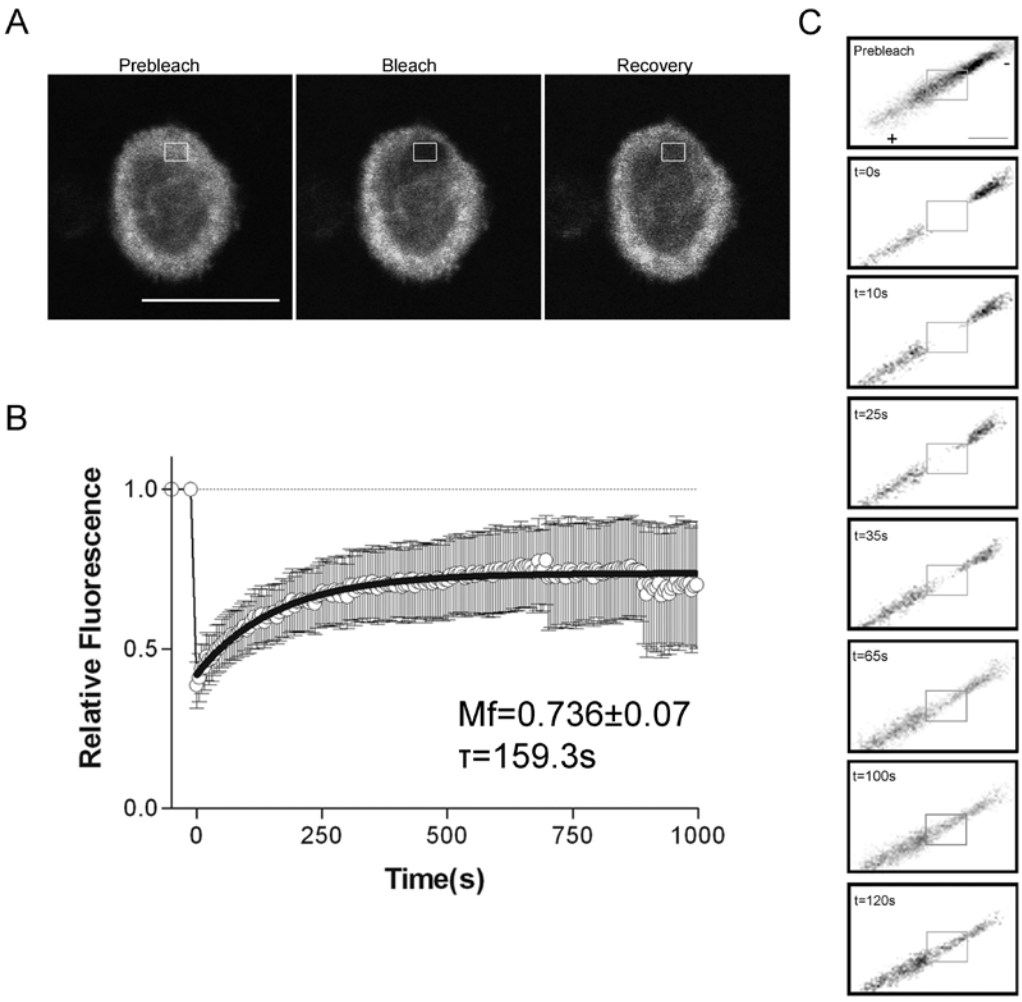

Figure 2.12 Recovery of CNGA2-Citrine after Photobleaching in MDCK Cells.

(A) Average recovery for CNGA2-Citrine signal from the cytoplasm of MDCK cells at 25ºC (*n*=5 cells). Fit parameters: mobile fraction = 0.736±0.07, τ = 159.3 s R^2=0.942 **(B)** Selected images from a confocal FRAP experiment at 25ºC in live MDCK cells transfected with CNGA2-Citrine and CNGB1b-3xFlag showing fluorescence signal from CNGA2-citrine in the cytoplasm prebleach, immediately post-bleach (t = 0 s), and recovery (t = 200 s). Box represents area of photobleach (dimensions of box). Bar represents 10µm. **(C)** Selected images at indicated times showing dynamics of fluorescence recovery in cilia from live MDCK cells at 29ºC expressing CNGA2-Citrine and CNGB1b-3xFlag. Images were background subtracted and color inverted to improve visibility. Box represents area of photobleach. Bar represents 2µm, "+" represents plus end of microtubules (distal tip of cilium), and "–" represents minus end of microtubules (towards cytoplasm).

CHAPTER 3

PACS-1 MEDIATES PHOSPHORYLATION-DEPENDENT CILIARY TRAFFICKING OF THE CNG CHANNEL IN OLFACTORY SENSORY NEURONS

SUMMARY

Impaired ciliary protein transport in olfactory sensory neurons (OSNs) leads to anosmia, and is a newly recognized clinical manifestation of a class of human disorders called ciliopathies. Surprisingly little is known regarding the mechanisms controlling trafficking to this unique neuronal compartment. Here, we show a novel role for phosphofurin acidic cluster sorting protein 1 (PACS-1) in the ciliary trafficking of the olfactory CNG channel. PACS-1 is an intracellular sorting protein that mediates its effects through the binding of acidic clusters on cargo protein. This interaction is dependent on CK2 phosphorylation of both PACS-1 and its cargo. We show that CNGB1b contains two putative PACS-1 binding sites, which are phosphorylated by CK2. Additionally, we show that PACS-1 is expressed in OSNs and interacts in complex with the CNG channel. Inhibition of CK2 in native OSNs causes a loss of CNG channel from cilia and subsequent olfactory dysfunction, while adenoviral expression of mutant PACS-1 causes similar mislocalization. These results provide a mechanism for the subunit-

Chapter 3 is published as Jenkins, P.M., Zhang, L., Thomas, G., and Martens, J.R. (2009). PACS-1 mediates phosphorylation-dependent ciliary trafficking of the cyclic-nucleotide-gated channel in olfactory sensory neurons. J Neurosci *29*, 10541-10551. For copyright release, please see Appendix I. I would like to thank Gary Thomas for providing the PACS-1 plasmids and for review of the manuscript. Finally I would like to acknowledge the Jeffrey Martens laboratory, especially Lian Zhang for the preparation of various CNG channel mutant and PACS-1 constructs.

dependent ciliary trafficking of the CNG channel and offer further insight into the mechanisms of ciliary transport.

INTRODUCTION

The cilium is a microtubule-based organelle that can project from the surface of nearly any mammalian cell. Defects in cilia structure and function have been implicated in a growing number of human diseases involving multiple organ systems [157-159]. In the brain, many neurons and glia have been shown to possess primary cilia; however, their precise function remains obscure [160]. The olfactory system is one neuronal system that is critically dependent on the proper function of cilia. OSNs are unique in that cilia project from multiple basal bodies in the bulbous tip of their apical dendrite and make contact with the external environment [161]. Olfactory cilia act to compartmentalize signaling molecules, thereby allowing rapid and efficient activation of the signaling cascade.

Since cilia lack the machinery for protein synthesis, proteins must be produced in the cell and transported into the cilium via an evolutionarily-conserved process called intraflagellar transport (IFT) [24-25]. Entry into the cilium is regulated by a complex of proteins at the basal body which acts to restrict access to the cilium [24-25]. Alterations in the localization of ciliary proteins have been shown to underlie a number of human diseases including olfactory dysfunction, polycystic kidney disease, retinal degeneration, and primary ciliary dyskinesia [81-82, 95, 157, 159, 162]. Despite advances in the understanding of cilia formation and function, we still know little about the mechanisms regulating protein entry into the ciliary compartment.

All of the necessary components of the olfactory signal transduction cascade are enriched in cilia, including odorant receptors, the stimulatory G-protein (G_{olf}), adenylyl cyclase III (ACIII), and the olfactory cyclic-nucleotide-gated channel [141]. The olfactory CNG channel is a non-selective cation channel comprising 3 channel-forming subunits (CNGA2, CNGA4 and CNGB1b). Activation of the channel allows the initial depolarization of the OSN, and mislocalization of the CNG channel from cilia has been implicated in diseases, including anosmia and retinal degeneration [95, 144]. Previously,

we have shown that the CNGB1b subunit is necessary for ciliary localization of the olfactory CNG channel [68]; however, the mechanism of this subunit-dependent ciliary trafficking remained unknown.

Recently, the intracellular trafficking protein, phosphofurin acidic cluster sorting protein 1 (PACS-1) has been shown to localize to the base of human respiratory cilia and control the localization of nephrocystin 1 to the transition zone of respiratory cilia [85]. While PACS-1 has been shown to interact with acidic cluster-containing ion channels such as polycystin-2/TRPP2, TRPV4, and CLC-7 [81, 86], no direct role has been demonstrated in the control of ciliary localization of ion channels or other neuronal cargo.

Here, we have examined the subunit-dependent ciliary trafficking mechanisms of the olfactory CNG channel. We found that PACS-1 interacts with the CNGB1b subunit and is required for the control of its ciliary localization. Additionally, we found that CK2 phosphorylation of PACS-1 and of residues on two distinct CNGB1b amino terminal sites is necessary for this ciliary localization. These results represent the first report of a role for PACS-1 in the ciliary localization of membrane proteins, and also highlight a novel mechanism for the control of subcellular localization of neuronal cargo.

RESULTS

PACS-1 is expressed in Olfactory Sensory Neurons

To address the question of whether PACS-1 regulates ciliary trafficking of the olfactory CNG channel, we first examined expression of PACS-1 in native olfactory tissue. Using *in situ* hybridization performed with an anti-sense PACS-1 riboprobe on coronal sections from multiple mice, we found that PACS-1 mRNA, indicated by a dark purple precipitate, is present along the dorsal roof of the nasal cavity in a region corresponding to the OSN layer (Figure 3.1A, C). Using a control, sense riboprobe, we detected minimal reactivity (Figure 3.1B, D). These results clearly demonstrate the cellular distribution of PACS-1 mRNA in the olfactory epithelium and suggest that OSNs have the capacity to generate PACS-1 protein.

To determine if PACS-1 protein is expressed in OE, we performed Western blot analysis of native olfactory tissue homogenate. Using antibodies directed against PACS-1, we detected the presence of an immunoreactive band corresponding to the molecular weight of PACS-1 (~120 kDa) in adult mouse OE (Figure 3.1E lane 3). The specificity of this signal was confirmed in that we detected a band of similar molecular weight (Figure 3.1E lane 2) using lysates from HEK-293 cells transiently transfected with hemagglutinin (HA)-tagged PACS-1 but not untransfected HEK-293 cells (Figure 3.1E, lane 1). Using antibodies against the HA epitope, we verified that the 120 kDa band in lane 2 corresponds to PACS-1 (data not shown).

Since the OE comprises multiple cell types including OSNs, sustentacular cells and basal cells, we examined protein localization at the level of the OSN by immunostaining coronal sections of mouse OE. Single confocal planes of sections coimmunostained with antibodies against PACS-1 and γ tubulin demonstrated the presence of PACS-1 protein in the OSN (Figure 3.1F, G). Interestingly, PACS-1 localized to the dendritic knob, where it colocalized with the basal body marker, γ tubulin, but was undetectable in olfactory cilia. Together, these results demonstrate that PACS-1 is expressed in OSNs and localizes to the dendritic knob, where it may act as part of the basal body protein complex to regulate ciliary transport of the CNG channel.

The CNGB1b Subunit can Interact with PACS-1 and Serve as a Substrate for CK2 Phosphorylation

Previously, we have shown that the CNGB1b subunit is necessary for ciliary targeting of the olfactory CNG channel [68]; however, the mechanism of this regulation remained unknown. The intracellular sorting protein PACS-1 interacts with its cargo through phosphorylated serines or threonines contained in a cluster of acidic residues on the cargo protein to control its subcellular localization. Interestingly, using amino acid sequence analysis of the 3 olfactory CNG channel subunits, we identified two highly conserved acidic clusters in the amino terminus of the CNGB1b subunit which contain putative CK2 consensus phosphorylation sites (Figure 3.2A). In contrast, no consensus PACS-1 binding sites were identified in CNGA2 or CNGA4.

To examine interactions between PACS-1 and CNGB1b we used immunoprecipitation experiments from both transfected cells and native olfactory tissue. Immunoprecipitations of CNGB1b from HEK293 cells transiently transfected with CNGB1b-3xFlag and HA-PACS-1 demonstrated an *in vitro* interaction that was confirmed using the reverse immunoprecipitation (Figure 3.2B). Importantly, we observed an interaction between the endogenous CNG channel and PACS-1 in native mouse olfactory epithelium, while negative control antibodies showed no detectable immunoprecipitation (Figure 3.2C). Taken together these results indicate that CNGB1b and PACS-1 can interact in complex both *in vitro* and *in vivo*.

We next tested if the CNGB1b subunit could serve as a substrate for CK2 phosphorylation. *In vitro* kinase reactions were performed on immunoprecipitated protein (CNGA2, CNGA4, CNGB1b, or PACS-1) from transiently-transfected HEK293 cells using recombinant CK2 and [γ-^{32}P] *ATP*. As predicted from the sequence analysis, we found that CNGB1b serves as a substrate for CK2 (Figure 3.2D), while PACS-1 was also phosphorylated by CK2 as previously described [163]. In contrast, despite efficient immunoprecipitation (Figure 3.3), neither CNGA2 nor CNGA4 were phosphorylated (Figure 3.2D), demonstrating a subunit-specificity for CK2 phosphorylation.

Finally, we used alanine substitution to determine if the putative CK2 sites at serines 132 and 208 within CNGB1b are capable of being phosphorylated by the enzyme. For these experiments, we created three mutant forms of CNGB1b (S132A, S208A, and S132A/S208A double mutant) and performed *in vitro* kinase reactions on immunoprecipitated proteins. Despite equal immunoprecipitation, the CNGB1b S132A/S208A mutant exhibited a significant decrease (~35%) in phosphorylation by CK2 compared to wild-type (Figure 3.2D). Mutation of either serine alone (S132A or S208A) caused an intermediate decrease in phosphorylation (data not shown). These results demonstrate that CK2 is capable of phosphorylating S132 and S208 located within acidic clusters on CNGB1b, which may serve to regulate CNGB1b ciliary trafficking.

Mutation of the CK2 Phosphorylation Sites on CNGB1b Inhibits Ciliary Delivery of the CNG Channel

Since mutation of CK2 phosphorylation sites within PACS-1 cargo has been shown to impair intracellular trafficking [164], we tested CNG channel trafficking using phosphorylation-deficient CNGB1b mutants. Previously, we have demonstrated that ciliated MDCK cells represent a suitable model to study ciliary trafficking of olfactory signaling proteins [68]. Confocal images of individual cells clearly show that mutation of both putative CK2 sites (S132A + S208A double mutant) caused a dramatic loss of CNGB1b and its heteromeric partner CNGA2-mCitrine from the cilia of MDCK cells (Figure 3.4A-B, 3.8). Importantly, averaged data from multiple cells indicate an almost complete absence of CNG channel ciliary localization in the presence of the CNGB1b double mutant (Figure 3.4C, D). Mutation of either S132 or S208 alone caused an intermediate decrease in ciliary trafficking of the channel (Figure 3.6). Together these data indicate that, while either CK2 site is sufficient for ciliary trafficking, both sites are necessary for ciliary enrichment of the CNG channel.

Loss of PACS-1 Function Impairs CNG Channel Ciliary Transport

To ascertain a functional role for PACS-1 in the ciliary targeting of the olfactory CNG channel we generated retroviral stable MDCK cells expressing either wild-type PACS-1 or the dominant-negative, non-phosphorylatable PACS-1 S278A mutant. It is thought that phosphorylation of an autoregulatory domain of PACS-1 at serine 278 causes the protein to unfold, allowing the binding and subsequent trafficking of cargo protein. This phosphorylation-dependent function is inhibited by mutation of S278 to alanine [163]. Expression of CNGA2-mCitrine and CNGB1b in PACS-1 S278A stable MDCK cells resulted in impaired ciliary localization, whereas in cells stably overexpressing wild-type PACS-1 the channel localized to cilia as expected (Figure 3.7A-B, 3.8). As an additional control, MDCK cells stably expressing the phosphomimic form of PACS-1 (PACS-1 S278D) demonstrated normal ciliary localization of the CNG channel (data not shown). These data indicate that loss of the autoregulatory phosphorylation site on PACS-1 inhibits ciliary trafficking of the CNG channel.

One limitation of using the non-phosphorylatable mutant PACS-1 is that its overexpression may sequester trafficking partners within the cell, leading to non-specific effects. To overcome this limitation, we utilized retrovirally-delivered short hairpin RNA (shRNA) in MDCK cells to silence PACS-1 expression. MDCK cells express endogenous PACS-1 which was efficiently silenced using a 21 nucleotide sequence directed against PACS-1 (human 1345-1365) while a validated negative control shRNA had no effect on PACS-1 protein levels (Figure 3.9). In MDCK cells stably expressing PACS-1 shRNA, we failed to detect localization of CNGA2-mCitrine to cilia in the presence of CNGB1b, whereas, in cells stably expressing negative control shRNA, we found normal ciliary localization of the CNG channel (Figure 3.7C-D). Interestingly, mutation or shRNA-mediated suppression of PACS-1 had no effect on cilia length or gross morphology (Figure 3.9). These results, together with the results from the non-phosphorylatable mutant PACS-1, indicate that diminished PACS-1 function, either by mutation of the autoregulatory domain or loss of protein, leads to impaired ciliary trafficking of the olfactory CNG channel.

Inhibition of CK2 Alters CNG Channel Localization

Pharmacological inhibition of CK2 enzymatic activity has been shown to impair PACS-1 activity [163-165]. To directly examine the CK2 phosphorylation dependence of ciliary trafficking of the olfactory CNG channel we transfected MDCK cells with both CNGA2-mCitrine and CNGB1b, allowed 48 hours for channel to reach cilia, and then treated cells with the cell-permeant, selective CK2 inhibitor, 4,5,6,7-Tetrabromotriazole (TBB). Inhibition of CK2 for 4 hours with 20 μM TBB led to a loss of CNG channel from the cilia of MDCK cells (Figure 3.10A). Mislocalized channel formed bright puncta at the base of the cilium, which can be seen more clearly in an X-Z projection (Figure 3.10B). Consistent with the effects of phosphodeficient PACS-1 shown above, treatment of MDCK cells with 20 μM TBB for 4 hours had no effect on average cilia length (Figure 3.11). Together, these indicate that the processes necessary for maintenance of cilia length are not dependent on CK2 phosphorylation.

CK2 Phosphorylation is Necessary for the Ciliary Localization of CNG Channel *In Vivo* and Proper Olfactory Function

Our results indicate an important role for PACS-1 and CK2 phosphorylation in the ciliary trafficking of ectopically-expressed CNG channels *in vitro*. We next tested the hypothesis that these mechanisms were operating in native olfactory tissue and were necessary for proper olfactory function. To this end, the selective CK2 inhibitor TBB was delivered directly to the olfactory epithelium using intranasal injections into adult CD1 mice. Using this method, we found that the area of greatest exposure to the inhibitor were regions of the ventral OE, especially turbinates III and IV. This was confirmed using the fluorescent tracer, carboxyfluorescein diacetate, succinimidyl ester (data not shown). Fluorescence immunohistochemistry on fixed tissue was used to examine the subcellular distribution of CNG channels. Coronal sections from mice injected with control solution (0.1% DMSO) exhibited normal CNG channel enrichment in cilia, as indicated by colocalization with the ciliary marker, acetylated α tubulin (Figure 3.10C). Sections from mice injected with 20 μM TBB followed by 4 hours of recovery demonstrated a dramatic loss of CNG channel from the cilia layer and a lower level of total CNG channel protein in the olfactory epithelium (Figure 3.10D). This loss of channel protein is consistent with previous work demonstrating that mislocalized CNG channel out of the cilia is degraded in OSNs [95]. These results demonstrate that the ciliary trafficking of the CNG channel in native olfactory tissue is dependent on CK2 phosphorylation.

Mislocalization of olfactory signaling proteins from cilia leads to olfactory dysfunction [82, 95]. To assess the effect of CK2 inhibition on olfactory function we measured the odor-evoked electrical response in OSNs using electroolfactogram (EOG) recordings from the surface of mouse OE. The head was split sagitally at the midline to expose the olfactory turbinates. Solutions (Ringer's buffer control or Ringer's plus 20 μM TBB) were applied directly to either turbinate and evoked potentials in response to the odorant amyl acetate were measured every 5 minutes from two recording electrodes placed on opposite sides of the OE (See diagram in Figure 3.12). In paired recordings

from 5 mice, inhibition of CK2 with TBB caused a significant and almost complete loss of the response to amyl acetate within 25 minutes. Treatment with control solution caused only a slight decrease (Figure 3.12A, B) consistent with rundown of the odor-evoked signal [166]. To confirm that the mechanism for the loss of EOG response was due to an alteration in the ciliary localization of the CNG channel, we treated mouse OE with TBB or control solution for 25 minutes in the same manner as performed for EOG recordings. Medial surfaces of the olfactory turbinates, which correspond to regions of the OE that would have been exposed to drug, demonstrated a dramatic decrease in ciliary localization of the CNG channel compared to control (Figure 3.12C). After only 25 minutes, mislocalized channel protein appeared to accumulate on microtubule tracks of the dendrite indicating a possible retrograde trafficking of the channel in response to CK2 inhibition. Interestingly, ACIII ciliary localization was unaffected by the 25 minute CK2 inhibition (Figure 3.11). These data demonstrate that inhibition of CK2 causes a selective mislocalization of olfactory CNG channels from cilia and subsequent olfactory dysfunction.

Adenoviral Expression of Non-Phosphorylatable PACS-1 in Native OSNs Impairs Ciliary Localization of the Endogenous CNG Channel

Since inhibition of CK2 in native OSNs causes a selective mislocalization of the CNG channel from cilia, we examined if this effect included inhibition of PACS-1 function. Mice were infected intranasally with adenovirus carrying either non-phosphorylatable PACS-1 S278A IRES GFP or GFP alone. Infection of OSNs with adenovirus carrying the non-phosphorylatable form of PACS-1 (S278A) caused a mislocalization of the endogenous ciliary CNG channel, but no detectable change in the cilia layer as indicated by acetylated α tubulin staining (Figure 3.13A, top). Expression of PACS-1 S278A, however, had no effect on ciliary ACIII localization, consistent with the specificity measured by pharmacological inhibition of CK2 (Figure 3.13A, bottom). A surprising result was the malformation of the dendrite in OSN infected with the functionally-impaired S278A mutant. In these neurons, marked by GFP, there was an obvious swelling of the knob and thickening of the dendritic shaft compared to controls

(Figure 3.13A, B), however these cells were localized deep within the OMP-positive cell body layer as would be expected for mature OSNs (Figure 3.14). This unanticipated result suggests that, although we observe no accumulation of CNG channel, inhibition of PACS-1-mediated trafficking may cause the accumulation of other dendritic or ciliary cargo.

DISCUSSION

The results of these studies define a mechanism for the subunit-dependent ciliary trafficking of the olfactory CNG channel. The intracellular sorting protein, PACS-1, is expressed in OSNs and localizes to the dendritic knob, which is the site of protein entry and exit from olfactory cilia. We discovered that PACS-1 binds to the CNGB1b subunit and controls its proper ciliary localization. This mechanism is dependent on CK2 phosphorylation at sites on both PACS-1 and two distinct sites on the amino terminus of the CNGB1b subunit. Importantly, this work provides new insight into the requirements for the ciliary trafficking of polytopic membrane proteins and demonstrates for the first time a functional role for PACS-1 in neurons.

This is the first report for the direct mechanistic role of PACS-1 in the ciliary trafficking of membrane proteins. Previously, a role for PACS-1 in the localization of nephrocystin to the ciliary base/transition zone in epithelial cells was reported [85]. This work relied solely on the expression of non-phosphorylatable dominant-negative constructs to implicate PACS-1 in the localization. However, overexpression of this mutant protein may lead to non-specific effects through the sequestration of important binding partners. To overcome this limitation, we confirmed our dominant-negative results using shRNA-mediated gene silencing of PACS-1 to confirm its role in the ciliary localization of the olfactory CNG channel.

Although never directly addressed, there are other reports that are consistent with a role for PACS-1 in the trafficking of olfactory cargo. Some PACS-1 binding partners, such as the AP-1 adaptor complex, have been shown to be necessary for proper PACS-1-mediated trafficking through the budding of clathrin-coated vesicles from the trans-Golgi network [167]. Interestingly, components of the Golgi-localized clathrin trafficking

machinery as well as members of IFT complex, which participate in ciliary transport, share significant homology [73]. In addition, the clathrin AP-1 μ adaptor UNC-101 has been shown to be responsible for the localization of odorant receptors to the cilia of C. *elegans* [74]. These peripherally-related reports may suggest that PACS-1 participates in a common transport pathway for all olfactory ciliary proteins. Our results in native olfactory tissue, however, indicate that the requirement of CK2 phosphorylation does not apply to all olfactory signaling proteins.

There has been controversy in the role of CK2 in the regulation of the subcellular localization of other ciliary ion channels. For example, recent work reports that inhibition of CK2, despite altering the subcellular localization of the TRP-channel polycystin-2, had no effect on ciliary expression in MDCK cells [168]. In contrast, other work in *C. elegans*, demonstrated that a non-phosphorylatable mutant of polycystin-2 localizes to cilia whereas the phosphomimetic form of the protein fails to traffic to cilia [169]. Additionally, work in zebrafish demonstrated that deletion of a region of polycystin-2 corresponding to an acidic cluster with a CK2 phosphorylation site causes mislocalization of polycystin-2 to the apical cell membrane [170]. These findings may highlight differences in trafficking pathways for polycystin-2 and the CNG channel or differences between model systems. Interestingly, polycystin-2 and the CNGB1b subunit share a common "RVxP" trafficking motif, and mutation of this motif causes mislocalization of both proteins from cilia [68, 88].

The dynamics of intraciliary movement and the time for entry and exit from the cilia compartment is an area of intense interest. Very little is known regarding the residence time of proteins, including ion channels, within the ciliary membrane. Our results demonstrate that inhibition of CK2 causes a near-complete loss of CNG channel from the cilia of OSNs in ~25 minutes. Additionally, as shown in Figure 3.12, upon inhibition of CK2, the CNG channel displays an increased localization along the microtubule tracks of the dendrites. This rapid loss of channel from cilia can result from inhibiting entry or accelerating exit of channels from the ciliary compartment. This disruption of the steady-state channel localization implies a bidirectional movement of channel protein on a time scale shorter than 25 minutes. Qin *et al.* previously

demonstrated that the *C. elegans* TRPV channels OSM-9 and OCR-2 move bidirectionally along the ciliary axoneme at rates comparable to IFT (~1 μm/sec) [92]. If this applies to movement into and out of the cilium, it suggests a very short residence time for individual channels within the cilia. Our previous work demonstrated that the rate of olfactory CNG channel movement within MDCK cell cilia is on the order of diffusion with a τ of ~10 minutes [68], which predicts a greater latency for the channel. Therefore, we cannot exclude the possibility of an active cargo retrieval process initiated upon CK2 inhibition. The failure to detect PACS-1 in the cilia of OSNs (Fig. 3.1), however, suggests that PACS-1 is not the protein responsible for this potential scavenging mechanism. Ultimately, elucidation of the dynamics of protein movement into and out of the cilium will require advanced imaging techniques with the appropriate temporal and spatial resolution.

In summary, our results demonstrate that PACS-1 and CK2 are important players in the regulation of the localization of select olfactory cilia cargo. Chronic inhibition of PACS-1 function using dominant-negative constructs or shRNA-mediated gene silencing impairs the steady-state ciliary localization of the olfactory CNG channel in MDCK cells. Interestingly, expression of non-phosphorylatable PACS-1 in native OSNs, in addition to causing mislocalization of ciliary CNG channel, also leads to a dramatic thickening of the dendrite and flattening of the dendritic knob. These results may implicate PACS-1 in the trafficking of other dendritic or ciliary cargo. Interestingly, however, expression of this dominant-negative PACS-1 did not alter localization of ACIII, suggesting that PACS-1 controls the subcellular localization of only a subset of neuronal cargo. In contrast to the long-term, steady-state effects seen with dominant-negative expression, pharmacological inhibition of CK2 phosphorylation causes an acute and rapid mislocalization of the CNG channel, while also not affecting other members of the olfactory signaling cascade. Since activation of the CNG channel in cilia serves as the trigger for action potential generation in the OSN, CK2 phosphorylation-dependent trafficking may represent a novel mechanism for the fine tuning of responses to sensory stimuli. In addition to these physiological implications, our results clearly link PACS-1 to the subunit-dependent

ciliary localization of the olfactory CNG channel and highlight a novel role for PACS-1 in the regulation of subcellular protein trafficking in neurons.

EXPERIMENTAL PROCEDURES

Antibodies

Monoclonal anti-acetylated tubulin (1:1000) and anti-flag M2 antibodies (1 μg for immunoprecipitation) were from Sigma-Aldrich. Monoclonal anti-PACS-1 (1:500) antibodies were from BD Biosciences. Polyclonal anti-CNGA2 (1:200) antibodies were from Alomone Labs. Polyclonal anti-HA (1:500 for immunostaining, 1 μg for Immunoprecipitation) antibodies were from Santa Cruz Biotechnology. AlexaFluor-conjugated secondary antibodies (1:1000) were from Invitrogen.

Cell culture

Madin Darby Canine Kidney (MDCK) cells were cultured, transfected and prepared as described previously [68]. Briefly, MDCK cells were grown for 7 days post-confluence on Transwell filter supports (Corning Costar) and transfected with 0.5 μg per DNA construct and Lipofectamine plus reagent (Invitrogen) according to manufacturer's protocol. HEK293 cells were cultured in DMEM containing 10% fetal bovine serum, 100 units/mL penicillin, and 100 μg/mL streptomycin at 37°C and 5% CO_2. For immunoprecipitation, HEK293 cells were plated on 100 mm dishes at 50% confluence and transfected with 1 μg cDNA and 3 μL Lipofectamine 2000 (Invitrogen) according to manufacturer's protocol. CNGB1b serine to alanine mutations were performed using QuikChange Site-Directed Mutagenesis Kit purchased from Stratagene (La Jolla, CA) according to manufacturer's protocol.

Adenovirus Preparation

PACS-1 S278A IRES eGFP was cloned into the adenoviral shuttle plasmid, pDC315, and adenovirus was prepared using the Admax Adenoviral Preparation Kit (Microbix Biosystems) according to manufacturer's protocol. Adenovirus was amplified by

infection of HEK293 cells in 150 cm^2 flasks which were harvested at approximately 50% cytopathic effect and virus was purified using the Adeno-X Maxi Prep Kit (Clontech) according to manufacturer's protocol. Virus was dialyzed into a solution of 2.5% glycerol, 25mM NaCl, and 20 mM Tris-HCl pH8.0 and stored at -80°C until use. Viral titer was calculated using an adenoviral plaque assay according to Adeno-X Maxi Prep Kit instructions.

Intranasal injection

All animals were handled according to the guidelines for animal care at the University of Michigan. Adult CD1 mice (2-5 months) were anesthetized by intraperitoneal injection with 100 mg/kg ketamine and 5 mg/kg xylazine. Animals were placed on their backs and PE10 tubing was inserted into the right nostril to a depth of 7 mm. Adenoviral solutions were delivered in a total volume of 50μL of sterile 0.9% saline mixed with 0.02% fast green dye at a rate of 4 μL per minute (2.5×10^8 pfu for PACS-1 S278A IRES eGFP adenovirus; 1×10^9 pfu for eGFP adenovirus) for three consecutive days. Drug delivery was performed in a total volume of 25 μL of sterile 0.9% saline mixed with 0.02% fast green dye at a rate of 4 μL per minute (± 20 μM CK2 inhibitor, 4,5,6,7-Tetrabromotriazole (TBB). Animals were allowed 30 minutes to recover from anesthesia on their backs before being returned to their home cage. Mice infected with virus were allowed 4 days for expression of ectopic protein. Those injected with CK2 inhibitor were allowed 4 hours of recovery.

Tissue preparation

For immunostaining, adult CD1 mice (2-5 months) were deeply anesthetized and sacrificed by cardiac perfusion with 50 mL PBS followed by 50 mL 4% paraformaldehyde (PF) at a rate of 10 mL per minute. Olfactory epithelium was removed and post-fixed in 4% PF for 1 hour at 4°C, cryoprotected in 30% sucrose overnight at 4°C, and embedded in OCT compound (Tissuetek). Cryostat sections were sliced at a thickness of 20 μm and allowed to dry onto Superfrost Plus slides (Fisher Scientific) for 20 minutes at room temperature.

Immunostaining

Olfactory epithelium sections were permeabilized in PBS containing 0.3% Triton X-100 and 2% goat serum for 20 minutes at room temperature. MDCK cells were fixed for 7 minutes with 4% PF, permeabilized for 10 minutes in PBS containing 0.1% Triton X-100, and blocked in PBS with 2% goat serum for at least 10 minutes. Samples were incubated in primary antibodies diluted in 2% goat serum PBS for 1 hour at room temperature and washed three times for 2 minutes in PBS (anti-CNGA2 antibody incubation was overnight at 4°C in humidified chamber). Samples were incubated in fluorescently-conjugated secondary antibodies diluted in 2% goat serum/PBS for 1 hour, washed 3 times for 2 minutes in PBS, and mounted using Prolong Gold anti-fade reagent (Invitrogen).

Confocal Imaging

Confocal imaging was performed as described previously [68]. Images of transfected cells displaying fluorescent signals were acquired on an Olympus Fluoview 500 confocal microscope with a 60 × 1.40 N.A. or 100 × 1.35 N.A. oil objective. Exposure times were adjusted so that the maximal pixel intensities were at least half saturation. Images were obtained by taking a series of stacks every 0.5 μm through the cell (generally 3–5 μm) and combining the images into a composite stack. For MDCK cell experiments, while the entire confocal stack containing sections through the whole cell was used to generate images for display, fluorescence intensity analysis and colocalization were measured in images generated only from focal planes containing cilia (Figure 3.8). For adenoviral OE experiments, in order to minimize contribution of ciliary protein localization from uninfected OSNs, we used compressed Z stacks corresponding only to the thickness of the infected OSN. Images were analyzed with ImageJ software (NIH, Bethesda, MD), and statistics were performed with Prism 5 software from Graphpad Prism Software (San Diego, CA). Adjustments of contrast and brightness were performed using Adobe Photoshop 9.0 (San Jose, CA).

In situ hybridization

In situ hybridization was performed on mounted coronal sections of p1.5 CD1 mouse head using an 800bp digoxigenin-labeled, anti-sense PACS-1 riboprobe or the control, sense probe, with a hybridization temperature of 65°C as described previously [171]. 800 nucleotides of cDNA corresponding to the 3' coding sequence of PACS-1 were amplified by polymerase chain reaction using mouse brain cDNA (Generous gift of Dr. Donna Martin, University of Michigan) and cloned into pGem-T Easy. Probes were generated using digoxigenin-labeling kit (Roche Applied Science) according to manufacturer's protocol and detected using alkaline phosphatase-conjugated anti-digoxigenin antibodies with 5-Bromo-4-Chloro-3'-Indolyphosphate p-Toluidine Salt and Nitro-Blue Tetrazolium Chloride.

Immunoprecipitations

Protein G agarose beads were preincubated with antibodies for 2-4 hours on a nutator at 4°C in immunoprecipitation (IP) buffer containing: 20 mM Tris–HCl, pH 7.5, 1% Triton X-100, 25 mM NaF, 12.5 mM $Na_4P_2O_7$, 0.1 mM EDTA, 100 mM NaCl, 2 mM Na_3VO_4 and protease inhibitors with 1% Triton X-100. 24 hours post-transfection, HEK293 cells were lysed on ice for 30 minutes in 500μL IP buffer. After douncing, cells were centrifuged at 1,000×g for 5 minutes and supernatant was incubated overnight at 4°C with antibody-conjugated beads. 5% of supernatant was used for starting material. Beads were washed three times for 5 minutes with IP buffer with 1% Triton X-100 and once with IP buffer without Triton X-100. Supernatant was either analyzed by SDS-PAGE as described previously [68], or used for *in vitro* kinase reactions.

In vitro kinase reactions

Kinase reactions were performed essentially as described previously [172]. Briefly, immunoprecipates bound to beads were incubated with recombinant CK2 (New England Biolabs) in the presence of 10 μCi/mL [γ–^{32}P] ATP and 200 μM MgATP for 30 minutes at 30°C according to manufacturer's protocol. Samples were processed by SDS-PAGE

and gels were exposed to phosphorimager screen for one hour and read on a Typhoon Variable Mode Imager (GE Healthcare).

RNAi and retrovirus

Short-hairpin RNA for PACS-1 (5'- sense GAT GAC AGC TTG ACT GAA ACA loop TTC AAG AGA anti-sense TGT TTC AGT CAA GCT GTC ATC -3') or Clontech negative control shRNA sequence was cloned into pSiren RetroQ (Clontech) and retrovirus was generated according to manufacturer's protocol. Stable MDCK cell lines were created by infection with shRNA retrovirus followed by selection using 5μg/mL Puromycin.

Electroolfactograms

Summated potentials from mouse olfactory epithelium (OE) were recorded essentially as described previously [82]. Briefly, adult mice were euthanized by carbon dioxide inhalation and the head was bisected laterally at the midline. Solutions were added for 5 minutes directly to the epithelial surface (Ringer's or Ringer's + 20 μM TBB). Recording electrodes were placed on either side of the head in the region of turbinate II or IIb and electrical responses to odorant (amyl acetate at 10 mM) perfused across the OE in the vapor phase in a stream of humidified oxygen were recorded. We analyzed data with Clampfit (Molecular Devices) and determined peak heights from prepulse baseline.

ACKNOWLEDGEMENTS

We thank Kristen Verhey and Toby Hurd (University of Michigan) for helpful discussions and critical review of the manuscript. We also thank Donna Martin and her laboratory (University of Michigan) for assistance with the *in situ* hybridization. This work was supported by National Institutes of Health grants DC009606 (JRM), DK37274 (GT), AI49793 (GT), GM007767 (PMJ), DC00011 (PMJ), and NRSA fellowship DC009524 (PMJ).

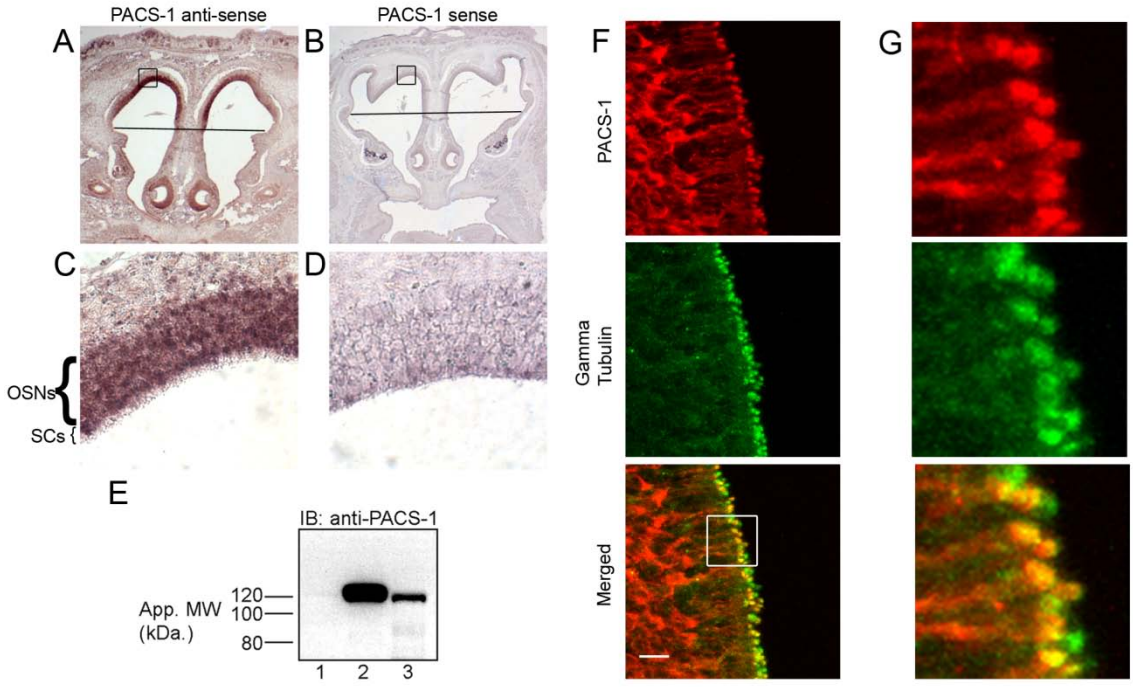

Figure 3.1 PACS-1 is Expressed in OSNs.

(A-D) *In situ* hybridizations performed on coronal sections from p1.5 CD1 mice were probed with digoxigenin-labeled antisense riboprobes for PACS-1 (A,C) or control, sense probes (B, D). PACS-1 mRNA is present in OSNs as indicated by dark purple precipitate (panel C). Line denotes transition from olfactory epithelium (top) to respiratory epithelium (bottom). Boxes in panels A and B represent regions of interest shown at higher magnification in panels C and D, respectively. **(E)** Western blot results from lysates of (1) untransfected HEK293 cells, (2) HEK293 cells expressing human PACS-1 with HA tag, or (3) p18 mouse olfactory epithelium. Molecular weight markers are indicated on the left in kDa. **(F)** Immunostaining of coronal sections from adult CD1 mouse OE demonstrates PACS-1 (red) is expressed in OSNs where it is enriched at the dendritic knob as indicated by colocalization with gamma tubulin (green). Merged image shown on bottom. Bars represent 10 μm. **(G)** Higher magnification image from boxed region of interest in panel F, bottom, demonstrating colocalization of PACS-1 and gamma tubulin.

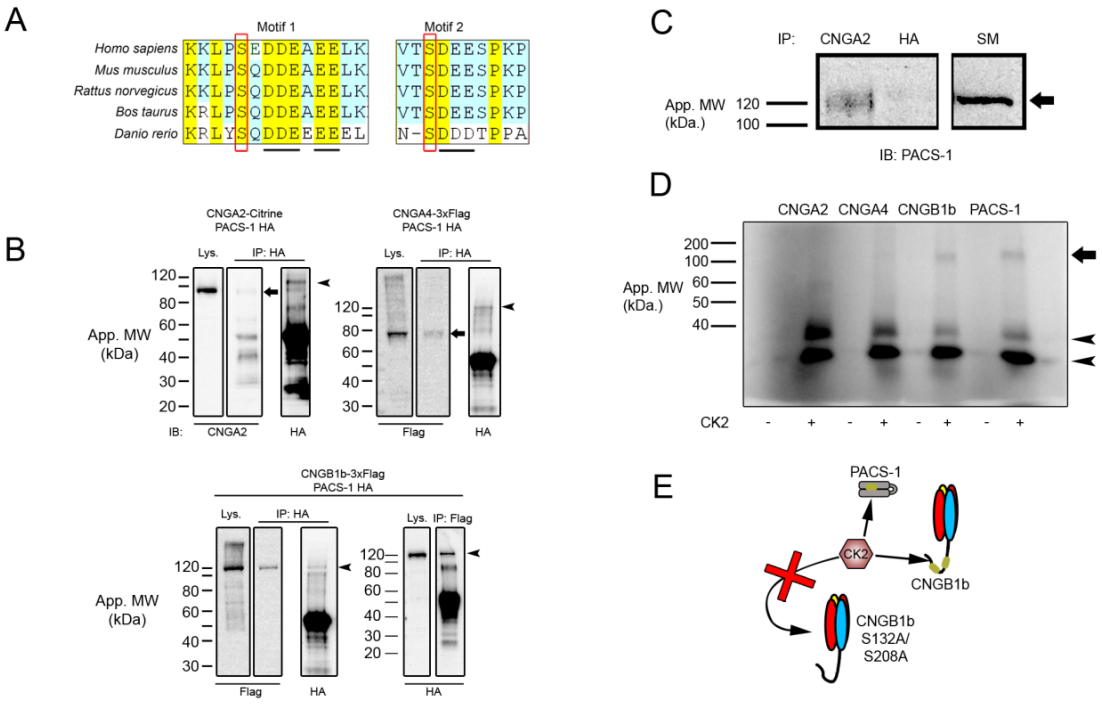

Figure 3.2 CNGB1b Contains Acidic Clusters, Interacts with PACS-1, and can Serve as a Substrate for CK2.

(A) Amino acid sequence alignment of the CNGB1b subunit from *Homo sapiens*, *Mus musculus*, *Rattus norvegicus*, *Bos taurus*, and *Danio rerio*. Acidic clusters marked by underline and putative CK2 phosphorylation sites marked by red rectangle. **(B)** Immunoprecipitation experiments from HEK293 cells cotransfected with HA-PACS-1 and CNGB1b-3xFlag. Immunoprecipitations were performed with either rabbit anti-Flag (left) or rabbit anti-HA (right) and blots were probed with rabbit anti-HA (left) or mouse anti-Flag M2 (right). Arrows mark PACS-1 (left) and CNGB1b (right). Arrowheads represent heavy and light IgG. Lys. = lysates IP = Immunoprecipitation. **(C)** Immunoprecipitation experiment from adult CD1 mouse olfactory epithelial lysates. Immunoprecipitations of endogenous protein were performed either with anti-CNGA2 or negative control, anti-HA antibodies. Blot was probed with anti-PACS-1 antibodies. Arrow marks PACS-1 protein at approximately 120 kDa. SM = 10% starting material. **(D)** (Top) Autoradiograph from *in vitro* kinase reaction performed on immunoprecipitated proteins (CNGA2, CNGA4, CNGB1b, or PACS-1) in the presence (+) or absence (-) of recombinant CK2. Autophosphorylated CK2 bands marked with arrowheads. Arrow marks approximate molecular weight of PACS-1 and CNGB1b. (Bottom left) Model depicting predicted CK2-mediated phosphorylation of both PACS-1 and CNGB1b, but not CNGB1b S132A/S208A. (Bottom right) Quantification of CK2-mediated phosphorylation of CNGB1b (white) or CNGB1b S132A/S208A (black). Data are shown as Mean ± SEM. (CNGB1b S132A/S208A 66.44 ± 1.958% compared to CNGB1b wild-type. n=3 experiments, $p<0.0001$ unpaired *t* test).

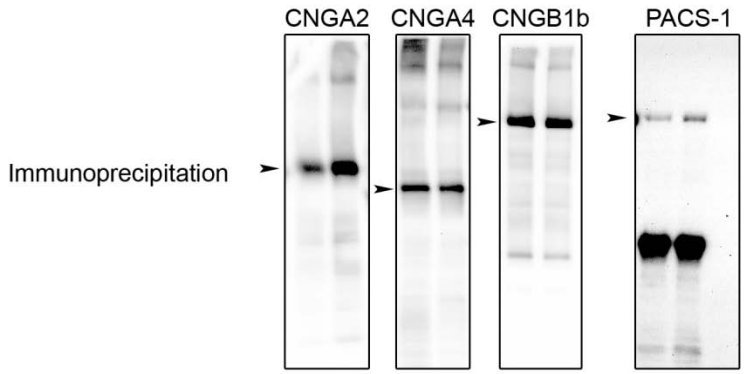

Figure 3.3 Immunoprecipitation of CNGA2, CNGA4, and CNGB1b prior to *in vitro* CK2 kinase reaction.

Western blot results from immunoprecipitation experiments from HEK293 cells transfected with CNGA2-3xFlag, CNGA4-3xFlag, CNGB1b3xFlag, or HA-PACS-1. Samples containing immunoprecipitates bound to beads were split, and half was used for the in vitro kinase reaction in Figure 3.2D. Arrowheads mark proteins of interest. Immunoprecipitations were performed with polyclonal anti-Flag (CNGA2, CNGA4, and CNGB1b) or polyclonal anti-HA (PACS-1) antibodies.

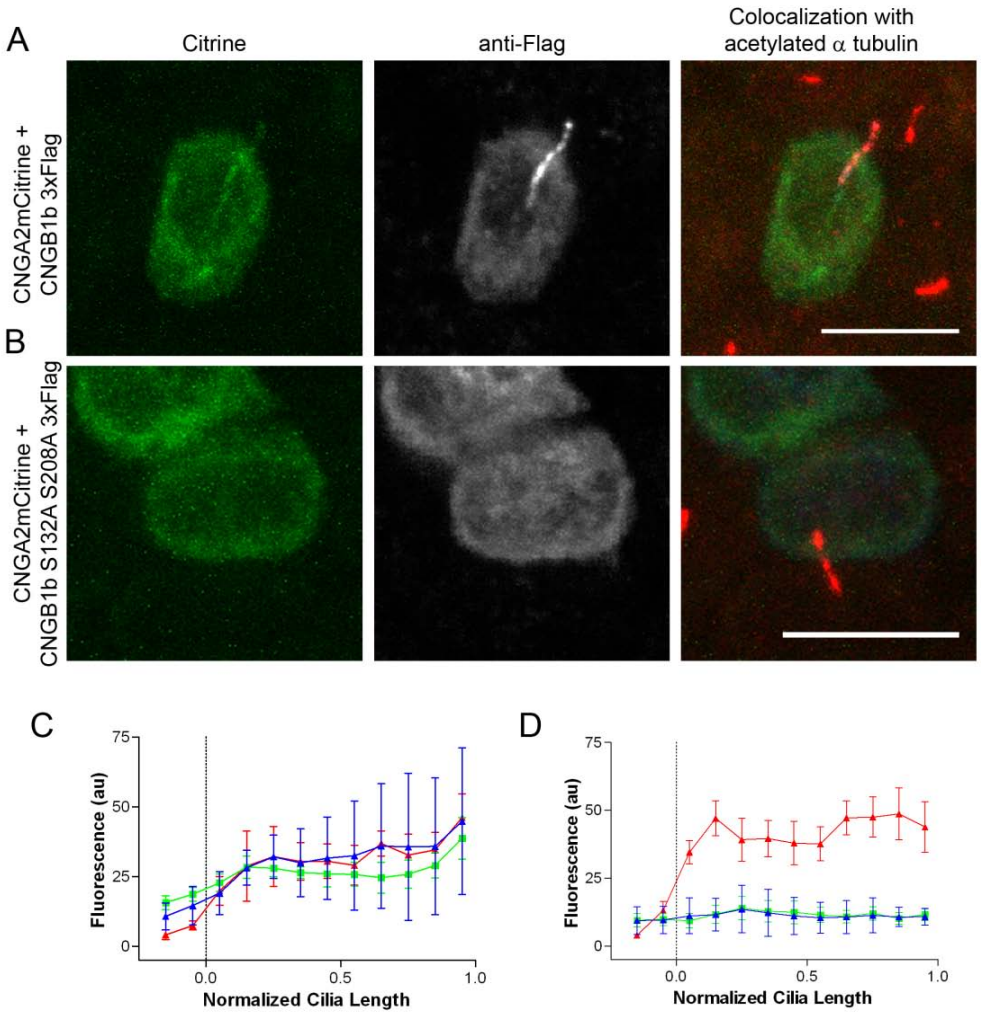

Figure 3.4 Mutation of CK2 Phosphorylation Sites on the N-terminus of CNGB1b Impairs Ciliary Trafficking of the CNG Channel.

Representative confocal images of MDCK cells transfected with CNGA2-mCitrine and **(A)** CNGB1b-3xFlag or **(B)** CNGB1b S132A, S208A-3xFlag. Citrine signal is on left (green). Flag immunostaining for CNGB1b is in middle (grayscale). Merged image with staining for acetylated α tubulin (red) is on right. Bar represents 10 μm. Average data from multiple cells (n=6-7) shown for **(C)** CNGB1b wild-type or **(D)** CNGB1b S132A, S208A. Data were apportioned into bins of $1/10^{th}$ of normalized cilia length. Acetylated tubulin signal shown in red, CNGA2-mCitrine fluorescence shown in green, and anti-Flag immunostaining signal shown in blue (arbitrary fluorescent units).

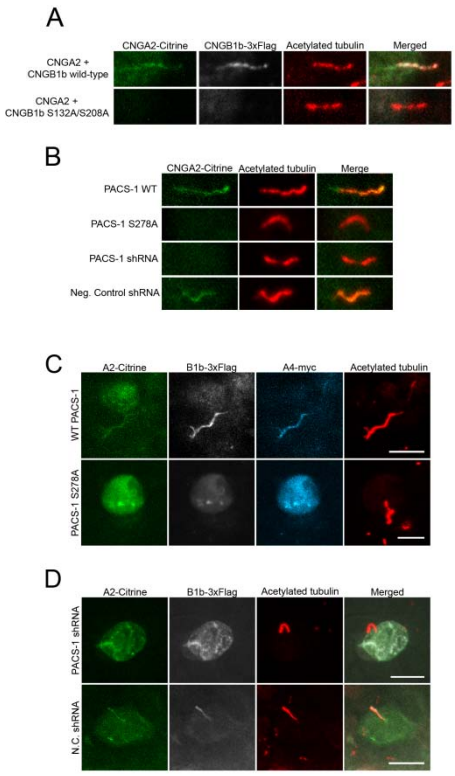

Figure 3.5 Alteration of PACS-1 Function Causes Impaired Ciliary Localization of the Complete CNG Channel Heterotetramer

Representative collapsed confocal images from MDCK cells shown in Figure 3.4 **(A)** and Figure 3.7 **(B). (A)** Representative confocal images of MDCK cells transfected with CNGA2-mCitrine and CNGB1b-3xFlag or CNGB1b S132A, S208A-3xFlag. Citrine signal is on left (green). Flag immunostaining for CNGB1b is in middle (grayscale). Merged image shown with for acetylated α tubulin (red) is on right. **(B)** Representative confocal images of MDCK cells transfected with CNGA2-mCitrine and CNGB1b-3xFlag stably-expressing either PACS-1 WT, PACS-1 S278A, PACS-1 shRNA, or negative control shRNA. Signal from CNGA2-mCitrine is shown on the left (green) and acetylated tubulin is in the middle (red). Merged image on the right. **(C)** Representative confocal images of MDCK cells transfected with CNGA2-mCitrine, CNGA4-myc, and CNGB1b-3xFlag stably-expressing either PACS-1 WT or PACS-1 S278A. Signal from CNGA2-mCitrine is shown on the left (green), immunostaining for CNB1b-3x flag is shown 2nd from the left (grayscale), immunostaining for CNGA4-myc flag is shown 3rd from the left (cyan) and acetylated tubulin signal is on the right (red). **(D)** Representative confocal images of MDCK cells transfected with CNGA2-mCitrine, and CNGB1b-3xFlag stably-expressing either PACS-1 shRNA (top) or negative control shRNA (N.C. shRNA, bottom). Signal from CNGA2-mCitrine is shown on the left (green), immunostaining for CNB1b-3x flag is shown 2nd from the left (grayscale), acetylated tubulin signal marking the ciliary axoneme is 3rd from the left (red), and the merged image is on the right. All bars represent 10 μm.

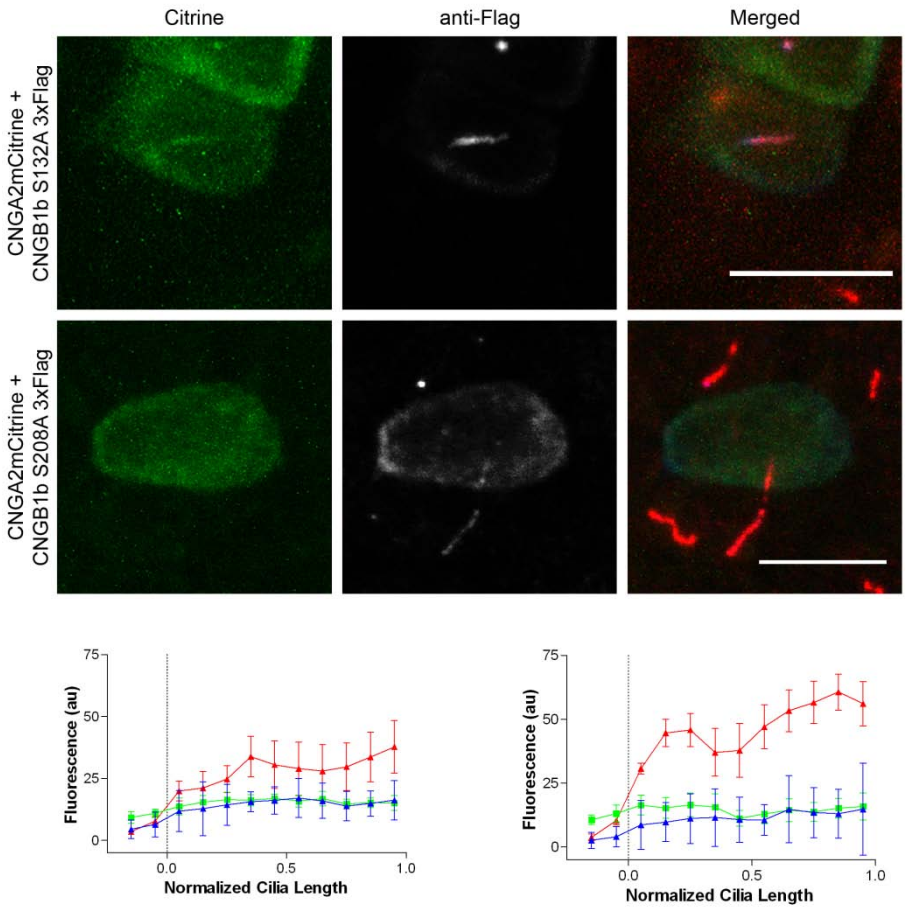

Figure 3.6 Mutation of Either S132 or S208 Leads to Diminished Ciliary Trafficking of the CNG Channel

Representative confocal images of MDCK cells transfected with CNGA2-mCitrine and **(top images)** CNGB1b S132A-3xFlag or **(bottom images)** CNGB1b S208A-3xFlag. Citrine signal is on left (green). Flag immunostaining for CNGB1b is in middle (grayscale). Merged image with staining for acetylated α tubulin (red) is on right. Bar represents 10 μm. Average data from multiple cells (n=6-7) shown for **(bottom left)** CNGB1b S132A or **(bottom right)** CNGB1b S208A. Data were apportioned into bins of $1/10^{th}$ of normalized cilia length. Acetylated tubulin signal shown in red, CNGA2-mCitrine fluorescence shown in green, and anti-Flag immunostaining signal shown in blue (arbitrary fluorescent units).

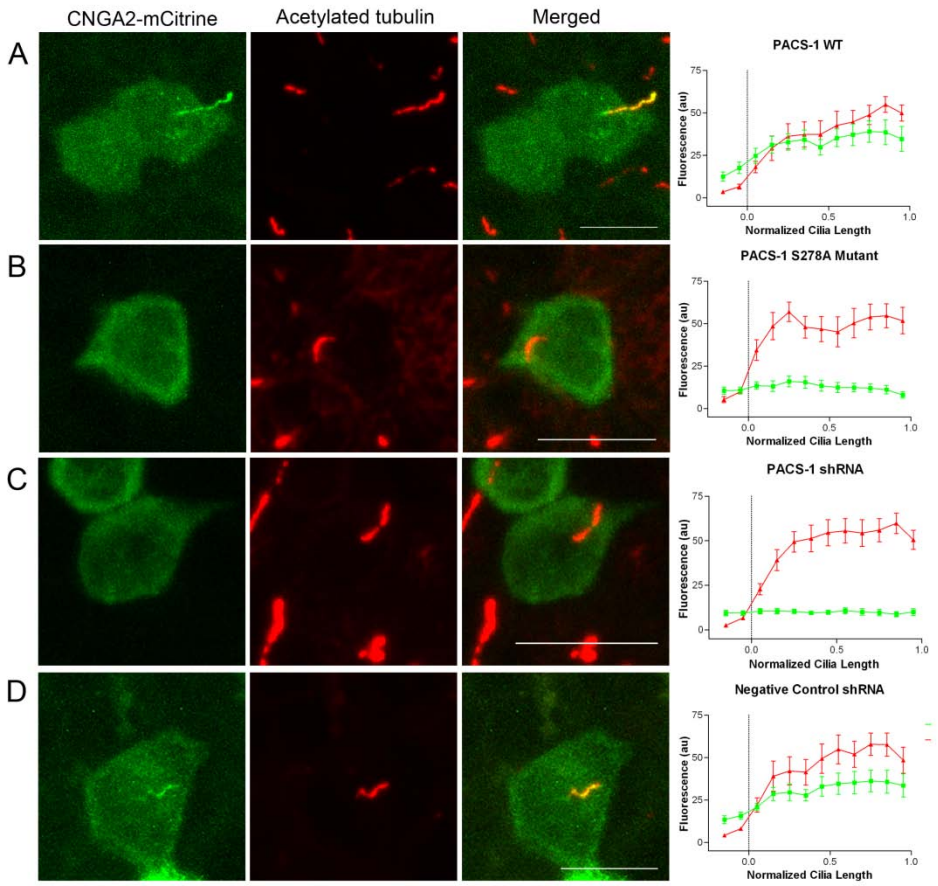

Figure 3.7 PACS-1 Regulates Ciliary Trafficking of the Olfactory CNG Channel.

CNGA2-mCitrine and CNGB1b-3xFlag were transfected into MDCK stable cell lines expressing **(A)** wild-type PACS-1, **(B)** PACS-1 S278A non-phosphorylatable mutant, **(C)** shRNA directed against PACS-1, or **(D)** negative control shRNA. Signal from CNGA2-mCitrine is shown on the left (green) and acetylated tubulin signal marking the ciliary axoneme is in the middle (red), with the merged image on the right. Bars represent 10 μm. Average data from multiple cells (n=9-11 for each condition) shown on far right. Data were apportioned into bins of $1/10^{th}$ of normalized cilia length. Acetylated tubulin signal shown in red and CNGA2-mCitrine fluorescence shown in green (arbitrary fluorescent units).

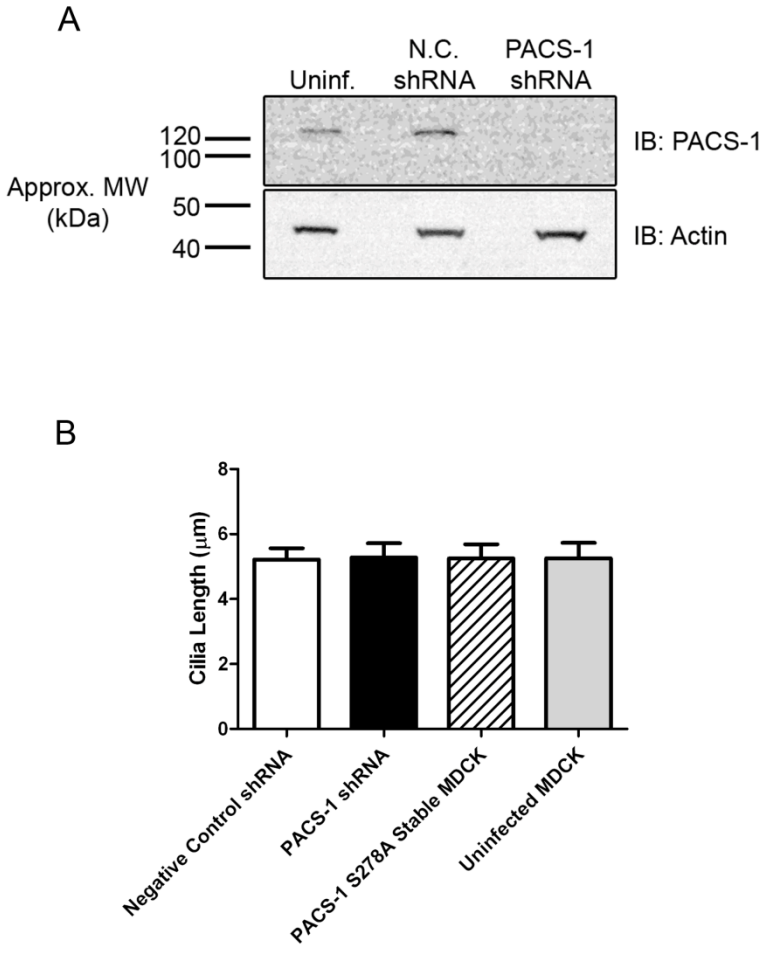

Figure 3.8 Retrovirally-Delivered shRNA Effectively Silences PACS-1 Expression but Does Not Affect Cilia Length

(A) Western blot results from lysates prepared from uninfected MDCK cells (Uninf.), MDCK cells stably-expressing negative control shRNA (N.C. shRNA), or MDCK cells stably expressing shRNA directed against PACS-1 (PACS-1 shRNA). (Top) Blot probed for PACS-1 indicates loss of expression in PACS-1 shRNA stable MDCK cells. (Bottom) Loading control blot for actin demonstrates equal loading of protein. Markers for approximate molecular weight (kDa) are shown on left. **(B)** Average cilia length of filter-grown MDCK cells stably-expressing Negative Control shRNA, PACS-1 shRNA, PACS-1 S278A, versus uninfected MDCK cells. Data are represented as mean ± SEM. No statistical significance was detected (n=15 for each condition; One-way ANOVA p=0.9998).

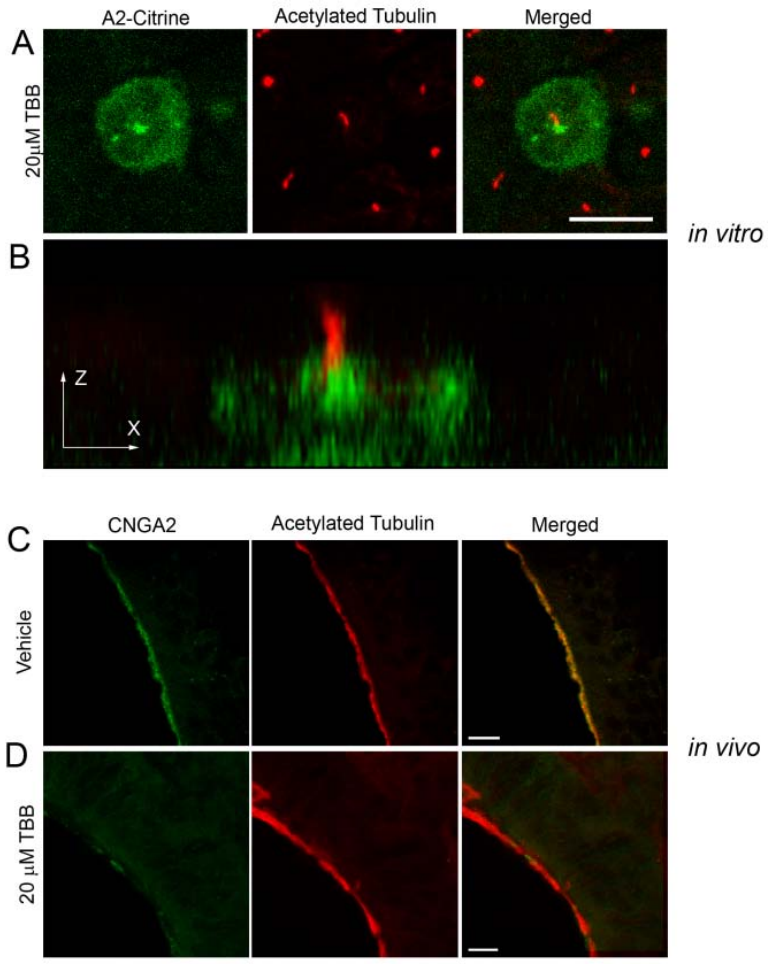

Figure 3.9 Inhibition of CK2 Activity Causes a Loss of CNG Channel Localization to Cilia in MDCK Cells and Olfactory Sensory Neurons.

(A,B) MDCK cells were transfected with CNGA2-mCitrine and CNGB1b-3xFlag and allowed time for ciliary delivery followed by 4 hours of treatment with 20 μM of the CK2 inhibitor, TBB. (A) Compressed confocal image of a MDCK cell with CNGA2-mCitrine fluorescence shown in green and acetylated tubulin staining marking cilia shown in red. Bar represents 10 μm. (B) X-Z projection of the cell from panel A demonstrating concentration of CNG channel at base of cilium. **(C)** Average cilia length of filter-grown MDCK cells treated with 0.01% DMSO vehicle (empty bar, 5.323 ± 0.552 n=33) or 20 μM TBB (filled bar, 5.230 ± 0.329 n=33). p=0.885, unpaired *t* test. Data are represented as mean ± SEM. **(C, D)** Representative compressed confocal stacks of coronal sections from OE from intranasally-injected CD1 mice. Confocal images of OE from adult CD1 mice treated with (A) DMSO vehicle or (B) 20 μM TBB for four hours. Signals shown are CNGA2 immunostaining (green, left), and acetylated tubulin immunostaining (red, middle). Merged images shown on right. Bars represent 10 μm.

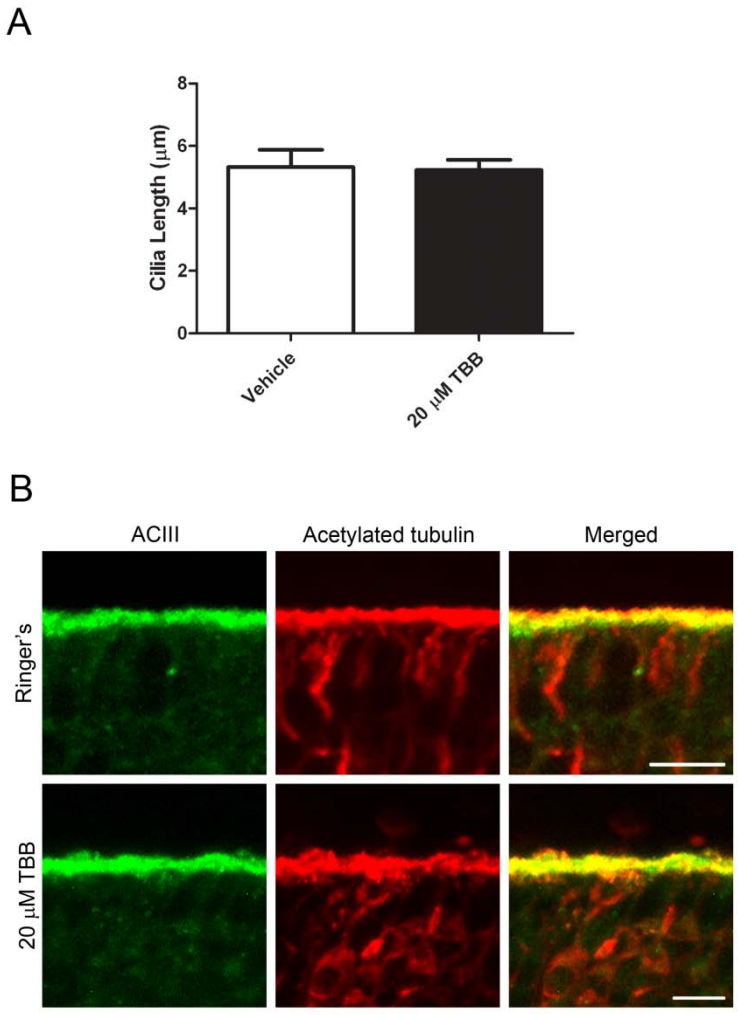

Figure 3.10 Cilia Length and ACIII Ciliary Localization are Unaffected by CK2 Inhibition.

(A) Average cilia length of filter-grown MDCK cells treated with 0.01% DMSO vehicle (empty bar, 5.323 ± 0.552 n=33) or 20 μM TBB (filled bar, 5.230 ± 0.329 n=33). p=0.885, unpaired *t* test. Data are represented as mean ± SEM. **(B)** Representative images taken from the medial surface of the olfactory turbinates exposed to either Ringer's control (top) or 20 μM TBB (bottom) for 25 minutes. Sections were coimmunostained with antibodies against ACIII (left, green) and acetylated α tubulin (middle, red). Merged images shown on right. Bars represent 10 μm.

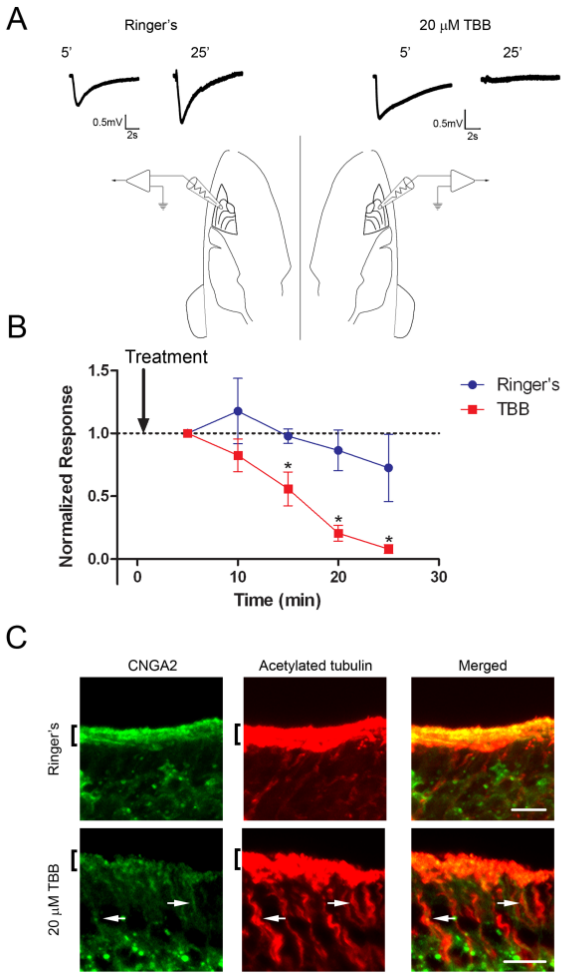

Figure 3.11 Inhibition of CK2 Alters the Ciliary Localization of Olfactory Signaling Proteins. CK2 Inhibition Impairs Olfactory Function.

(A) Representative traces from paired EOG recordings from turbinate II or IIb in response to amyl acetate. Mice were prepared as indicated in Materials and Methods and two electrodes were placed on the surface of the OE on opposite sides of the head. OE was treated with Ringer's solution control (left) or Ringer's plus 20 μM TBB (right) for 5 minutes and then EOG responses were recorded every 5 minutes. Representative traces are shown at 5 and 25 minutes for both treatments. Scale bars represent 0.5 mV and 2 seconds. **(B)** Average data demonstrate a rapid loss of EOG response from the TBB-treated OE (n=5) (* $p < 0.05$; paired t-test). Responses were normalized to the first trace taken at 5 minutes after treatment. Arrow indicates time of drug delivery. **(C)** Representative images taken from the medial surface of the olfactory turbinates exposed to either Ringer's control (top) or 20 μM TBB (bottom) for 25 minutes. Sections were coimmunostained with antibodies against CNGA2 (left, green) and acetylated α tubulin (middle, red). Merged images shown on right. Bars represent 10 μm. Arrows mark dendritic tracks with concentrated CNGA2 signal. Brackets denote cilia layer.

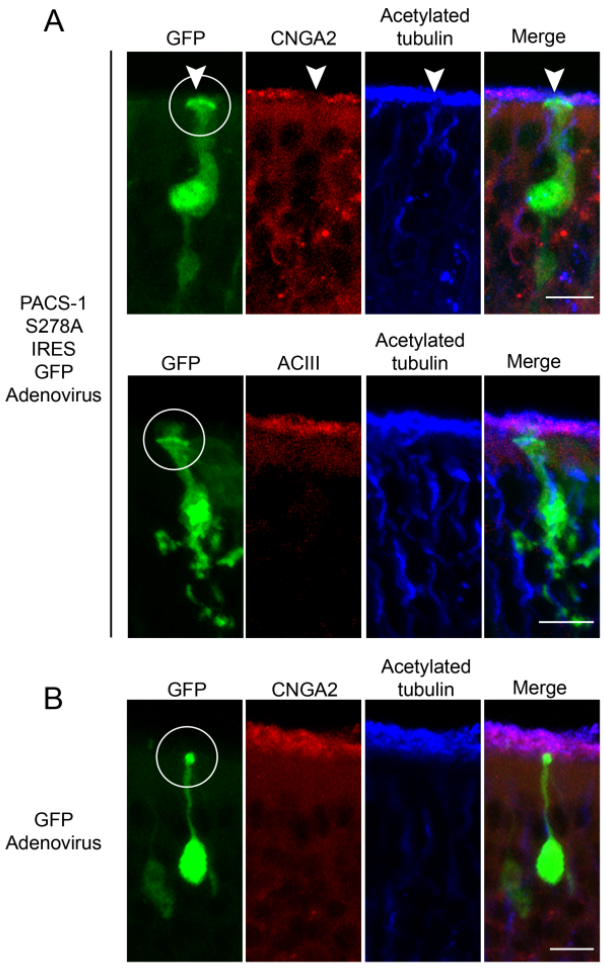

Figure 3.12 Expression of Mutant PACS-1 in Native OSNs Causes Mislocalization of the CNG Channel, but not ACIII.

Representative collapsed confocal images of coronal sections of OE from adenovirally-infected mice. **(A)** (top) Immunostaining of a PACS-1 S278A IRES GFP-infected OSN (green) with antibodies against CNGA2 (red) and acetylated α tubulin (blue) demonstrates a loss of ciliary CNG channel from the infected OSN (white arrowhead) with no change in the cilia layer. (bottom) Immunostaining of a PACS-1 S278A IRES GFP-infected OSN (green) with antibodies against ACIII (red) and acetylated α tubulin (blue) demonstrates no detectable change in ciliary ACIII or the cilia layer from the infected OSN. **(B)** Immunostaining of a GFP-infected OSN (green) with antibodies against CNGA2 (red) and acetylated α tubulin (blue) demonstrates no detectable change in ciliary CNG channel or the cilia layer from the infected OSN. For all conditions, merged image shown on right (Merge), white circles mark dendritic knobs, and bars represent 10 μm.

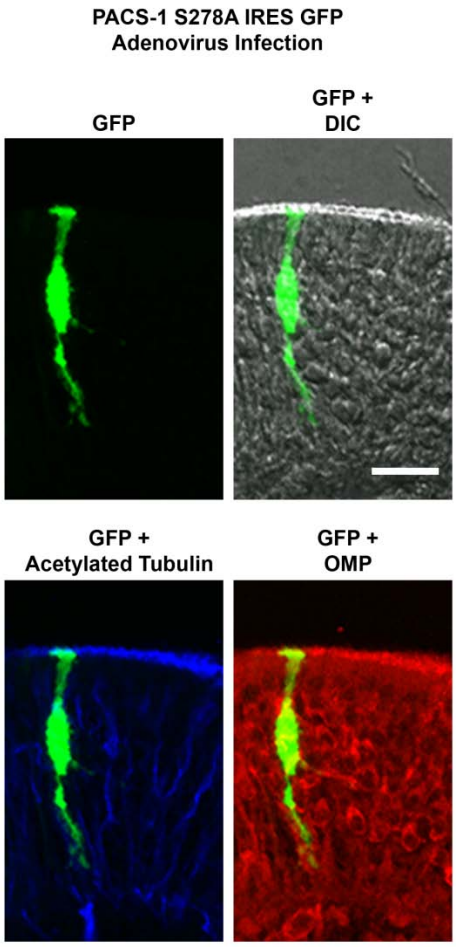

Figure 3.13 Adenovirally-Infected Cells with Altered Morphology are Mature OSNs

Representative collapsed confocal images of a coronal section of OE from adenovirally-infected mouse. A PACS-1 S278A IRES GFP-infected OSN (green, top left) can be visualized deep in the layer of OSNs as determined by overlay with a differential interference contrast image (top right). This localization can be confirmed by immunostaining and colocalization with antibodies against the ciliary marker, acetylated α tubulin (blue, bottom left) and the marker of mature OSNs, olfactory marker protein (OMP) (red, bottom right). Bar represents 20 μm.

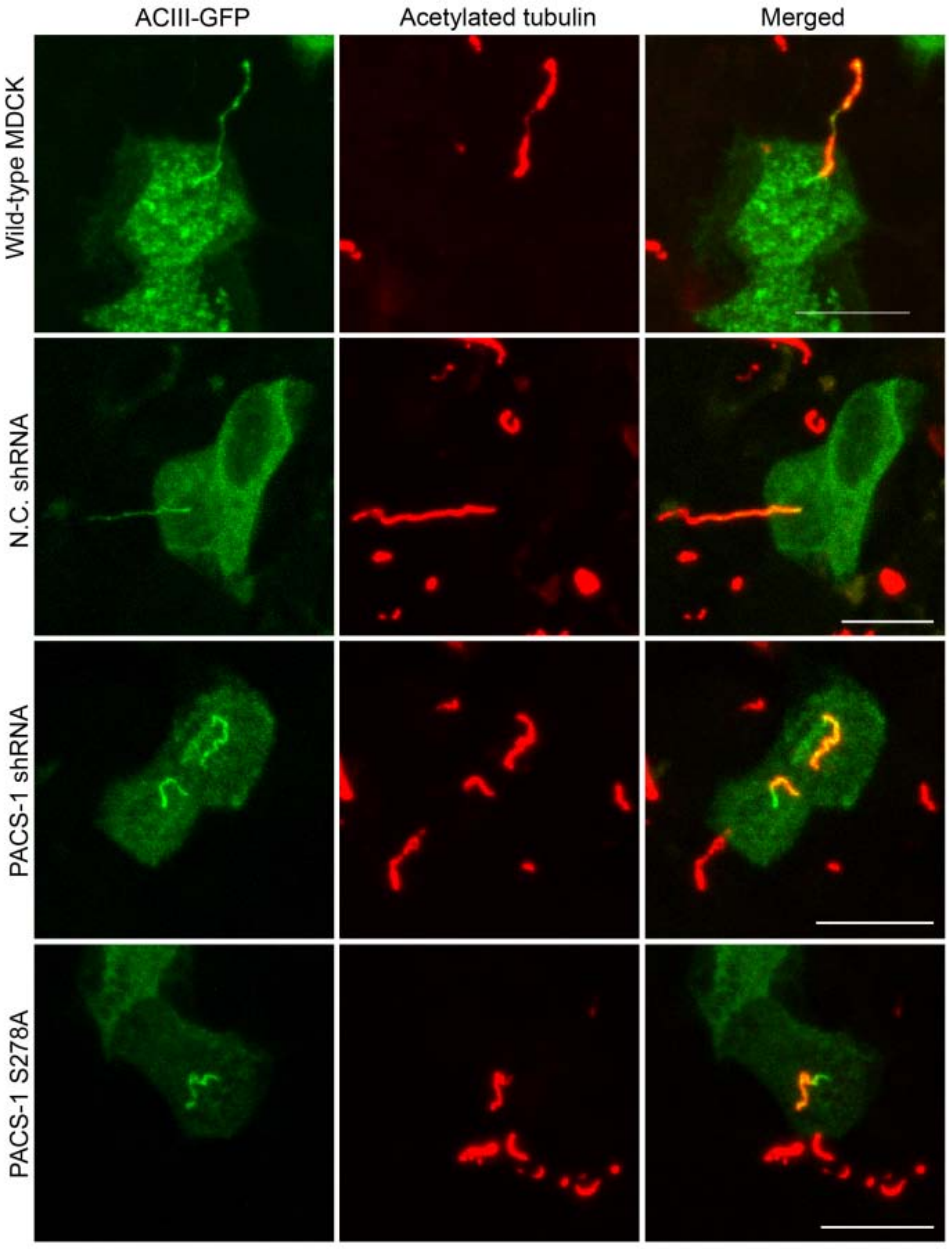

Figure 3.14 Ciliary Localization of ACIII-GFP is Unaffected by Alterations in PACS-1 Function

Representative confocal images of wild-type MDCK cells (top) or MDCK cells stably-expressing either negative control shRNA, PACS-1 shRNA, or PACS-1 S278A transfected with ACIII-GFP. Signal from ACIII-GFP is shown on the left (green) and acetylated tubulin signal marking the ciliary axoneme is in the middle (red), with the merged image on the right. Bars represent 10 μm.

CHAPTER 4

CONCLUSION

INTRODUCTION

Through the work of this thesis, we have established that heteromeric assembly with the CNGB1b subunit of the olfactory CNG channel is necessary for delivery of the channel to cilia of OSNs, where it functions as a major target of the olfactory signaling cascade. In addition, we determined that a carboxyl-terminal RVxP motif is necessary, but not sufficient, for this ciliary targeting (see summary in Illustration 4.1). After our work demonstrating the necessity of CNGB1b for olfactory CNG channel ciliary localization, it was confirmed that mice lacking the CNGB1b subunit exhibited a loss of ciliary CNG channel [95]. However, the mechanism for this subunit-dependent trafficking remained unknown.

We showed that CNGB1b associates with the intracellular trafficking protein PACS-1, and that proper function of PACS-1 is necessary for CNG channel ciliary localization. Since PACS-1 binds cargo on clusters of acidic amino acids containing CK2 phosphorylation sites, we identified two amino terminal PACS-1 binding sites on CNGB1b and show that mutation of these sites impaired ciliary targeting (Illustration

4.1). Importantly, we were able to validate these results from our model cell culture system in native OSNs.

Finally, we demonstrated a role for the kinesin motor, KIF17, in the ciliary localization of the CNG channel. Work in invertebrates has previously shown that heterotrimeric kinesin 2 and homodimeric Osm3 (invertebrate homolog of KIF17) function in IFT. Here we show for the first time that KIF17, initially thought to be a brain-specific molecular motor, functions outside of the central nervous system and plays a role in the transport of ciliary cargo. In addition to my work, KIF17 has also been found to function in cargo transport in photoreceptors where loss of KIF17 function leads to photoreceptor degradation [130], and has also been found in the placenta [173].

These findings are significant since they represent the first demonstration of a role for KIF17 in mammalian ciliary transport. Additionally, they show a CNGB1b-dependent trafficking of the olfactory CNG channel suggesting a delegation of functional responsibilities among CNG channel subunits. These reports also define the mechanism for this subunit-dependent trafficking and give us some idea of the stability of membrane proteins once inserted in the ciliary compartment. Finally, this work elucidates some of the processes controlling entry of cargo into the ciliary compartment, which may give us some insight into mechanisms of human disease.

CILIARY TARGETING MOTIFS

As described in Chapter 2, we found a carboxyl-terminal RVxP amino acid motif on CNGB1b that was necessary, but not sufficient, for delivery of the channel to cilia.

This motif was originally identified as a ciliary targeting motif in the TRP channel, polycystin-2 [88]. Interestingly, as opposed to our studies, Geng *et al.* found that this motif was both necessary and sufficient for ciliary trafficking. This may represent a difference between the cell lines used (MDCK cells versus LLC-PK1 cells) or the cargos in which the motif was inserted (CNGA2 versus transferrin receptor). Recently, it was shown that a similar ciliary trafficking motif found in rhopodsin (xVxP) binds to the small GTPase, Arf4 [89, 174]. Interference with the GTPase activity of Arf4 caused a mislocalization of rhodopsin from the outer segments of transgenic mice. It would be interesting to determine if the RVxP motif found in CNGB1b is also responsible for channel trafficking via the actions of Arf4. Finally, a stretch of amino acids on the intracellular carboxyl-terminal tail of polycystin 1 was found to be necessary for its ciliary localization [175]. Although the exact sequence necessary for this trafficking was not examined further, this stretch does contain an xVxP motif on the distal end of its carboxyl terminus.

In addition to xVxP, several other ciliary targeting motifs have been identified. For example, a recent study showed that several ciliary G protein-coupled receptors contain a loosely-conserved AX[S/A]XQ motif in their 3rd intracellular loop and that this sequence is necessary and sufficient for ciliary trafficking of receptors in IMCD-3 cells. Another group found that the ciliary localization of the small protein cystin is dependent on an AxEGG motif [176]. Finally, we and others have found that the PACS-1 binding motif, consisting of acidic amino acid clusters containing phosphorylatable serine or threonine residues, is necessary for ciliary transport [85, 177].

From these reports it is clear that, although several different trafficking sequences have been identified, there is not a unique, ubiquitous ciliary trafficking motif. In fact, amino acid sequence analysis of known ciliary proteins fails to yield a conserved ciliary targeting sequence. For example, the AX[S/A]XQ motif, found by Berbari *et al,.* exists only in a few of the over 350 predicted odorant receptors found in humans. How are the other ORs entering cilia? Do they still utilize the same cellular machinery despite the lack of this trafficking motif? Future work to identify the interacting partners of these ciliary targeting signals will allow us to determine the exclusivity of the interactions between motors and cargos.

One interesting idea is that kinesin motors interact with their cargo indirectly through intermediate partners such as scaffolding proteins. For example, kinesin 1 interacts with ApoER2 through the intermediate JNK-interacting proteins (JIPs) which serve as cellular scaffolds [178]. In addition, KIF17 was shown to interact with the NMDA receptor through members of the LIN complex [146]. It is interesting to speculate that these different targeting motifs serve to allow interaction of members of the signaling cascade with each other through a scaffolding protein.

The preformation of signaling proteins as a complex, before entry into the cilium, may allow a more efficient organization of the signaling cascades. After all, the olfactory signaling cascade involves the coordination of a multitude of signaling proteins within a tiny subcellular compartment with millisecond temporal precision. Since OSNs are constantly regenerating, this targeting process recurs multiple times, which highlights the need for a rapid and efficient process. Virtually no information is known regarding the

timing of signaling complex assembly. In addition, most mutations to known ciliary transport proteins cause a loss of the cilium itself. This confounds the analysis of the function of the remaining ciliary transport proteins. However, recently we have uncovered a mutation that impairs transport of some, but not all, of the members of the olfactory signaling cascade. Hypomorphic mutations in CEP290 cause a mislocalization of the olfactory G proteins, without affecting ACIII, the CNG channel, or the ORs. In addition, work presented in this thesis shows that inhibition of PACS-1 function impairs CNG channel ciliary localization without affecting ACIII. These results could mean two possibilities regarding the timing of signal complex formation: members of the signaling cascade are transported into the cilium independently and then interact as part of a complex or they form a complex before entry into the cilium with no requirements for the presence of the entire signaling cascade. Future work will allow us to differentiate between these possibilities and perhaps identify the adaptor proteins that allow interaction of olfactory ciliary cargo with their respective kinesin motors.

Differences between Cilia Types

It has been suggested that cilia and flagella are conserved organelles both between species and within a single organism. Much of this has been based on the high level of homology of ciliary genes between species as well as the broad range of phenotypes seen with mutations of ciliary genes. Early work on ciliopathies identified numerous cilia-related phenotypes that seemed to be shared (e.g. polycystic kidneys, retinal degeneration, *situs inversus*, hydrocephaly, infertility, anosmia). However, recent work has highlighted differences in ciliated systems. For example, OSM-3 has been clearly

shown to play a role in maintenance of cilia length in *C. elegans;* however, inhibition of the mammalian homolog of OSM-3, KIF17, had no effect on cilia length [68-69]. LCA patients with hypomorphic mutations in CEP290 exhibit anosmia and early-onset retinal degeneration without a renal phenotype [82, 129], indicating variable requirements for CEP290 in normal cilia function. Mice lacking BBS4 have been shown to be deficient in sperm flagellum formation, but not in the formation of other cilia types within the same animal [121]. Despite the existence of proteins that are required for all cilia types (e.g. KIF3a), we are now beginning to find proteins that are only necessary for a subset of ciliated/flagellated cells.

One reason for the divergent phenotypes seen between ciliated cells upon mutation/loss of cilia-related proteins is the dependence of these systems on different signaling cascades. For example, mutation of a protein that specifically alters CNG channel ciliary transport would be predicted to affect retina and OE, but not other systems that do not rely on the CNG channel for signaling. This is demonstrated by the case of hypomorphic CEP290 mutations, which affect ciliary G protein localization in the OE and interactions with RPGR in the retina. However, the renal cilia signaling cascade (including polycystin 1 and 2) is likely unaffected since mice with these mutations lack an apparent renal phenotype. The specificity of the trafficking defect is likely due, at least in part, to interactions with adaptor proteins and scaffolds at the ciliary transition zone.

It is becoming clear that that the divergent phenotypes seen with mutations in various ciliary proteins is due, at least in part, to differences in the cargo that is affected

by the mutation. One pleiotropic ciliopathy with a wide range of phenotypes is Bardet-Biedl syndrome. Mutations in the core members of the BBS complex cause a range of symptoms including polycystic kidneys, retinal degeneration, polydactyly, and olfactory dysfunction. Often, mutation of BBS proteins causes a loss, or at least a time-dependent degradation, of cilia. However, sperm flagella formation is critically-dependent on proper BBS protein function [121]. The loss of cilia in these systems has hindered elucidation of BBS protein function in ciliary transport. However, a recent study using *C. reinhardtii* was able to purify members of the core BBS complex (BBS1/2/4/5/7/8/9) and examine the dysfunction resulting from mutations in these proteins [179]. Mutants for BBS1, 4 and 7 are able to assemble full-length flagella, but are unable to perform phototaxis indicating a defect in signaling in these flagella. Interestingly, the BBS4 mutants still exhibit normal IFT suggesting that BBS4 may be necessary to link some signaling proteins to IFT machinery. Indeed, a subset of putative signaling proteins, including phospholipase D and a serine/threonines kinase, were found to be accumulated in flagella from these mutants. It was also found in this study that mutants for BBS1 had a dramatic loss of BBS4 protein, which supports the previous finding that BBS1 is a core interacting protein for the BBSome [180]. Therefore, a loss of function of certain BBS proteins can affect the localization of specific ciliary proteins, which may help to explain the divergent phenotypes seen in different ciliopathies.

Many ciliary proteins, such as the BBS and IFT proteins, form complexes that are transported along the ciliary axoneme and are responsible for interactions with ciliary cargo. However, as previously described, mutations or loss of these proteins affect

subsets of ciliary cargo. It is likely that these proteins have several cytoplasmic faces responsible for interacting with multiple ciliary cargos. Thus, mutation in one cargo interaction site may not affect transport of other cargo, whereas mutation of a site necessary for interaction with the entire IFT complex may interfere with transport of a larger number of proteins. The idea that BBS is caused by mutations in any member of the BBSome and that mutations at different sites within a single BBS protein may affect different cargos could explain the various phenotypes seen within the BBS patient population. Future work to identify the exact function of ciliary transport proteins, such as the IFT or BBS complexes, will allow further insight into the mechanisms contributing to the diverse phenotypes seen with different ciliopathies.

Basal Body/ Transition Zone Protein Complex

A major site for the regulation of cargo entry into the cilium is the basal body/transition zone. The basal body is a modified centriole from which the ciliary microtubules project. The transition zone is a region between the triplet microtubules of the basal body and the double microtubules of the ciliary axoneme. A complex of proteins exists at the transition zone that acts as a docking site for cargo and IFT proteins and serves to restrict access to the cilium. For instance, even overexpression of small non-ciliary proteins such as GFP will not force aberrant entry of this protein into the ciliary compartment. Specific interactions of the members of this protein complex with ciliary cargo likely mediate the differential trafficking phenotypes seen with loss or mutation of complex proteins.

Although some of the members of the basal body "gate" complex have been identified, very little is known about how these proteins function or what other potential partners also localize to this critical region. It has been shown that some members of the nephrocystin family are localized to the ciliary base in several cell types, including respiratory cells and OSNs [82, 85]. Members of the BBS family of proteins are often found at the base of cilia; however their localization in OSNs remains virtually unexplored, with only one report localizing BBS4 to the "ciliated border" of the OE [84]. One member of the nephrocystin family, CEP290, is also found in the dendritic knob [82]. Finally, PACS-1 is highly localized in the dendritic knob. These proteins most likely represent only a fraction of the constituents of the basal body/transition zone complex. In addition, due to the complex nature of the dendritic knob, high-resolution microscopy, such as immunogold localization, is necessary to pinpoint the exact location of these proteins with respect to the basal body and transition zone.

While the exact function and structural components of the ciliary "gate" remain poorly understood, there are some striking similarities between this barrier and the nuclear pore complex. For example, some members of the IFT complex share homology with the COPI vesicle proteins, which are structurally similar to components of the nuclear pore complex [181]. Transport through the nuclear pore is regulated by RAN GTPase, which interacts with cargo containing nuclear localization signals. Interestingly, work done in collaboration with the Kristen Verhey laboratory has found that the ciliary motor KIF17 contains an amino acid sequence similar to a nuclear localization signal, which is necessary for entry into the cilium. Interestingly, the fragment containing this

sequence is also able to enter the nucleus, presumably thought the nuclear pore complex. In addition to these findings, the Retinitis Pigmentosa G-protein Regulator protein, which also functions as a guanine nucleotide exchange factor, has been found at or near the transition zone in several cell types [182]. It will be interesting to see if there are further similarities between the nuclear pore complex and the molecular gate at the ciliary transition zone.

ROLE OF KIF17 IN CILIA TRANSPORT

While we demonstrated that KIF17 is essential for ciliary localization of the olfactory CNG channel, the exact role KIF17 is playing in this pathway remains unclear. KIF17 was found along the ciliary axoneme in MDCK cells and in the ciliated border of the OE, which would suggest that KIF17 is functioning in IFT like its invertebrate homolog Osm3. However, IFT occurs at a relatively fast rate, on the order of 1-2 microns/sec. Analysis of CNG channel mobility in MDCK primary cilia showed an extremely long time of recovery, with a time constant over 10 minutes. This indicates that it is unlikely that KIF17 is actively moving the CNG channel within the cilium.

If KIF17 is not actively transporting the channel along the ciliary axoneme, how is it controlling the channel's ciliary localization? One explanation could be that KIF17 is responsible for the transport across the transition zone. There is evidence of a vesicular pool near the basal body, however the site of vesicle fusion where transmembrane proteins like the CNG channel are inserted remains poorly understood. Perhaps ciliary transmembrane proteins are transported on vesicles by cellular kinesin and myosin

molecular motors, inserted into the plasma membrane, and then transported across the transition zone by KIF17.

Another possibility is that KIF17 does not participate in IFT or in moving proteins across the transition zone, but rather delivers cargo-containing vesicles to the site of fusion at the base of the cilium. In this case, one would expect that inhibition of KIF17 function, as is found with the use of a KIF17DN would still impair ciliary localization of its cargo. Interestingly, KIF17 has been shown to be involved in a direct transport of NMDA receptor-containing vesicles from the ER to Golgi outposts in the dendrites of hippocampal neurons [183]. Also, work on nephrocystin ciliary trafficking found areas of the Golgi marker, Golgin97, at the ciliary base in respiratory epithelial cells [85]. Perhaps KIF17 is involved in the transport of the CNG channel through the secretory pathway by directing trafficking from the ER to Golgi protein-rich regions at the base of the cilium. Future work is necessary to differentiate between these possibilities.

FUNCTIONAL COOPERATION OF MAMMALIAN CILIARY KINESIN MOTORS

Most of the early advances in the understanding of cilia biology came from the use of invertebrate systems. In fact, the discovery of IFT was made in the laboratory of Joel Rosenbaum using the biflagellate green alga *Chlamydomonas* [62]. It was found in *C. elegans* that there were two molecular motors responsible for building cilia: heterotrimeric kinesin II and homodimeric Osm3 [184]. These two motors function in a coordinated manner to build the cilium, with kinesin II building the 4 μm-long microtubule doublets extending from the basal body, and Osm3 forming the 2.5 μm-long distal microtubule singlets [66]. Interestingly, we found no effect on average cilia length

when KIF17 function was inhibited in MDCK cell primary cilia [68]. This apparent difference between invertebrate and mammalian cilia could arise from a functional specialization of duties for the two ciliary kinesin motors, where kinesin II is responsible for the assembly and maintenance of cilia while KIF17 is important for the delivery of signaling proteins into the ciliary compartment. However, it is also important to note that, in *C. elegans*, Osm3 is required for building the distal segments of cilia, which are composed of singlet microtubules. Transmission electron microscopy experiments performed in our laboratory failed to detect the existence of a singlet microtubule "distal segment" in MDCK primary cilia, leaving open the possibility that KIF17 does play some role in maintenance of cilia length at least in the case of cilia with singlet microtubule extensions. Interestingly, mammalian olfactory cilia axonemes contain extremely long singlet microtubule extensions which extend over 50 microns. It would be interesting to perform experiments examining the role of KIF17 in ciliary transport in native OE by examining OSN structure in the presence of the KIF17DN or in a KIF17-null background.

SUMMARY

In summary, the work of this thesis has shown that heteromeric assembly with the CNGB1b subunit of the olfactory CNG channel is necessary for ciliary trafficking in OSNs, where it functions as a major target of the olfactory signaling cascade. We demonstrated that a carboxyl-terminal RVxP motif is necessary, but not sufficient, for this ciliary targeting (see summary in Illustration 4.1). We were able to define the mechanism for subunit-dependent CNG channel trafficking by demonstrating that

CNGB1b associates with the intracellular trafficking protein PACS-1, and showing that PACS-1 function is necessary for CNG channel ciliary localization. In addition, we have shown a role for the kinesin motor, KIF17, in the ciliary localization of the CNG channel: the first report of KIF17 participating in mammalian ciliary transport. Importantly, we were able to confirm much of this work by examining mechanisms of ciliary transport in native OSNs.

Additional experiments are necessary to further elucidate the mechanisms of mammalian ciliary transport. Hopefully the work of this thesis will provide a starting point for studies of cilia trafficking in OSNs, and will allow the further expansion of our thinking regarding the mechanisms a cell utilizes to control subcellular localization of signaling proteins. I am glad that I was able to contribute to this exciting and rapidly expanding field of cilia biology.

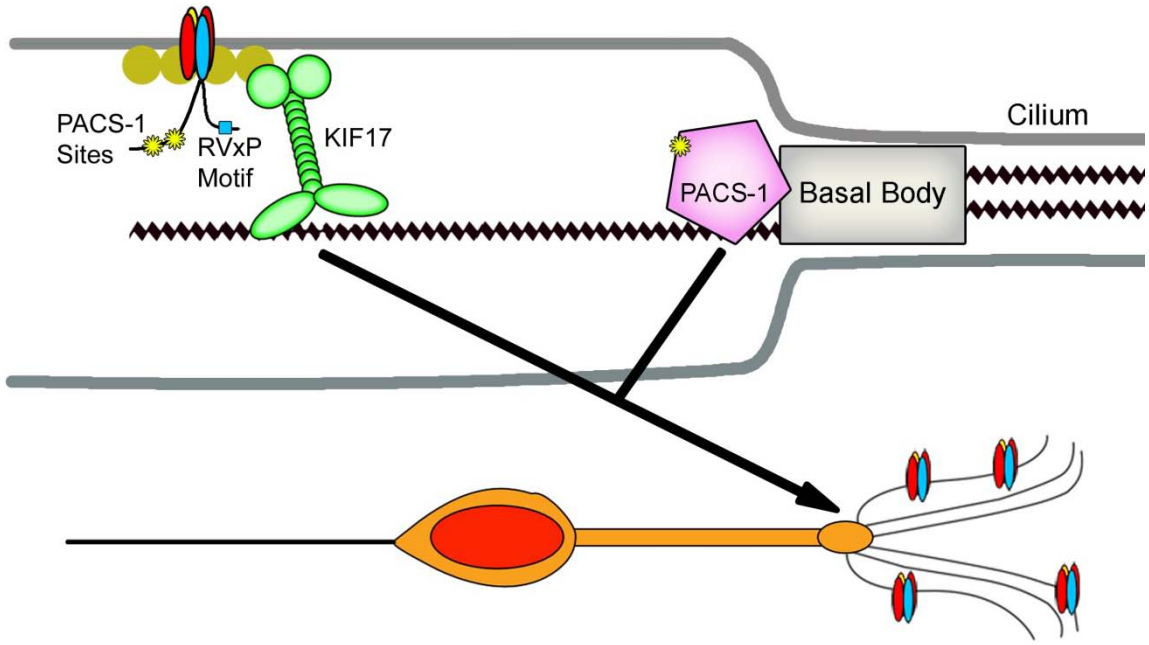

Illustration 4.1 Model of Requirements for Olfactory CNG Channel Ciliary Localization

The olfactory CNG channel comprises 3 subunits: CNGA2 (red), CNGA4 (yellow) and CNGB1b (blue). CNGB1b contains two amino-terminal PACS-1 binding sites (yellow stars) which can be phosphorylated by CK2. In addition, CNGB1b contains a carboxy-terminal RVxP motif, which is necessary, but not sufficient for CNG channel ciliary localization. The CNG channel is transported into cilia through the actions of the homodimeric kinesin motor, KIF17 (green). PACS-1, which is also phosphorylated by CK2, localizes to the basal body-containing dendritic knob and controls ciliary localization of the CNG channel in OSNs (shown in orange).

APPENDIX I

COPYRIGHT RELEASES

- Jenkins, P.M., McEwen, D.P., and Martens, J.R. (2009). Olfactory cilia: linking sensory cilia function and human disease. Chem Senses *34,* 451-64.

  Page 105

- Jenkins, P.M., Hurd, T.W., Zhang, L., McEwen, D.P., Brown, R.L., Margolis, B., Verhey, K.J., and Martens, J.R. (2006). Ciliary targeting of olfactory CNG channels requires the CNGB1b subunit and the kinesin-2 motor protein, KIF17. Curr Biol *16*, 1211-1216.

  Page 106

- Jenkins, P.M., Zhang, L., Thomas, G., and Martens, J.R. (2009). PACS-1 mediates phosphorylation-dependent ciliary trafficking of the cyclic-nucleotide-gated channel in olfactory sensory neurons. J Neurosci *29*, 10541-10551.

  Page 107

License Details

This is a License Agreement between Paul M Jenkins ("You") and Oxford University Press ("Oxford University Press"). The license consists of your order details, the terms and conditions provided by Oxford University Press, and the payment terms and conditions.

Get the printable license.

License Number	2325461312334
License date	Dec 10, 2009
Licensed content publisher	Oxford University Press
Licensed content publication	Chemical Senses
Licensed content title	Olfactory Cilia: Linking Sensory Cilia Function and Human Disease
Licensed content author	Paul M. Jenkins, et. al.
Licensed content date	June 2009
Type of Use	Thesis / Dissertation
Institution name	UMI Dissertation Publishing (a division of ProQuest)
Title of your work	Mechanisms of Ciliary Targeting of the Olfactory CNG Channel
Publisher of your work	UMI Dissertation Publishing (a division of ProQuest)
Expected publication date	Jan 2010
Billing type	Invoice
Company	Paul M Jenkins
Billing address	1301 MSRBIII 1150 W. Medical Center Dr. Ann Arbor, MI 48109-5632 United States
Customer reference info	
Permissions cost	0.00 USD
Value added tax	0.00 USD
Total	0.00 USD

BACK

Powered by RIGHTSLINK COPYRIGHT CLEARANCE CENTER, INC. Home Help

Logged in as:
Paul Jenkins
Account #:
3000260989
LOGOUT

License Details

Thank you for placing your Rightslink license request for reuse of Elsevier Limited content.

Get the printable license.

License Number	2325470300818
License date	Dec 10, 2009
Licensed content publisher	Elsevier
Licensed content publication	Current Biology
Licensed content title	Ciliary Targeting of Olfactory CNG Channels Requires the CNGB1b Subunit and the Kinesin-2 Motor Protein, KIF17
Licensed content author	Paul M. Jenkins, Toby W. Hurd, Lian Zhang, Dyke P. McEwen, R. Lane Brown, Ben Margolis, Kristen J. Verhey and Jeffrey R. Martens
Licensed content date	20 June 2006
Volume number	16
Issue number	12
Pages	6
Type of Use	Thesis / Dissertation
Portion	Full article
Format	Both print and electronic
You are the author of this Elsevier article	Yes
Are you translating?	No
Order Reference Number	
Expected publication date	Jan 2010
Elsevier VAT number	GB 494 6272 12
Billing type	Invoice
Company	Paul M Jenkins
Billing address	1301 MSRBIII 1150 W. Medical Center Dr. Ann Arbor, MI 48109-5632 United States
Customer reference info	
Permissions price	0.00 USD
Value added tax 0.0%	0.00 USD
Total	0.00 USD

BACK

COPYRIGHT CLEARANCE CENTER

Confirmation Number: 2407351
Order Date: 12/10/2009

Customer Information

Customer: Paul Jenkins
Account Number: 3000260989
Organization: Paul Jenkins
Email: pjenkins@umich.edu
Phone: +1 (734)6473132
Payment Method: Invoice

Order Details

JOURNAL OF NEUROSCIENCE. ONLINE
Order detail ID: 38602949

ISBN/ISSN: 1529-2401
Publication Year: 2009
Publisher: SOCIETY FOR NEUROSCIENCE
Rightsholder: SOCIETY FOR NEUROSCIENCE
Author/Editor: Paul Jenkins

Permission Status: **Granted**
Permission type: Republish into a book, journal, newsletter...
Requested use: Dissertation
Republication title: CILIARY TARGETING OF THE OLFACTORY CNG CHANNEL
Republishing organization: UMI (A DIVISION OF PROQUEST)
Organization status: For profit
Republication date: 01/29/2010
Circulation/Distribution: 10
Type of content: Full article chapter
Description of requested content: Graduate Dissertation
Page range(s): 10541-10551
Requested content's publication date: 08/26/2009
Your reference: PAUL'S THESIS, CHAPTER 3

Billing Status: **Not Billed**

$3.00

Order Total: $3.00

BIBLIOGRAPHY

1. Carr, V.M., Menco, B.P., Yankova, M.P., Morimoto, R.I., and Farbman, A.I. (2001). Odorants as cell-type specific activators of a heat shock response in the rat olfactory mucosa. J Comp Neurol *432*, 425-439.

2. Hegg, C.C., Greenwood, D., Huang, W., Han, P., and Lucero, M.T. (2003). Activation of purinergic receptor subtypes modulates odor sensitivity. J Neurosci *23*, 8291-8301.

3. Kern, R.C., and Pitovski, D.Z. (1997). Localization of 11 beta-hydroxysteroid dehydrogenase: specific protector of the mineralocorticoid receptor in mammalian olfactory mucosa. Acta oto-laryngo logica *117*, 738-743.

4. Menco, B.P., Birrell, G.B., Fuller, C.M., Ezeh, P.I., Keeton, D.A., and Benos, D.J. (1998) . Ultrastructural localization of amiloride-sensitive sodium channels and Na+,K(+)-ATPase in the rat's olfactory epithelial surface. Chemical senses *23*, 137-149.

5. Lin, W., Margolskee, R., Donnert, G., Hell, S.W., and Restrepo, D. (2007). Olfactory neurons expressing transient receptor potential channel M5 (TRPM5) are involved in sensing semiochemicals. Proceedings of the National Academy of Sciences of the United States of America *104*, 2471-2476.

6. Moran, D.T., Rowley, J.C., 3rd, and Jafek, B.W. (1982). Electron microscopy of human olfactory epithelium reveals a new cell type: the microvillar cell. Brain Res *253*, 39-46.

7. Moran, D.T., Rowley, J.C., 3rd, Jafek, B.W., and Lovell, M.A. (1982). The fine structure of the olfactory mucosa in man. J Neurocytol *11*, 721-746.

8. Rowley, J.C., 3rd, Moran, D.T., and Jafek, B.W. (1989). Peroxidase backfills suggest the mammalian olfactory epithelium contains a second morphologically distinct class of bipolar sensory neuron: the microvillar cell. Brain Res *502*, 387-400.

9. Murdoch, B., and Roskams, A.J. (2007). Olfactory epithelium progenitors: insights from transgenic mice and in vitro biology. J Mol Histol *38*, 581-599.

10. Cuschieri, A., and Bannister, L.H. (1975). The development of the olfactory mucosa in the mouse: light microscopy. J Anat *119*, 277-286.

11. Cuschieri, A., and Bannister, L.H. (1975). The development of the olfactory mucosa in the mouse: electron microscopy. J Anat *119*, 471-498.

12. Wheatley, D.N., Wang, A.M., and Strugnell, G.E. (1996). Expression of primary cilia in mammalian cells. Cell Biol Int *20*, 73-81.

13. Okada, Y., Takeda, S., Tanaka, Y., Belmonte, J.C., and Hirokawa, N. (2005). Mechanism of nodal flow: a conserved symmetry breaking event in left-right axis determination. Cell *121*, 633-644.

14. Menco, B.P. (1984). Ciliated and microvillous structures of rat olfactory and nasal respiratory epithelia. A study using ultra-rapid cryo-fixation followed by freeze-substitution or freeze-etching. Cell and tissue research *235*, 225-241.

15. Dabdoub, A., and Kelley, M.W. (2005). Planar cell polarity and a potential role for a Wnt morphogen gradient in stereociliary bundle orientation in the mammalian inner ear. J Neurobiol *64*, 446-457.

16. Reese, T.S. (1965). Olfactory cilia in the frog. The Journal of cell biology *25*, 209-230.

17. Lidow, M.S., and Menco, B.P. (1984). Observations on axonemes and membranes of olfactory and respiratory cilia in frogs and rats using tannic acid-supplemented fixation and photographic rotation. J Ultrastruct Res *86*, 18-30.

18. Bronshtein, A.A., and Minor, A.V. (1973). [Significance of flagellae and their mobility for olfactory receptor function]. Doklady Akademii nauk SSSR *213*, 987-989.

19. Mair, R.G., Gesteland, R.C., and Blank, D.L. (1982). Changes in morphology and physiology of olfactory receptor cilia during development. Neuroscience *7*, 3091-3103.

20. Menco, B.P., and Morrison, E.E. (2003). Morphology of the Mammalian Olfactory Epithelium: Form, Fine Structure, Function, and Pathology. In Handbook on Olfaction and Gustation, 2 Edition, R.L. Doty, ed. (New York: Informa Health Care), pp. 17-49.

21. Menco, B.P. (1980). Qualitative and quantitative freeze-fracture studies on olfactory and nasal respiratory epithelial surfaces of frog, ox, rat, and dog. II. Cell apices, cilia, and microvilli. Cell and tissue research *211*, 5-29.

22. Menco, B.P. (1997). Ultrastructural aspects of olfactory signaling. Chemical senses *22*, 295-311.

23. Menco, B. (1992). Ultrastructural studies on membrane, cytoskeletal, mucous, and protective compartments in olfaction. Microscopy research and technique *22*, 215-224.

24. Rosenbaum, J.L., and Witman, G.B. (2002). Intraflagellar Transport. Nat Rev Mol Cell Biol *3*, 813-825.

25. Scholey, J.M. (2003). Intraflagellar transport. Annual review of cell and developmental biology *19*, 423-443.

26. Hammond, J.W., Cai, D., and Verhey, K.J. (2008). Tubulin modifications and their cellular functions. Curr Opin Cell Biol *20*, 71-76.

27. Pathak, N., Obara, T., Mangos, S., Liu, Y., and Drummond, I.A. (2007). The zebrafish fleer gene encodes an essential regulator of cilia tubulin polyglutamylation. Mol Biol Cell *18*, 4353-4364.

28. Schwarzenbacher, K., Fleischer, J., and Breer, H. (2005). Formation and maturation of olfactory cilia monitored by odorant receptor-specific antibodies. Histochem Cell Biol *123*, 419-428.

29. Flannery, R.J., French, D.A., and Kleene, S.J. (2006). Clustering of cyclic-nucleotide-gated channels in olfactory cilia. Biophysical journal *91*, 179-188.

30. Matsuzaki, O., Bakin, R.E., Cai, X., Menco, B.P., and Ronnett, G.V. (1999). Localization of the olfactory cyclic nucleotide-gated channel subunit 1 in normal, embryonic and regenerating olfactory epithelium. Neuroscience *94*, 131-140.

31. Brady, J.D., Rich, T.C., Le, X., Stafford, K., Fowler, C.J., Lynch, L., Karpen, J.W., Brown, R.L., and Martens, J.R. (2004). Functional role of lipid raft microdomains in cyclic nucleotide-gated channel activation. Mol Pharmacol *65*, 503-511.

32. Schreiber, S., Fleischer, J., Breer, H., and Boekhoff, I. (2000). A possible role for caveolin as a signaling organizer in olfactory sensory membranes. The Journal of biological chemistry *275*, 24115-24123.

33. Kobayakawa, K., Hayashi, R., Morita, K., Miyamichi, K., Oka, Y., Tsuboi, A., and Sakano, H. (2002). Stomatin-related olfactory protein, SRO, specifically expressed in the murine olfactory sensory neurons. J Neurosci *22*, 5931-5937.

34. Goldstein, B.J., Kulaga, H.M., and Reed, R.R. (2003). Cloning and characterization of SLP3: a novel member of the stomatin family expressed by olfactory receptor neurons. J Assoc Res Otolaryngol *4*, 74-82.

35. Tillman, T.S., and Cascio, M. (2003). Effects of membrane lipids on ion channel structure and function. Cell Biochem Biophys *38*, 161-190.

36. Andrews, D., and Nelson, D.L. (1979). Biochemical studies of the excitable membrane of Paramecium tetraurelia. II. Phospholipids of ciliary and other membranes. Biochim Biophys Acta *550*, 174-187.

37. Hennessey, T.M., Andrews, D., and Nelson, D.L. (1983). Biochemical studies of the excitable membrane of Paramecium tetraurelia. VII. Sterols and other neutral lipids of cells and cilia. J Lipid Res *24*, 575-587.

38. Chailley, B., Boisvieux-Ulrich, E., and Sandoz, D. (1983). Evolution of filipin-sterol complexes and intramembrane particle distribution during ciliogenesis. J Submicrosc Cytol *15*, 275-280.

39. Andres, K.H. (1969). Der olfaktorische Saum der Katze. Z Zellforsch Mikrosk Anat *96*, 140-154.

40. Gilula, N.B., and Satir, P. (1972). The ciliary necklace. A ciliary membrane specialization. The Journal of cell biology *53*, 494-509.

41. Menco, M. (1980). Qualitative and quantitative freeze-fracture studies on olfactory and respiratory epithelial surfaces of frog, ox, rat, and dog. IV. Ciliogenesis and ciliary necklaces (including high-voltage observations). Cell and tissue research *212*, 1-16.

42. Satir, P., and Christensen, S.T. (2007). Overview of structure and function of mammalian cilia. Annual review of physiology *69*, 377-400.

43. Carson, J.L., Collier, A.M., Knowles, M.R., Boucher, R.C., and Rose, J.G. (1981). Morphometric aspects of ciliary distribution and ciliogenesis in human nasal epithelium. Proceedings of the National Academy of Sciences of the United States of America *78*, 6996-6999.

44. Deane, J.A., Cole, D.G., Seeley, E.S., Diener, D.R., and Rosenbaum, J.L. (2001). Localization of intraflagellar transport protein IFT52 identifies basal body transitional fibers as the docking site for IFT particles. Curr Biol *11*, 1586-1590.

45. Dirksen, E.R. (1974). Ciliogenesis in the mouse oviduct. A scanning electron microscope study. J Cell Biol *62*, 899-904.

46. Hagiwara, H., Ohwada, N., and Takata, K. (2004). Cell biology of normal and abnormal ciliogenesis in the ciliated epithelium. Int Rev Cytol *234*, 101-141.

47. Burton, P.R. (1992). Ultrastructural studies of microtubules and microtubule organizing centers of the vertebrate olfactory neuron. Microscopy research and technique *23*, 142-156.

48. Burton, P.R., and Laveri, L.A. (1985). The distribution, relationships to other organelles, and calcium-sequestering ability of smooth endoplasmic reticulum in frog olfactory axons. J Neurosci *5*, 3047-3060.

49. Engelmann, T.W. (1880). Zur anatomie und physiologie der flimmerzellen. Arch gel Physiol. *23*, 505-535.

50. Yang, J., Liu, X., Yue, G., Adamian, M., Bulgakov, O., and Li, T. (2002). Rootletin, a novel coiled-coil protein, is a structural component of the ciliary rootlet. The Journal of cell biology *159*, 431-440.

51. Farbman, A.I., and Gesteland, R.C. (1974). Fine structure of olfactory epithelium in the mud puppy, Necturus maculosus. Am J Anat *139*, 227-243.

52. Naguro, T., and Iwashita, K. (1992). Olfactory epithelium in young adult and aging rats as seen with high-resolution scanning electron microscopy. Microscopy research and technique *23*, 62-75.

53. Yamamoto, M. (1976). An electron microscopic study of the olfactory mucosa in the bat and rabbit. Archivum histologicum Japonicum *38*, 359-412.

54. McClintock, T.S., Glasser, C.E., Bose, S.C., and Bergman, D.A. (2008). Tissue expression patterns identify mouse cilia genes. Physiol Genomics *32*, 198-206.

55. Menco, B.P. (1980). Qualitative and quantitative freeze-fracture studies on olfactory and nasal respiratory epithelial surfaces of frog, ox, rat, and dog. III. Tight-junctions. Cell Tissue Res *211*, 361-373.

56. Menco, B.P., and Farbman, A.I. (1985). Genesis of cilia and microvilli of rat nasal epithelia during pre-natal development. II. Olfactory epithelium, a morphometric analysis. J Cell Sci *78*, 311-336.

57. Seifert, K. (1971). [Light and electron microscopic studies on the organ of Jacobson (vomero-nasal organ) of cats]. Arch Klin Exp Ohren Nasen Kehlkopfheilkd *200*, 223-251.

58. Margalit, T., and Lancet, D. (1993). Expression of olfactory receptor and transduction genes during rat development. Brain Res Dev Brain Res *73*, 7-16.

59. Saito, H., Mimmack, M., Kishimoto, J., Keverne, E.B., and Emson, P.C. (1998). Expression of olfactory receptors, G-proteins and AxCAMs during the development and maturation of olfactory sensory neurons in the mouse. Brain Res Dev Brain Res *110*, 69-81.

60. Schwarzenbacher, K., Fleischer, J., Breer, H., and Conzelmann, S. (2004). Expression of olfactory receptors in the cribriform mesenchyme during prenatal development. Gene Expr Patterns *4*, 543-552.

61. Strotmann, J., Wanner, I., Helfrich, T., and Breer, H. (1995). Receptor expression in olfactory neurons during rat development: in situ hybridization studies. Eur J Neurosci *7*, 492-500.

62. Kozminski, K.G., Johnson, K.A., Forscher, P., and Rosenbaum, J.L. (1993). A motility in the eukaryotic flagellum unrelated to flagellar beating. Proceedings of the National Academy of Sciences of the United States of America *90*, 5519-5523.

63. Scholey, J.M. (2008). Intraflagellar transport motors in cilia: moving along the cell's antenna. The Journal of cell biology *180*, 23-29.

64. Pazour, G.J., Wilkerson, C.G., and Witman, G.B. (1998). A dynein light chain is essential for the retrograde particle movement of intraflagellar transport (IFT). The Journal of cell biology *141*, 979-992.

65. Cole, D.G., Diener, D.R., Himelblau, A.L., Beech, P.L., Fuster, J.C., and Rosenbaum, J.L. (1998). Chlamydomonas kinesin-II-dependent intraflagellar transport (IFT): IFT particles contain proteins required for ciliary assembly in Caenorhabditis elegans sensory neurons. The Journal of cell biology *141*, 993-1008.

66. Snow, J.J., Ou, G., Gunnarson, A.L., Walker, M.R., Zhou, H.M., Brust-Mascher, I., and Scholey, J.M. (2004). Two anterograde intraflagellar transport motors cooperate to build sensory cilia on C. elegans neurons. Nat Cell Biol *6*, 1109-1113.

67. Lin, F., Hiesberger, T., Cordes, K., Sinclair, A.M., Goldstein, L.S., Somlo, S., and Igarashi, P. (2003). Kidney-specific inactivation of the KIF3A subunit of kinesin-II inhibits renal ciliogenesis and produces polycystic kidney disease. Proceedings of the National Academy of Sciences of the United States of America *100*, 5286-5291.

68. Jenkins, P.M., Hurd, T.W., Zhang, L., McEwen, D.P., Brown, R.L., Margolis, B., Verhey, K.J., and Martens, J.R. (2006). Ciliary targeting of olfactory CNG channels requires the CNGB1b subunit and the kinesin-2 motor protein, KIF17. Curr Biol *16*, 1211-1216.

69. Ou, G., Blacque, O.E., Snow, J.J., Leroux, M.R., and Scholey, J.M. (2005). Functional coordination of intraflagellar transport motors. Nature *436*, 583-587.

70. Cole, D.G. (2003). The intraflagellar transport machinery of Chlamydomonas reinhardtii. Traffic *4*, 435-442.

71. Blacque, O.E., Cevik, S., and Kaplan, O.I. (2008). Intraflagellar transport: from molecular characterisation to mechanism. Front Biosci *13*, 2633-2652.

72. Tsujikawa, M., and Malicki, J. (2004). Intraflagellar transport genes are essential for differentiation and survival of vertebrate sensory neurons. Neuron *42*, 703-716.

73. Avidor-Reiss, T., Maer, A.M., Koundakjian, E., Polyanovsky, A., Keil, T., Subramaniam, S., and Zuker, C.S. (2004). Decoding cilia function: defining specialized genes required for compartmentalized cilia biogenesis. Cell *117*, 527-539.

74. Dwyer, N.D., Adler, C.E., Crump, J.G., L'Etoile, N.D., and Bargmann, C.I. (2001). Polarized dendritic transport and the AP-1 mu1 clathrin adaptor UNC-101 localize odorant receptors to olfactory cilia. Neuron *31*, 277-287.

75. Mukhopadhyay, S., Lu, Y., Shaham, S., and Sengupta, P. (2008). Sensory signaling-dependent remodeling of olfactory cilia architecture in C. elegans. Dev Cell *14*, 762-774.

76. Roayaie, K., Crump, J.G., Sagasti, A., and Bargmann, C.I. (1998). The G alpha protein ODR-3 mediates olfactory and nociceptive function and controls cilium morphogenesis in C. elegans olfactory neurons. Neuron *20*, 55-67.

77. Farbman, A.I., Brunjes, P.C., Rentfro, L., Michas, J., and Ritz, S. (1988). The effect of unilateral naris occlusion on cell dynamics in the developing rat olfactory epithelium. J Neurosci *8*, 3290-3295.

78. Northcutt, R.G., and Gans, C. (1983). The genesis of neural crest and epidermal placodes: a reinterpretation of vertebrate origins. Q Rev Biol *58*, 1-28.

79. Inglis, P.N., Boroevich, K.A., and Leroux, M.R. (2006). Piecing together a ciliome. Trends Genet *22*, 491-500.

80. Iannaccone, A., Mykytyn, K., Persico, A.M., Searby, C.C., Baldi, A., Jablonski, M.M., and Sheffield, V.C. (2005). Clinical evidence of decreased olfaction in Bardet-Biedl syndrome caused by a deletion in the BBS4 gene. Am J Med Genet A *132*, 343-346.

81. Kulaga, H.M., Leitch, C.C., Eichers, E.R., Badano, J.L., Lesemann, A., Hoskins, B.E., Lupski, J.R., Beales, P.L., Reed, R.R., and Katsanis, N. (2004). Loss of BBS proteins causes anosmia in humans and defects in olfactory cilia structure and function in the mouse. Nature genetics *36*, 994-998.

82. McEwen, D.P., Koenekoop, R.K., Khanna, H., Jenkins, P.M., Lopez, I., Swaroop, A., and Martens, J.R. (2007). Hypomorphic CEP290/NPHP6 mutations result in anosmia caused by the selective loss of G proteins in cilia of olfactory sensory neurons. Proceedings of the National Academy of Sciences of the United States of America *104*, 15917-15922.

83. Kim, J., Krishnaswami, S.R., and Gleeson, J.G. (2008). CEP290 interacts with the centriolar satellite component PCM-1 and is required for Rab8 localization to the primary cilium. Hum Mol Genet *17*, 3796-3805.

84. Kim, J.C., Badano, J.L., Sibold, S., Esmail, M.A., Hill, J., Hoskins, B.E., Leitch, C.C., Venner, K., Ansley, S.J., Ross, A.J., et al. (2004). The Bardet-Biedl protein BBS4 targets cargo to the pericentriolar region and is required for microtubule anchoring and cell cycle progression. Nature genetics *36*, 462-470.

85. Schermer, B., Hopker, K., Omran, H., Ghenoiu, C., Fliegauf, M., Fekete, A., Horvath, J., Kottgen, M., Hackl, M., Zschiedrich, S., et al. (2005). Phosphorylation by casein kinase 2 induces PACS-1 binding of nephrocystin and targeting to cilia. Embo J *24*, 4415-4424.

86. Youker, R.T., Shinde, U., Day, R., and Thomas, G. (2008). At the Crossroads of Homeostasis and Disease: Roles of the PACS proteins in Membrane Traffic and Apoptosis. Biophys J. (In Press).

87. Mashukova, A., Spehr, M., Hatt, H., and Neuhaus, E.M. (2006). Beta-arrestin2-mediated internalization of mammalian odorant receptors. J Neurosci *26*, 9902-9912.

88. Geng, L., Okuhara, D., Yu, Z., Tian, X., Cai, Y., Shibazaki, S., and Somlo, S. (2006). Polycystin-2 traffics to cilia independently of polycystin-1 by using an N-terminal RVxP motif. J Cell Sci *119*, 1383-1395.

89. Mazelova, J., Astuto-Gribble, L., Inoue, H., Tam, B.M., Schonteich, E., Prekeris, R., Moritz, O.L., Randazzo, P.A., and Deretic, D. (2009). Ciliary targeting motif VxPx directs assembly of a trafficking module through Arf4. EMBO J.

90. Berbari, N.F., Johnson, A.D., Lewis, J.S., Askwith, C.C., and Mykytyn, K. (2008). Identification of Ciliary Localization Sequences within the Third Intracellular Loop of G Protein-coupled Receptors. Mol Biol Cell *19*, 1540-1547.

91. Dwyer, N.D., Troemel, E.R., Sengupta, P., and Bargmann, C.I. (1998). Odorant receptor localization to olfactory cilia is mediated by ODR-4, a novel membrane-associated protein. Cell *93*, 455-466.

92. Qin, H., Burnette, D.T., Bae, Y.K., Forscher, P., Barr, M.M., and Rosenbaum, J.L. (2005). Intraflagellar transport is required for the vectorial movement of TRPV channels in the ciliary membrane. Curr Biol *15*, 1695-1699.

93. Wigley, W.C., Fabunmi, R.P., Lee, M.G., Marino, C.R., Muallem, S., DeMartino, G.N., and Thomas, P.J. (1999). Dynamic association of proteasomal machinery with the centrosome. The Journal of cell biology *145*, 481-490.

94. Gerdes, J.M., Liu, Y., Zaghloul, N.A., Leitch, C.C., Lawson, S.S., Kato, M., Beachy, P.A., Beales, P.L., DeMartino, G.N., Fisher, S., et al. (2007). Disruption of the basal body compromises proteasomal function and perturbs intracellular Wnt response. Nature genetics *39*, 1350-1360.

95. Michalakis, S., Reisert, J., Geiger, H., Wetzel, C., Zong, X., Bradley, J., Spehr, M., Huttl, S., Gerstner, A., Pfeifer, A., et al. (2006). Loss of CNGB1 protein leads to olfactory dysfunction and subciliary cyclic nucleotide-gated channel trapping. The Journal of biological chemistry *281*, 35156-35166.

96. Blacque, O.E., Li, C., Inglis, P.N., Esmail, M.A., Ou, G., Mah, A.K., Baillie, D.L., Scholey, J.M., and Leroux, M.R. (2006). The WD repeat-containing protein IFTA-1 is required for retrograde intraflagellar transport. Mol Biol Cell *17*, 5053-5062.

97. Li, J.B., Gerdes, J.M., Haycraft, C.J., Fan, Y., Teslovich, T.M., May-Simera, H., Li, H., Blacque, O.E., Li, L., Leitch, C.C., et al. (2004). Comparative genomics identifies a flagellar and basal body proteome that includes the BBS5 human disease gene. Cell *117*, 541-552.

98. Pazour, G.J., Agrin, N., Leszyk, J., and Witman, G.B. (2005). Proteomic analysis of a eukaryotic cilium. J Cell Biol *170*, 103-113.

99. Smith, J.C., Northey, J.G., Garg, J., Pearlman, R.E., and Siu, K.W. (2005). Robust method for proteome analysis by MS/MS using an entire translated genome: demonstration on the ciliome of Tetrahymena thermophila. J Proteome Res *4*, 909-919.

100. Stolc, V., Samanta, M.P., Tongprasit, W., and Marshall, W.F. (2005). Genome-wide transcriptional analysis of flagellar regeneration in Chlamydomonas reinhardtii identifies orthologs of ciliary disease genes. Proc Natl Acad Sci U S A *102*, 3703-3707.

101. Klimmeck, D., Mayer, U., Ungerer, N., Warnken, U., Schnolzer, M., Frings, S., and Mohrlen, F. (2008). Calcium-signaling networks in olfactory receptor neurons. Neuroscience *151*, 901-912.

102. Ostrowski, L.E., Blackburn, K., Radde, K.M., Moyer, M.B., Schlatzer, D.M., Moseley, A., and Boucher, R.C. (2002). A proteomic analysis of human cilia: identification of novel components. Mol Cell Proteomics *1*, 451-465.

103. Sammeta, N., Yu, T.T., Bose, S.C., and McClintock, T.S. (2007). Mouse olfactory sensory neurons express 10,000 genes. J Comp Neurol *502*, 1138-1156.

104. Su, A.I., Wiltshire, T., Batalov, S., Lapp, H., Ching, K.A., Block, D., Zhang, J., Soden, R., Hayakawa, M., Kreiman, G., et al. (2004). A gene atlas of the mouse and human protein-encoding transcriptomes. Proc Natl Acad Sci U S A *101*, 6062-6067.

105. Mayer, U., Kuller, A., Daiber, P.C., Neudorf, I., Warnken, U., Schnolzer, M., Frings, S., and Mohrlen, F. (2008). The proteome of rat olfactory sensory cilia. Proteomics.

106. Mayer, U., Ungerer, N., Klimmeck, D., Warnken, U., Schnolzer, M., Frings, S., and Mohrlen, F. (2008). Proteomic analysis of a membrane preparation from rat olfactory sensory cilia. Chemical senses *33*, 145-162.

107. Toller, S.V. (1999). Assessing the impact of anosmia: review of a questionnaire's findings. Chemical senses *24*, 705-712.

108. Murphy, C., Schubert, C.R., Cruickshanks, K.J., Klein, B.E., Klein, R., and Nondahl, D.M. (2002). Prevalence of olfactory impairment in older adults. Jama *288*, 2307-2312.

109. Nguyen-Khoa, B.A., Goehring, E.L., Jr., Vendiola, R.M., Pezzullo, J.C., and Jones, J.K. (2007). Epidemiologic study of smell disturbance in 2 medical insurance claims populations. Arch Otolaryngol Head Neck Surg *133*, 748-757.

110. Jafek (2000). Evaluation and treatment of anosmia. Current opinion in otolaryngology & head and neck surgery *8*, 63-67.

111. Douek, E., Bannister, L.H., and Dodson, H.C. (1975). Recent advances in the pathology of olfaction. Proc R Soc Med *68*, 467-470.

112. Afzelius, B.A. (2004). Cilia-related diseases. J Pathol *204*, 470-477.

113. Bardet, G. (1995). On congenital obesity syndrome with polydactyly and retinitis pigmentosa (a contribution to the study of clinical forms of hypophyseal obesity). 1920. Obes Res *3*, 387-399.

114. Beales, P.L., Elcioglu, N., Woolf, A.S., Parker, D., and Flinter, F.A. (1999). New criteria for improved diagnosis of Bardet-Biedl syndrome: results of a population survey. J Med Genet *36*, 437-446.

115. Biedl, A. (1995). A pair of siblings with adiposo-genital dystrophy. 1922. Obes Res *3*, 404.

116. Klysik, M. (2008). Ciliary syndromes and treatment. Pathol Res Pract *204*, 77-88.

117. Beales, P.L., Badano, J.L., Ross, A.J., Ansley, S.J., Hoskins, B.E., Kirsten, B., Mein, C.A., Froguel, P., Scambler, P.J., Lewis, R.A., et al. (2003). Genetic interaction of BBS1 mutations with alleles at other BBS loci can result in non-Mendelian Bardet-Biedl syndrome. Am J Hum Genet *72*, 1187-1199.

118. Hichri, H., Stoetzel, C., Laurier, V., Caron, S., Sigaudy, S., Sarda, P., Hamel, C., Martin-Coignard, D., Gilles, M., Leheup, B., et al. (2005). Testing for triallelism: analysis of six BBS genes in a Bardet-Biedl syndrome family cohort. Eur J Hum Genet *13*, 607-616.

119. Mykytyn, K., Nishimura, D.Y., Searby, C.C., Beck, G., Bugge, K., Haines, H.L., Cornier, A.S., Cox, G.F., Fulton, A.B., Carmi, R., et al. (2003). Evaluation of complex inheritance involving the most common Bardet-Biedl syndrome locus (BBS1). Am J Hum Genet *72*, 429-437.

120. Stoetzel, C., Laurier, V., Davis, E.E., Muller, J., Rix, S., Badano, J.L., Leitch, C.C., Salem, N., Chouery, E., Corbani, S., et al. (2006). BBS10 encodes a vertebrate-specific chaperonin-like protein and is a major BBS locus. Nat Genet *38*, 521-524.

121. Mykytyn, K., Mullins, R.F., Andrews, M., Chiang, A.P., Swiderski, R.E., Yang, B., Braun, T., Casavant, T., Stone, E.M., and Sheffield, V.C. (2004). Bardet-Biedl syndrome type 4 (BBS4)-null mice implicate Bbs4 in flagella formation but not global cilia assembly. Proceedings of the National Academy of Sciences of the United States of America *101*, 8664-8669.

122. Nishimura, D.Y., Fath, M., Mullins, R.F., Searby, C., Andrews, M., Davis, R., Andorf, J.L., Mykytyn, K., Swiderski, R.E., Yang, B., et al. (2004). Bbs2-null mice have neurosensory deficits, a defect in social dominance, and retinopathy associated with mislocalization of rhodopsin. Proc Natl Acad Sci U S A *101*, 16588-16593.

123. Mokrzan, E.M., Lewis, J.S., and Mykytyn, K. (2007). Differences in renal tubule primary cilia length in a mouse model of Bardet-Biedl syndrome. Nephron Exp Nephrol *106*, e88-96.

124. Eichers, E.R., Abd-El-Barr, M.M., Paylor, R., Lewis, R.A., Bi, W., Lin, X., Meehan, T.P., Stockton, D.W., Wu, S.M., Lindsay, E., et al. (2006). Phenotypic characterization of Bbs4 null mice reveals age-dependent penetrance and variable expressivity. Hum Genet *120*, 211-226.

125. Leber, T. (1869). Uber retinitis pigmentosa und angeborene amaurose. Graefes Arch Clin Exp Ophthalmol *15*, 1-25.

126. Koenekoop, R.K. (2004). An overview of Leber congenital amaurosis: a model to understand human retinal development. Surv Ophthalmol *49*, 379-398.

127. den Hollander, A.I., Koenekoop, R.K., Yzer, S., Lopez, I., Arends, M.L., Voesenek, K.E., Zonneveld, M.N., Strom, T.M., Meitinger, T., Brunner, H.G., et al. (2006). Mutations in the CEP290 (NPHP6) gene are a frequent cause of Leber congenital amaurosis. Am J Hum Genet *79*, 556-561.

128. Cideciyan, A.V., Aleman, T.S., Jacobson, S.G., Khanna, H., Sumaroka, A., Aguirre, G.K., Schwartz, S.B., Windsor, E.A., He, S., Chang, B., et al. (2007). Centrosomal-ciliary gene CEP290/NPHP6 mutations result in blindness with unexpected sparing of photoreceptors and visual brain: implications for therapy of Leber congenital amaurosis. Hum Mutat *28*, 1074-1083.

129. Chang, B., Khanna, H., Hawes, N., Jimeno, D., He, S., Lillo, C., Parapuram, S.K., Cheng, H., Scott, A., Hurd, R.E., et al. (2006). In-frame deletion in a novel centrosomal/ciliary protein CEP290/NPHP6 perturbs its interaction with RPGR and results in early-onset retinal degeneration in the rd16 mouse. Hum Mol Genet *15*, 1847-1857.

130. Insinna, C., Pathak, N., Perkins, B., Drummond, I., and Besharse, J.C. (2008). The homodimeric kinesin, Kif17, is essential for vertebrate photoreceptor sensory outer segment development. Dev Biol *316*, 160-170.

131. Doty, R.L. (2008). The olfactory vector hypothesis of neurodegenerative disease: is it viable? Ann Neurol *63*, 7-15.

132. Doty, R.L., Perl, D.P., Steele, J.C., Chen, K.M., Pierce, J.D., Jr., Reyes, P., and Kurland, L.T. (1991). Odor identification deficit of the parkinsonism-dementia complex of Guam: equivalence to that of Alzheimer's and idiopathic Parkinson's disease. Neurology *41*, 77-80; discussion 80-71.

133. Baker, H., and Genter, M.B. (2003). The olfactory system and the nasal mucosa as portals of entry of viruses, drugs, and other exogenous agents into the brain. In Handbook on Olfaction and Gustation, 2 Edition, R.L. Doty, ed. (New York: Informa Health Care), pp. 909-950.

134. Ding, X., and Dahl, A.R. (2003). Olfactory Mucosa: Composition, Enzymatic Localization, and Metabolism. In Handbook on Olfaction and Gustation, 2 Edition, R.L. Doty, ed. (New York: Informa Health Care), pp. 98-135.

135. Flexner, S. (1917). Mechanisms that Defend the Body from Poliomyelitic Infection, (a) External or Extra-Nervous, (b) Internal or Nervous. Proc Natl Acad Sci U S A *3*, 416-418.

136. Brodie, M., and Elvidge, A.R. (1934). The Portal of Entry and Transmission of the Virus of Poliomyelitis. Science *79*, 235-236.

137. Schultz, E.W., and Gebhardt, L.P. (1936). Chemoprophylaxis of Poliomyelitis: A Progress Report. Cal West Med *45*, 138-140.

138. Tabaton, M., Monaco, S., Cordone, M.P., Colucci, M., Giaccone, G., Tagliavini, F., and Zanusso, G. (2004). Prion deposition in olfactory biopsy of sporadic Creutzfeldt-Jakob disease. Annals of neurology *55*, 294-296.

139. Firestein, S., and Werblin, F. (1989). Odor-induced membrane currents in vertebrate-olfactory receptor neurons. Science *244*, 79-82.

140. Nakamura, T., and Gold, G.H. (1987). A cyclic nucleotide-gated conductance in olfactory receptor cilia. Nature *325*, 442-444.

141. Ronnett, G.V., and Moon, C. (2002). G proteins and olfactory signal transduction. Annual review of physiology *64*, 189-222.

142. Bonigk, W., Bradley, J., Muller, F., Sesti, F., Boekhoff, I., Ronnett, G.V., Kaupp, U.B., and Frings, S. (1999). The native rat olfactory cyclic nucleotide-gated channel is composed of three distinct subunits. J Neurosci *19*, 5332-5347.

143. Trudeau, M.C., and Zagotta, W.N. (2002). An intersubunit interaction regulates trafficking of rod cyclic nucleotide-gated channels and is disrupted in an inherited form of blindness. Neuron *34*, 197-207.

144. Huttl, S., Michalakis, S., Seeliger, M., Luo, D.G., Acar, N., Geiger, H., Hudl, K., Mader, R., Haverkamp, S., Moser, M., et al. (2005). Impaired channel targeting and retinal degeneration in mice lacking the cyclic nucleotide-gated channel subunit CNGB1. J.Neurosci. *25*, 130-138.

145. Evans, J.E., Snow, J.J., Gunnarson, A.L., Ou, G., Stahlberg, H., McDonald, K.L., and Scholey, J.M. (2006). Functional modulation of IFT kinesins extends the sensory repertoire of ciliated neurons in Caenorhabditis elegans. The Journal of cell biology *172*, 663-669.

146. Setou, M., Nakagawa, T., Seog, D.H., and Hirokawa, N. (2000). Kinesin superfamily motor protein KIF17 and mLin-10 in NMDA receptor-containing vesicle transport. Science *288*, 1796-1802.

147. Zheng, J., and Zagotta, W.N. (2004). Stoichiometry and assembly of olfactory cyclic nucleotide-gated channels. Neuron *42*, 411-421.

148. Snapp, E.L., and Landfear, S.M. (1999). Characterization of a targeting motif for a flagellar membrane protein in Leishmania enriettii. J.Biol.Chem. *274*, 29543-29548.

149. Nishimura, T., Kato, K., Yamaguchi, T., Fukata, Y., Ohno, S., and Kaibuchi, K. (2004). Role of the PAR-3-KIF3 complex in the establishment of neuronal polarity. Nat.Cell Biol. *6*, 328-334.

150. Marszalek, J.R., Liu, X., Roberts, E.A., Chui, D., Marth, J.D., Williams, D.S., and Goldstein, L.S. (2000). Genetic evidence for selective transport of opsin and arrestin by kinesin-II in mammalian photoreceptors. Cell *102*, 175-187.

151. Noda, Y., Okada, Y., Saito, N., Setou, M., Xu, Y., Zhang, Z., and Hirokawa, N. (2001). KIFC3, a microtubule minus end-directed motor for the apical transport of annexin XIIIb-associated Triton-insoluble membranes. J.Cell Biol. *155*, 77-88.

152. Bakalyar, H.A., and Reed, R.R. (1990). Identification of a specialized adenylyl cyclase that may mediate odorant detection. Science *250*, 1403-1406.

153. Griesbeck, O., Baird, G.S., Campbell, R.E., Zacharias, D.A., and Tsien, R.Y. (2001). Reducing the environmental sensitivity of yellow fluorescent protein. Mechanism and applications. J.Biol.Chem. *276*, 29188-29194.

154. Saxton, M.J., and Jacobson, K. (1997). Single-particle tracking: applications to membrane dynamics. Annu.Rev.Biophys.Biomol.Struct. *26*, 373-399.

155. O'Connell, K.M., and Tamkun, M.M. (2005). Targeting of voltage-gated potassium channel isoforms to distinct cell surface microdomains. J.Cell Sci. *118*, 2155-2166.

156. Peden, E.M., and Barr, M.M. (2005). The KLP-6 kinesin is required for male mating behaviors and polycystin localization in Caenorhabditis elegans. Curr Biol *15*, 394-404.

157. Pazour, G.J., and Rosenbaum, J.L. (2002). Intraflagellar transport and cilia-dependent diseases. Trends in cell biology *12*, 551-555.

158. Badano, J.L., Mitsuma, N., Beales, P.L., and Katsanis, N. (2006). The ciliopathies: an emerging class of human genetic disorders. Annual review of genomics and human genetics *7*, 125-148.

159. Christensen, S.T., Pedersen, L.B., Schneider, L., and Satir, P. (2007). Sensory cilia and integration of signal transduction in human health and disease. Traffic *8*, 97-109.

160. Fuchs, J.L., and Schwark, H.D. (2004). Neuronal primary cilia: a review. Cell Biol Int *28*, 111-118.

161. Menco, B.P. (1994). Ultrastructural aspects of olfactory transduction and perireceptor events. Seminars in cell biology *5*, 11-24.

162. Otto, E.A., Loeys, B., Khanna, H., Hellemans, J., Sudbrak, R., Fan, S., Muerb, U., O'Toole, J.F., Helou, J., Attanasio, M., et al. (2005). Nephrocystin-5, a ciliary IQ domain protein, is mutated in Senior-Loken syndrome and interacts with RPGR and calmodulin. Nature genetics *37*, 282-288.

163. Scott, G.K., Gu, F., Crump, C.M., Thomas, L., Wan, L., Xiang, Y., and Thomas, G. (2003). The phosphorylation state of an autoregulatory domain controls PACS-1-directed protein traffic. Embo J *22*, 6234-6244.

164. Jones, B.G., Thomas, L., Molloy, S.S., Thulin, C.D., Fry, M.D., Walsh, K.A., and Thomas, G. (1995). Intracellular trafficking of furin is modulated by the phosphorylation state of a casein kinase II site in its cytoplasmic tail. Embo J *14*, 5869-5883.

165. Scott, G.K., Fei, H., Thomas, L., Medigeshi, G.R., and Thomas, G. (2006). A PACS-1, GGA3 and CK2 complex regulates CI-MPR trafficking. Embo J *25*, 4423-4435.

166. Scott, J.W., Acevedo, H.P., and Sherrill, L. (2006). Effects of concentration and sniff flow rate on the rat electroolfactogram. Chemical senses *31*, 581-593.

167. Crump, C.M., Xiang, Y., Thomas, L., Gu, F., Austin, C., Tooze, S.A., and Thomas, G. (2001). PACS-1 binding to adaptors is required for acidic cluster motif-mediated protein traffic. Embo J *20*, 2191-2201.

168. Kottgen, M., Benzing, T., Simmen, T., Tauber, R., Buchholz, B., Feliciangeli, S., Huber, T.B., Schermer, B., Kramer-Zucker, A., Hopker, K., et al. (2005). Trafficking of TRPP2 by PACS proteins represents a novel mechanism of ion channel regulation. Embo J *24*, 705-716.

169. Hu, J., Bae, Y.K., Knobel, K.M., and Barr, M.M. (2006). Casein kinase II and calcineurin modulate TRPP function and ciliary localization. Mol Biol Cell *17*, 2200-2211.

170. Obara, T., Mangos, S., Liu, Y., Zhao, J., Wiessner, S., Kramer-Zucker, A.G., Olale, F., Schier, A.F., and Drummond, I.A. (2006). Polycystin-2 immunolocalization and function in zebrafish. J Am Soc Nephrol *17*, 2706-2718.

171. Martin, D.M., Skidmore, J.M., Fox, S.E., Gage, P.J., and Camper, S.A. (2002). Pitx2 distinguishes subtypes of terminally differentiated neurons in the developing mouse neuroepithelium. Dev Biol *252*, 84-99.

172. Boehning, D., Moon, C., Sharma, S., Hurt, K.J., Hester, L.D., Ronnett, G.V., Shugar, D., and Snyder, S.H. (2003). Carbon monoxide neurotransmission activated by CK2 phosphorylation of heme oxygenase-2. Neuron *40*, 129-137.

173. Sati, L., Seval-Celik, Y., Unek, G., Korgun, E.T., and Demir, R. (2009). The presence of kinesin superfamily motor proteins KIFC1 and KIF17 in normal and pathological human placenta. Placenta *30*, 848-854.

174. Deretic, D., Williams, A.H., Ransom, N., Morel, V., Hargrave, P.A., and Arendt, A. (2005). Rhodopsin C terminus, the site of mutations causing retinal disease, regulates trafficking by binding to ADP-ribosylation factor 4 (ARF4). Proceedings of the National Academy of Sciences of the United States of America *102*, 3301-3306.

175. Xu, C., Rossetti, S., Jiang, L., Harris, P.C., Brown-Glaberman, U., Wandinger-Ness, A., Bacallao, R., and Alper, S.L. (2007). Human ADPKD primary cyst epithelial cells with a novel, single codon deletion in the PKD1 gene exhibit defective ciliary polycystin localization and loss of flow-induced Ca2+ signaling. Am J Physiol Renal Physiol *292*, F930-945.

176. Tao, B., Bu, S., Yang, Z., Siroky, B., Kappes, J.C., Kispert, A., and Guay-Woodford, L.M. (2009). Cystin localizes to primary cilia via membrane microdomains and a targeting motif. J Am Soc Nephrol *20*, 2570-2580.

177. Jenkins, P.M., Zhang, L., Thomas, G., and Martens, J.R. (2009). PACS-1 mediates phosphorylation-dependent ciliary trafficking of the cyclic-nucleotide-gated channel in olfactory sensory neurons. J Neurosci *29*, 10541-10551.

178. Verhey, K.J., Meyer, D., Deehan, R., Blenis, J., Schnapp, B.J., Rapoport, T.A., and Margolis, B. (2001). Cargo of kinesin identified as JIP scaffolding proteins and associated signaling molecules. J Cell Biol *152*, 959-970.

179. Lechtreck, K.F., Johnson, E.C., Sakai, T., Cochran, D., Ballif, B.A., Rush, J., Pazour, G.J., Ikebe, M., and Witman, G.B. (2009). The Chlamydomonas

reinhardtii BBSome is an IFT cargo required for export of specific signaling proteins from flagella. J Cell Biol *187*, 1117-1132.

180. Tayeh, M.K., Yen, H.J., Beck, J.S., Searby, C.C., Westfall, T.A., Griesbach, H., Sheffield, V.C., and Slusarski, D.C. (2008). Genetic interaction between Bardet-Biedl syndrome genes and implications for limb patterning. Hum Mol Genet *17*, 1956-1967.

181. Devos, D., Dokudovskaya, S., Alber, F., Williams, R., Chait, B.T., Sali, A., and Rout, M.P. (2004). Components of coated vesicles and nuclear pore complexes share a common molecular architecture. PLoS Biol *2*, e380.

182. Hong, D.H., Pawlyk, B., Sokolov, M., Strissel, K.J., Yang, J., Tulloch, B., Wright, A.F., Arshavsky, V.Y., and Li, T. (2003). RPGR isoforms in photoreceptor connecting cilia and the transitional zone of motile cilia. Invest Ophthalmol Vis Sci *44*, 2413-2421.

183. Jeyifous, O., Waites, C.L., Specht, C.G., Fujisawa, S., Schubert, M., Lin, E.I., Marshall, J., Aoki, C., de Silva, T., Montgomery, J.M., et al. (2009). SAP97 and CASK mediate sorting of NMDA receptors through a previously unknown secretory pathway. Nat Neurosci *12*, 1011-1019.

184. Signor, D., Wedaman, K.P., Rose, L.S., and Scholey, J.M. (1999). Two heteromeric kinesin complexes in chemosensory neurons and sensory cilia of Caenorhabditis elegans. Mol Biol Cell *10*, 345-360.